ISSN 0915-6364

NATIONAL INSTITUTE FOR FUSION SCIENCE

Collisional-radiative Model for Neutral Helium in Plasma: Excitation Cross Section and Singlet-triplet Wavefunction Mixing

M. Goto and T. Fujimoto

(Received - July 10, 1997)

NIFS-DATA-43 Oct. 1997

RESEARCH REPORT
NIFS-DATA Series

NAGOYA, JAPAN

Collisional-radiative model for neutral helium in plasma: Excitation cross section and singlet-triplet wavefunction mixing

Motoshi Goto

National Institute for Fusion Science, Toki 509-52, Japan

Takashi Fujimoto

Department of Engineering Science, Kyoto 606-01, Japan

Abstract

We have revised the collisional-radiative (CR) model code of neutral helium (T. Fujimoto, JQSRT **21**, 1979). The spin-orbit interaction gives rise to mixing of the wavefunctions of the singlet and triplet states. The degree of the mixing depends on the magnetic field, and at the field strength of the level-anticrossings complete mixing, or complete breakdown of the L-S coupling scheme, occurs. We have approximately incorporated this effect into the code.

We have reviewed the excitation cross section data for electron impacts. For transitions starting from the ground state, the recent assessment by the group led by Dr. de Heer is judged satisfactory. For transitions from the metastable levels the assessment by the same group appears rather conservative; there remains a question about the cross section values near the threshold. For transitions between different-l levels within the same multiplicity and same n, a semi-empirical formula based on the Born cross section gives a good agreement with experiment. Proton impacts are also considered for these transitions.

We compare the new cross sections with those used in the original version. These cross sections for transitions starting from the metastable levels are fitted by analytical formulas and the parameter values are given. We also give parameter values for the excitation rate coefficient for these transitions as well as for transitions starting from the ground state. With all the above revisions incorporated into the CR model code, we have calculated the energy loss rates and the line intensity ratios for the purpose of plasma diagnostics, where the effect of a magnetic field is noted. The calculated population distribution over excited levels are compared with experiment, and a tentative conclusion is drawn concerning the excitation cross section from the metastable level.

KEYWORDS

helium, collisional-radiative model, wavefunction mixing, excitation cross section, l-changing collision, proton impacts

I. INTRODUCTION

Neutral helium has been one of the most common species for spectroscopy of laboratory and astrophysical plasmas. It played an important role in development of plasma spectroscopy. At present, with the D-T plasma in sight, the importance of spectroscopic plasma diagnostics on helium is even increasing. In order to perform quantitative spectroscopy on plasmas containing helium, a highly reliable model is indispensable that enables us to interpret the observed spectral line intensities in terms of the characteristics of the plasma; the electron temperature T_e and density n_e, the magnetic field, the particle transport and the ionization-recombination dynamics.

Almost two decades ago Fujimoto published a CR model for helium [1]. That code was constructed with application to positive-column plasmas of glow discharge in mind, and in it the set of atomic data was adopted that was judged best at that time. The details of the atomic data were published in a volume of IPPJ-AM-8 [2], the predecessor of this series. This code found use at various places, and even recently effective rate coefficients derived from the code were parametrized and distributed [3].

We began to feel that we should update this original CR model code; the collision cross sections should be replaced on the basis of the data accumulated during the last twenty years, and since we are interested in tokamak and other magnetically confined plasmas including the divertor plasmas, the cross section data should be handled so as to fit our objective. It should also include ion collisions which may be important for high temperature plasmas. Secondly, since the magnetically confined plasmas are in a magnetic field of significant strength, the singlet-triplet wavefunction mixing should be taken into account. We began this attempt several years ago. It was very fortunate that, at that time, a group of people led by de Heer was assessing the cross sections [4, 5] and Drake was finishing his calculation on helium wavefunctions [6]. We could obtain their valuable results, and in our revision we were able to use them.

In the following, we report the new versions of the set of cross section data and the CR model which should replace the original ones. In the present version we have dropped the part of the CR model which treated the effect of radiation trapping and the part for metastable-metastable collisions and diffusion of metastable

atoms. These parts could be incorporated rather easily.

II. COLLISIONAL-RADIATIVE MODEL

The temporal development of the population density $n(p)$ of level p is described by the differential equation,

$$\frac{\mathrm{d}n(p)}{\mathrm{d}t} = -\left\{\sum_{q\neq p} C(p,q)n_\mathrm{e} + \sum_{q<p} A(p,q) + S(p)n_\mathrm{e}\right\} n(p) + \sum_{q\neq p}\{C(q,p)n_\mathrm{e} + A(q,p)\}\, n(q) + \{\alpha(p)n_\mathrm{e} + \beta(p) + \beta_\mathrm{d}(p)\}\, n_\mathrm{i}n_\mathrm{e}, \quad (1)$$

which is coupled with similar equations for other levels. Here $q < p$ means that level q lies energetically lower than level p. $A(p,q)$ is the spontaneous transition probability from p to q, $C(p,q)$ and $S(p)$ are the rate coefficients for electron impact transition (excitation or deexcitation) and ionization, and $\alpha(p)$, $\beta(p)$ and $\beta_\mathrm{d}(p)$ are the rate coefficients for three-body, radiative and dielectronic recombination, respectively. We express the hydrogenlike ion density as n_i.

The energy level structure is the same as in [1] and is shown in Fig. 1. The term values of the levels are based on [7]. Several levels are grouped together, and Fig. 1 shows this grouping. All of the levels having principal quantum number $n \leq 7$ are treated as individual levels, except the levels having the orbital angular momentum $l \geq 3$. These latter levels with the same n are grouped together to form a single level denoted as '$F+$'. For the levels having $8 \leq n \leq 10$, all of the $S, P, D\ldots$ levels are grouped together. The levels with $n \geq 11$ are approximated by the hydrogenic levels having statistical weights twice those of hydrogen.

A. SINGLET-TRIPLET WAVEFUNCTION MIXING

Owing mainly to the spin-orbit interaction, wavefunctions between the singlet and triplet levels mix each other. Only states n^1L_L and n^3L_L mix, and the actual wavefunction $\psi(p)$ for them is expressed as

$$\psi(n^3L_L) = (1-\omega^2)^{1/2}\psi^0(n^3L_L) + \omega\psi^0(n^1L_L), \quad (2)$$

$$\psi(n^1L_L) = -\omega\psi^0(n^3L_L) + (1-\omega^2)^{1/2}\psi^0(n^1L_L), \quad (3)$$

where $\psi^0(p)$ denotes the wavefunction for the pure singlet or triplet level p. The mixing coefficients ω was calculated by Drake [6] and they are reproduced in Table I

and shown in Fig. 2. An experimental result [8] is also shown and it agrees with Drake's calculation. It is seen that for P and D levels the L-S coupling scheme is valid. Whereas for higher L levels, especially for $L \geq 4$, the L-S coupling scheme is inappropriate. Rather, the j-j coupling scheme is appropriate.

When a magnetic field is present, an energy-level splits into magnetic substates owing to the Zeeman or Paschen-Back effect. We take the substates with magnetic quantum number $m_J = 1$ of $3^{1,3}D$ levels as an example. There are four magnetic substates in terms of the L-S coupling scheme, i.e., $3^3D_{J=3,m_J=1}$, $3^3D_{2,1}$, $3^3D_{1,1}$ and $3^1D_{2,1}$. The elements of the secular matrix for the magnetic substate energies are expressed [9]

$$
\begin{aligned}
H_{11} &= E(3^3D_{3,1}) + \frac{1}{3}(2g_l + g_s)\mu_B B, && (4)\\
H_{12} &= \frac{4}{3\sqrt{5}}(g_l - g_s)\mu_B B, && (5)\\
H_{13} &= 0, && (6)\\
H_{14} &= 0, && (7)\\
H_{22} &= E(3^3D_{2,1}) + \frac{1}{6}(5g_l + g_s)\mu_B B, && (8)\\
H_{23} &= \frac{3}{2\sqrt{5}}(g_l - g_s)\mu_B B, && (9)\\
H_{24} &= \epsilon, && (10)\\
H_{33} &= E(3^3D_{1,1}) + \frac{1}{2}(3g_l - g_s)\mu_B B, && (11)\\
H_{34} &= 0, && (12)\\
H_{44} &= E(3^1D_{2,1}) + g_l\mu_B B. && (13)
\end{aligned}
$$

Here $E(3^{1,3}D_{J,m_J})$ denotes the pure substate energies, and the off diagonal element ϵ is the spin interactions term which causes the mixing between siglet and triplet levels. These values are taken from [6]. The parameters g_l, g_s and μ_B are the orbital and spin gyromagnetic ratios and the Bohr magneton, respectively. As a result of the diagonalization of the matrix, the dependence of the Zeeman or Paschen-Back shifts on the magnetic field strength is obtained. Figure 3 is the result for all the substates of $3^{1,3}D$ levels. With an increase in the field strength the energy separation between the substates having the same m_J decreases and the mixing occurs among these substates. In this case, the actual wavefunction for the $3^1D_{2,1}$ state, for example, is expressed as

$$
\psi(3^1D_{2,1}) = -\omega_1\psi^0(3^3D_{3,1}) - \omega_2\psi^0(3^3D_{2,1}) - \omega_3\psi^0(3^3D_{1,1})
$$

$$+(1-\omega^2)^{1/2}\psi^0(3^1D_{2,1}) \qquad (\omega_1{}^2+\omega_2{}^2+\omega_3{}^2=\omega^2), \qquad (14)$$

where the coefficients ω_i's are also determined by diagonalization of the secular matrix. The mixing degree ω^2 is calculated for each m_J and results are shown in Fig. 4. Starting from $\omega^2 = 2.44 \times 10^{-4}$ as given in Fig. 2 the ω^2 changes with an increase in the magnetic filed strength. Among the five sets of the substates only those with $m_J = 2, 1, 0, -1$ are strongly affected by the magnetic field. At the field strength about 7.3 T the singlet-triplet pairs having the same J and m_J undergo the 'level anticrossing' and the coefficient for each set reaches the maximum value $2^{-1/2}$. At the level anticrossing point the L-S coupling scheme completely breaks down.

From the standpoint of atomic physics, when the L-S coupling scheme becomes inadequate, a different coupling scheme should be employed. However, this procedure is inpractical for our purposes, and we retain the energy level scheme of Fig. 1 throughout. Instead we approximately take these effects into account by manipulating the transition rate coefficients. We assume that the population is equally distributed among the magnetic substates, and ω^2 is defined as an average of the five sets of the substates. In the case of no magnetic field, it is easily understood that one third of the triplet population can be mixed. That is also true when the energy levels are separated to the substates by a magnetic field and even when the triplet levels having $J \neq L$ take part in the mixing. The ω's are calculated for all the D and F levels, and the transition probabilities and rate coefficients concerning these levels are modified as follows. The secular matrix elements are taken from [9] for D levels and are constructed by the present authors for F levels.

For ionization originating from levels $n^{1,3}L$, the actual rate coefficient $S(n^{1,3}L)$ is expressed in terms of the rate coefficients calculated from the cross sections for the *pure* state,

$$S(n^1L) = (1-\omega^2)S^0(n^1L) + \omega^2 S^0(n^3L), \qquad (15)$$

$$S(n^3L) = \left(1-\frac{\omega^2}{3}\right)S^0(n^3L) + \frac{\omega^2}{3}S^0(n^1L). \qquad (16)$$

For recombination to levels $n^{1,3}L$, the actual rate coefficient $\beta(n^{1,3}L)$, for example, is expressed as

$$\beta(n^1L) = (1-\omega^2)\beta^0(n^1L) + \frac{\omega^2}{3}\beta^0(n^3L), \qquad (17)$$

$$\beta(n^3L) = \left(1 - \frac{\omega^2}{3}\right)\beta^0(n^3L) + \omega^2\beta^0(n^1L). \quad (18)$$

For transitions between levels $n^{1,3}L$ and $n'^{1,3}L'$, the actual electron impact transition rate coefficient $C(n^1L, n'^1L')$, for example, is expressed as

$$\begin{aligned} C(n^1L, n'^1L') &= (1-\omega^2)(1-\omega'^2)C^0(n^1L, n'^1L') \\ &\quad +(1-\omega^2)\frac{\omega'^2}{3}C^0(n^1L, n'^3L') \\ &\quad +\omega^2\frac{\omega'^2}{3}C^0(n^3L, n'^3L') + \omega^2(1-\omega'^2)C^0(n^3L, n'^1L'), \end{aligned} \quad (19)$$

and others are expressed in the similar way. The validity of this approximation is discussed later on.

B. FORMULATION I

We assume that the quasi-steady-state approximation is valid for the population of all the levels except the ground and the two metastable levels [10]. The time derivative of the population of the former levels is set equal to 0. The set of coupled differential equations for these levels reduces to a set of coupled linear equations. The solution is expressed as the sum of four terms,

$$n(p) = r_0(p)n_e n_i + r_1(p)n_e n(1^1S) + r_2(p)n_e n(2^1S) + r_3(p)n_e n(2^3S), \quad (20)$$

where $r_0(p)$, $r_1(p)$, $r_2(p)$ and $r_3(p)$ are the population coefficients which are functions of n_e and T_e. The subscripts 0, 1, 2 and 3 stand for the ion, 1^1S, 2^1S and 2^3S respectively. The rate equations (1) for these independent levels are rewritten as

$$\frac{d}{dt}n(1^1S) = k_{01}n_i n_e - k_1 n(1^1S)n_e + k_{21}n(2^1S)n_e + k_{31}n(2^3S)n_e, \quad (21)$$

$$\frac{d}{dt}n(2^1S) = k_{02}n_i n_e + k_{12}n(1^1S)n_e - k_2 n(2^1S)n_e + k_{32}n(2^3S)n_e, \quad (22)$$

$$\frac{d}{dt}n(2^3S) = k_{03}n_i n_e + k_{13}n(1^1S)n_e + k_{23}n(2^1S)n_e - k_3 n(2^3S)n_e, \quad (23)$$

where k's are the collisional-radiative coupling coefficients. They are given in terms of the population coefficients as functions of n_e and T_e as follows:

$$k_{01} = \sum_{q>3}\{C(q,1)n_e + A(q,1)\}\, r_0(q) + \alpha(1)n_e + \beta(1), \quad (24)$$

$$k_1 = \sum_{q\neq 1} C(1,q) - \sum_{q>3}[C(q,1) + A(q,1)/n_e]\, r_1(q)n_e + S(1), \quad (25)$$

$$k_{21} = \sum_{q>3} \{C(q,1) + A(q,1)/n_e\}\, r_2(q) n_e + C(2,1) + A(2,1)/n_e, \quad (26)$$

$$k_{31} = \sum_{q>3} \{C(q,1) + A(q,1)/n_e\}\, r_3(q) n_e + C(3,1) + A(3,1)/n_e, \quad (27)$$

$$k_{02} = \sum_{q>3} \{C(q,2) n_e + A(q,2)\}\, r_0(q) + \alpha(2) n_e + \beta(2), \quad (28)$$

$$k_{12} = \sum_{q>3} \{C(q,2) + A(q,2)/n_e\}\, r_1(q) n_e + C(1,2), \quad (29)$$

$$k_2 = \sum_{q\neq 2} C(2,q) - \sum_{q>3} \{C(q,2) + A(q,2)/n_e\}\, r_2(q) n_e \quad (30)$$

$$+S(2) + A(2,1)/n_e, \quad (31)$$

$$k_{32} = \sum_{q>3} \{C(q,2) + A(q,2)/n_e\}\, r_3(q) n_e + C(3,2) + A(3,2)/n_e, \quad (32)$$

$$k_{03} = \sum_{q>3} \{C(q,3) n_e + A(q,3)\}\, r_0(q) + \alpha(3) n_e + \beta(3), \quad (33)$$

$$k_{13} = \sum_{q>3} \{C(q,3) + A(q,3)/n_e\}\, r_1(q) n_e + C(1,3), \quad (34)$$

$$k_{23} = \sum_{q>3} \{C(q,3) + A(q,3)/n_e\}\, r_2(q) n_e + C(2,3), \quad (35)$$

$$k_3 = \sum_{q\neq 3} C(3,q) - \sum_{q>3} \{C(q,3) + A(q,3)/n_e\}\, r_3(q) n_e \quad (36)$$

$$+S(3) + \{A(3,2) + A(3,1)\}/n_e. \quad (37)$$

Here $q > 3$ means that level q stands for all the levels except for the ground state, singlet and triplet metastable levels.

C. FORMULATION II

When the plasma condition is such that the quasi-steady-state approximation is valid also for the population of the metastable levels, their time derivative may be set equal to 0. The population of all the levels except for the ground state and the ions is expressed as the sum of two terms as in the case of hydrogen and hydrogen like ions,

$$n(p) = R_0(p) n_e n_i + R_1(p) n_e n(1^1S), \quad (38)$$

where $R_0(p)$ and $R_1(p)$ are called the reduced population coefficients, which are again functions of n_e and T_e. Equation (21) is rewritten as

$$\frac{d}{dt} n(1^1S) = -S n(1^1S) n_e + \alpha n_i n_e, \quad (39)$$

where S and α are the collisional-radiative ionization and recombination rate coefficients, respectively, which are also functions of n_e and T_e. The coefficients in this

formulation are given in terms of the coefficients k's and r's in formulation I:

$$R_0(2^1S) = \frac{(k_{02}k_3 + k_{03}k_{32})}{(k_2k_3 - k_{23}k_{32})n_e}, \tag{40}$$

$$R_1(2^1S) = \frac{(k_{12}k_3 + k_{13}k_{32})}{(k_2k_3 - k_{23}k_{32})n_e}, \tag{41}$$

$$R_0(2^3S) = \frac{(k_{03}k_2 + k_{02}k_{23})}{(k_3k_2 - k_{32}k_{23})n_e}, \tag{42}$$

$$R_1(2^1S) = \frac{(k_{13}k_2 + k_{12}k_{22})}{(k_3k_2 - k_{33}k_{23})n_e}, \tag{43}$$

and

$$R_0(p) = r_0(p) + r_2(p)R_0(2^1S)n_e + r_3(p)R_0(2^3S)n_e, \tag{44}$$

$$R_1(p) = r_1(p) + r_2(p)R_1(2^1S)n_e + r_3(p)R_1(2^3S)n_e, \tag{45}$$

for excited levels p other than the metastable levels. The collisional-radiative ionization rate coefficient is then given as

$$S = k_1 - k_{21}R_1(2^1S)n_e - k_{31}R_1(2^3S)n_e, \tag{46}$$

and the recombination rate coefficient α is given as

$$\alpha = k_{01} + k_{21}R_0(2^1S)n_e + k_{31}R_0(2^3S)n_e. \tag{47}$$

III. EXCITATION CROSS SECTION

A. EXCITATION FROM THE GROUND STATE

Since the publication of the original CR model [1] several experimental and theoretical cross section data have been reported for excitation by electron impacts. For excitation from the ground state the group led by de Heer assessed the existing data and published their recommended cross sections [4]. Kato and Janev parametrized these cross sections [11]. Examples of their analytical fit are given in Figs. 5–7 together with the cross section adopted in the original CR model [1]. The excitation cross section σ_{pq} from p (1^1S in this case) to q is first expressed in terms of the collision strength $\Omega_{pq}(U)$,

$$\sigma_{pq} = \frac{\Omega_{pq}(U)}{g(p)E}\pi {a_0}^2, \tag{48}$$

where E is the energy of the incident electron in the Rydberg units, $g(p)$ is the statistical weight of the initial state ($g(1^1S) = 1$), and $U = E/\chi_{pq}$ is the collision

energy in the threshold units (χ_{pq} is the threshold energy) and a_0 is the first Bohr radius (5.29×10^{-11} m). The collision strength $\Omega_{pq}(U)$ is fitted with the following expressions.

1. $1^1S \rightarrow n^1P$

$$\Omega_{pq} = \left(a_1 + \frac{a_2}{U} + \frac{a_3}{U^2} + a_4 \ln U\right)\left(\frac{U-1}{U}\right)^{a_5}, \tag{49}$$

2. $1^1S \rightarrow n^1S, D, F; n^3P, D, F$

$$\Omega_{pq} = \left(a_1 + \frac{a_2}{U} + \frac{a_3}{U^2} + \frac{a_4}{U^3}\right)\left(\frac{U-1}{U}\right)^{a_5}, \tag{50}$$

3. $1^1S \rightarrow n^3S$

$$\Omega_{pq} = \left(\frac{a_1}{U} + \frac{a_2}{U^2} + \frac{a_3}{U^3} + \frac{a_4}{U^4}\right). \tag{51}$$

The parameter a_4 in Eq. (49) is fixed to its theoretical value,

$$a_4 = 4g(p)\frac{f_{pq}}{\chi_{pq}}. \tag{52}$$

The factor $[(U-1)/U]^{a_5}$ in Eqs. (49) and (50) is introduced for the purpose of adjusting the cross section values near the threshold (Figs 5 and 6). Since the $1^1S \rightarrow n^3S$ cross sections have finite values at the threshold (Fig. 7), the expression for these transitions does not have this factor. The parameters, a_1 to a_5, are reproduced from [11] in Table II.

For the optically forbidden transitions $1^1S \rightarrow 3^1D$ and $1^1S \rightarrow 2^3S$, discrepancies between de Heer's and the original data amount to a factor 2 in the high energy regions. The original semi-empirical formula had only three parameters, and emphasis was put on the low energy regions in the fitting procedure. This may explain the difference. For the transition $1^1S \rightarrow 2^3S$, recent cross section data tend to be larger in the high energy region, and the new assessment leads to the larger values.

The excitation rate coefficient

$$C(p,q) = \int_{v_{\rm th}}^{\infty} \sigma_{pq}(v) v f(v) dv \tag{53}$$

is given for electrons with velocity distribution, $f(v)$. Here $v_{\rm th}$ is the velocity corresponding to the threshold energy, and we assume $f(v)$ to be a Maxwellian. It is sometimes convenient to calculate the de-excitation rate coefficient $C(q,p)$ first. Examples are shown in Figs. 8. The excitation rate coefficient $C(p,q)$ is given by

$$C(p,q) = \frac{g(q)}{g(p)} C(q,p) e^{-u}, \tag{54}$$

where $u \equiv \chi_{pq}/kT_e$ (k is the Boltzmann constant). The numerically calculated de-excitation rate coefficient is fitted with a polynomial using natural logarithm,

$$\ln C(T_e) = \sum_{i=0}^{8} b_i (\ln T_e)^i. \tag{55}$$

Fitting has been done for the electron temperature range from 0.1 eV to 10 keV and the error is smaller than the line width in Fig. 8. The parameters, b_0 to b_8 are tabulated in Tables III-IV.

B. EXCITATION FROM THE METASTABLE LEVELS

For transitions from the metastable levels several experimental [12, 13] and theoretical [14–26] data have been reported, too. Examples are shown in Figs. 9–14 together with the recent assessment [5]. For the transitions between the singlet levels, agreement within a factor 2 is seen among the data except for the old calculation [14]. For the transitions between the triplet levels $2^3S \rightarrow 2, 3^3P$ and 3^3D, severe disagreement exists in the lower energy regions than 10–30 eV. It is sometimes by more than one order of magnitude. The recent calculation by the first order many body theory and the experiments tend to give larger values. The recommended cross sections [5] appear to be close to the lower end among the data. This point is discussed in Sec. V. The collision strength $\Omega_{pq}(U)$ is fitted to the recommended cross section by the expressions

1. $2^1S(2^3S) \rightarrow n^1P(n^3P)$

$$\Omega_{pq} = \left(a_1 + \frac{a_2}{U} + \frac{a_3}{U^2} + a_4 \ln U\right) \left(\frac{U - a_5}{U}\right)^{a_6}, \tag{56}$$

2. $2^1S(2^3S) \rightarrow n^1S, D(n^3S, D)$

$$\Omega_{pq} = \left(a_1 + \frac{a_2}{U} + \frac{a_3}{U^2} + \frac{a_4}{U^3}\right) \left(\frac{U - a_5}{U}\right)^{a_6}, \tag{57}$$

3. $2^1S(2^3S) \rightarrow n^3S, P, D(n^1S, P, D)$

$$\Omega_{pq} = \left(\frac{a_1}{U^2} + \frac{a_2}{U^3} + \frac{a_3}{U^4} + \frac{a_4}{U^5}\right) \left(\frac{U - a_5}{U}\right)^{a_6}. \tag{58}$$

Since several cross sections have finite values at the threshold energy, the parameter $a_5 (\leq 1)$ and a_6 are introduced. The parameter a_4 in Eq. (56) is fixed as given by Eq. (52). Examples of the fitting are shown in Figs. 15–20, where the cross section in

the original version is also compared. The first group is the optically allowed transitions (Figs. 15, 17 and 18), the second is the optically forbidden transitions without a spin change (Figs. 16 and 19) and the last is the transitions with a spin change (Fig. 20). These parameter values thus determined are tabulated in Tables V–VI.

The de-excitation rate coefficient is calculated and fitted by using Eq. (55). The parameters and examples are shown in Tables VII–X and Fig. 21, respectively.

C. *L*-CHANGING COLLISIONS

For transitions between the levels having the same principal quantum number, only a few experimental papers [27–29] are found and they give rate coefficients instead of cross sections. These rate coefficients are compared with three theoretical or semi-empirical formulas in Figs. 22-25. Here, the original rate coefficient in [27] has been multiplied by 10 on the assumptoin that the electron density was underestimated by the same factor in the original paper. Johnson's formula [30], which was employed in the original version, is based on the Born approximation and adjusted with several parameters to give a best fit to the existing data. Shevelko's formula [31] is also based on the Born approximation with the validity range of $kT_e \gg \chi_{pq}$. Dickinson [32] proposes formulas which are different for lower and higher energy collisions with the boundary energy corresponding to the speed of the target electron of nl. They are called the non-sudden and the sudden approximations, respectively. For the data in the figures only the sudden approximation is considered.

From the comparison with experiment we adopt the semi-empirical formula by Johnson [30]. The excitation cross section is expressed as

$$\sigma_{pq}(U) = \frac{4}{3}\frac{RS_{pq}}{\chi_{pq}g(p)}\pi {a_0}^2 \frac{1}{U}\left[1 - \exp\left\{-\beta\left(\frac{S_{pq}}{3g(p)}\right)^{-\gamma}(U+1)\right\}\right]\ln(U+\delta), \quad (59)$$

where $g(p)$ and R are the statistical weight of level p and the Rydberg constant (13.6 eV), respectively. The parameters β, γ and δ are given as 0.5, 0.7 and 0.2, respectively. The value S_{pq} is defined with the Bates-Damgaard notation [33]

$$S_{pq} = (2S+1)\left(\frac{3n_l^*}{2}\right)^2 \left|{n_l^*}^2 - l^2\right| l\,\varphi^2\left(n_{l-1}^*, n_l^*, l\right), \quad (60)$$

where

$$l = \mathrm{Max}(l_p, l_q). \quad (61)$$

The $\varphi(n_{l-1}^*, n_l^*, l)$ values are adopted from Oertel and Shomo [34] by interpolation.

Now the de-excitation rate coefficient is given as

$$C(q,p) = K\frac{g(p)}{g(q)}\left[\frac{1}{u}C_1(u) - \frac{\exp\left[-2\beta\left(\frac{S_{pq}}{3g(p)}\right)^{-\gamma}\right]}{\beta\left(\frac{S_{pq}}{3g(p)}\right)^{-\gamma}+u}C_2(u)\right], \tag{62}$$

with

$$C_1(u) = \ln(1+\delta) + \exp\left[(1+\delta)u\right]\left[-E_i\left\{-(1+\delta)u\right\}\right], \tag{63}$$

$$C_2(u) = \ln(1+\delta) + \exp\left[(1+\delta)\left(\beta\left(\frac{S_{pq}}{3g(p)}\right)^{-\gamma}+u\right)\right] \times\left[-E_i\left\{-(1+\delta)\left(\beta\left(\frac{S_{pq}}{3g(p)}\right)^{-\gamma}+u\right)\right\}\right], \tag{64}$$

where

$$K = 4\left(\frac{R}{kT_e}\right)^2 f_{pq}\sqrt{\pi}a_0^2\frac{2\sqrt{2}}{\sqrt{m_e}}\sqrt{kT_e}$$

$$= 2.19\times10^{-16}\left(\frac{R}{kT_e}\right)^2\sqrt{T_e}f_{pq} \qquad \mathrm{m^3s^{-1}}, \tag{65}$$

T_e is in the units of degree K. The exponential integral is defined as

$$E_i(-t) = -\int_t^\infty \frac{e^{-x}}{x}dx. \tag{66}$$

In this revision of the original CR model code many of the cross section data are replaced. For other transitions which are not shown in the tables, original data are used.

IV. Results

We incorporate the rate coefficients in Sec. III. into the CR model in Sec. II., and calculate various coefficients. Several examples of the results of calculation are shown: Fig. 26 shows the collisional-radiative coupling coefficients k in formulation I and the collisional-radiative ionization and recombination rate coefficients, S and α, of formulation II. For the sake of comparison, results of the original code [1] are also given with the dotted lines. Difference between the two calculations is small except for k_{23}, k_{31} and k_{32}. The latter differences stem from the large difference of the electron impact excitation cross section for the $2^3S \rightarrow 2^1S$ transition (Fig. 20)

adopted in the two calculations. Figures 27 and 28 show the T_e dependences of S and α, respectively.

Figures 29–32 show the n_e-dependence of the populations of several excited levels calculated in formulation II. The ionizing plasma component $R_1(p)n_e n(1^1S)$ is shown in Figs. 29 and 30, where the electron temperature is 30 eV and the population of the ground state is assumed to be 1 m^{-3}. Figures 31 and 32 show the recombining plasma component $R_0(p)n_e n_i$ devided by $n_e n_i$, where the electron temperature is 0.2 eV.

The radiative loss rate W_r (eV/$m^3 s$) and the electron cooling rate W_e (eV/$m^3 s$) are calculated with

$$W_r = \sum_i \left[n(i) \left\{ \sum_{j<i} A(i,j)\chi_{ji} \right\} + n_i n_e \beta_d(i) \chi_{(1s)i\,(2p)i} + n_i n_e \int_0^\infty \left(\frac{m_e v^2}{2} + \chi_i \right) \sigma_{\beta,i}(v) v f(v) dv \right], \quad (67)$$

and

$$W_e = \sum_i \left[n(i) \left\{ \sum_j C(i,j)\chi_{ji} + S(i)\chi_i \right\} n_e + n_i n_e \beta_d(i) \left\{ \chi_{(1s)i\,(2p)i} - \chi_i \right\} - n_i {n_e}^2 \alpha(i)\chi_i + n_i n_e \int_0^\infty \frac{m_e v^2}{2} \sigma_{\beta,i}(v) v f(v) dv \right], \quad (68)$$

respectively. Here χ_i is the ionization potential of level i, $\chi_{(1s)i\,(2p)i}$ is the transition energy between the doubly excited level $(2p, i)$ and the singly excited level $(1s, i)$, and $\sigma_{\beta,i}(v)$ is the cross sections of radiative recombination to level i. For the di-electronic recombination only the stabilizing transition $2p \rightarrow 1s$ is included, and as the radiation energy of such a transition the value of the hydrogenlike ion is used. Equations (67) and (68) are divided into two terms, each of which are proportional to n_i and $n(1)$, respectively, as

$$W_r = P_{r,0} n_e n_i + P_{r,1} n_e n(1), \quad (69)$$

$$W_e = P_{e,0} n_e n_i + P_{e,1} n_e n(1). \quad (70)$$

By using the relation

$$n(i) = R_0(i) n_e n_i + R_1(i) n_e n(1),$$

the coefficients in the above equations are expressed as

$$P_{\mathrm{r},0} = \sum_i \left[R_0(i) \left\{ \sum_{j<i} A(i,j)\chi_{ji} \right\} + \beta_{\mathrm{d}}(i)\chi_{(1s)i\,(2p)i} + \int_0^\infty \left(\frac{m_{\mathrm{e}}v^2}{2} + \chi_i \right) \sigma_{\beta,i}(v) v f(v) \mathrm{d}v \right], \tag{71}$$

$$P_{\mathrm{r},1} = \sum_i \left[R_1(i) \left\{ \sum_{j<i} A(i,j)\chi_{ji} \right\} \right], \tag{72}$$

$$P_{\mathrm{e},0} = \sum_i \left[R_0(i) \left\{ \sum_j C(i,j)\chi_{ji} + S(i)\chi_i \right\} n_{\mathrm{e}} + \beta_{\mathrm{d}}(i) \left\{ \chi_{(1s)i\,(2p)i} - \chi_i \right\} - n_{\mathrm{e}}\alpha(i)\chi_i + \int_0^\infty \frac{m_{\mathrm{e}}v^2}{2} \sigma_{\beta,i}(v) v f(v) \mathrm{d}v \right], \tag{73}$$

$$P_{\mathrm{e},1} = \sum_i \left[R_1(i) \left\{ \sum_j C(i,j)\chi_{ji} + S(i)\chi_i \right\} n_{\mathrm{e}} \right]. \tag{74}$$

Figures 33–36 show the electron temperature and density dependences of these coefficients calculated in formulation II.

Another example is the line intensity ratios which may be useful for plasma diagnostics [35]. In this calculation l-changing transitions by proton impacts are also considered. We assume that proton impacts have the same cross section value as that for the electron impacts at the same velocity. The proton impact cross section σ'_{pq} can be expressed as

$$\sigma'_{pq}(U) = \sigma_{pq}\left(\frac{m_{\mathrm{e}}}{m_{\mathrm{p}}} U \right), \tag{75}$$

where σ_{pq} is the electron impact cross section and m_{e}, m_{p} are the electron and proton masses, respectively. Under these assumptions the de-excitation rate coefficient is given by replacing u in the Eq. (62) with $(m_{\mathrm{p}}/m_{\mathrm{e}})u$ and multiplying the resulting equation by a factor $(m_{\mathrm{p}}/m_{\mathrm{e}})^{3/2}$. Before carring out this procedure, the original electron impacts data are modified to have a vanishing value at the threshold energy. As shown in Figs. 37–39, proton impacts play an important role in the high temperature regions. Figure 40 shows the ratio of the two line intensities $(n(p)A(p,q)\chi_{qp})$ corresponding to the $2^1P \leftarrow 3^1D$ and $2^1P \leftarrow 3^1S$ transitions calculated in formulation II under the assumption of the ionizing plasma. This ratio strongly depends on the electron density, and may be useful for its determination. Figure 41 shows

the result of $2^1P \leftarrow 3^1S$ and $2^3P \leftarrow 3^3S$ lines. It shows a strong dependence on the electron temperature, and can be used for its measurement. These results have been calculated with the assumption of no magnetic field. When a magnetic field is present, the line intensity may be affected, especially near the level anticrossing point. Figure 42 shows an example: at around the field strength of 7.3 T the line intensity of the $2^1P \leftarrow 3^1D$ transition strongly depends on the field strength. In the calculation the electron density and temperature are assumed to be 1.0×10^{19} m^{-3} and 100 eV, respectively.

V. Discussion

In our code (the effects of) the singlet-triplet wavefunction mixing is mimicked by the mixing of the transition rates, Eqs. (15)–(19). This approximation has yet to be verified. Figure 43 shows the dependence of the emission line intensities ($2^{1,3}P \leftarrow 4^{1,3}D$) from a discharge plasma on the magnetic field strength [36]. Since the electron density and temperature are not known, they are assumed to be 1.0×10^{18} m^{-3} and 30.0 eV, respectively. We compare our result with the experiment in Fig. 43. The decrease in the singlet line intensity and the corresponding increase in the triplet intensity near the level-anticrossing at 4.2 T is due to the larger excitation cross section to the singlet level 4^1D than that to the triplet level. We did a similar comparison for the $2^{1,3}P \leftarrow 3^{1,3}D$ lines near 7.2 T [36]. See also Fig. 42. In both the cases, the agreement of the emission line intensities is satisfactory, which indicates the validity of our approximation procedure. The above procedure is based on the assumption that the radiative transition and the cross section data which have been used are those for the *pure* singlet or triplet states. Obviously, this is not the case for experimental data. In the absence of the magnetic field, however, this inconsistency leads to an error less than 0.1 % in the experimental case, since the cross sections concerned are levels S, P and D, and for these levels the mixing is less than 0.1 %. For cross sections concerning levels F, for example $3^1D \rightarrow 4^1F$ and $\rightarrow 4^3F$, the available theoretical data differs by more than an order of magnitude. The true cross sections to the real levels should not differ by more than a factor of 2 for this example. This is because ω^2 for $4^{1,3}F$ levels is 0.36. Thus, we understood that the calculated cross sections are for *pure* states. Our procedure is justified also in this respect.

For the purpose of another comparison we take an experiment on an afterglow plasma [37] as shown in Fig. 44a. In the present plasma, which is a typical example of a recombining plasma, the higher lying levels are in local thermodynamic equilibrium with ions and continuum electrons (See Figs. 31 and 32). The electron density and temperature are determined from these populations to be 5.5×10^{19} m^{-3} and 0.20 eV, respectively. The populations of the lower-lying levels are controlled by individual transitions, so that they are sensitive to the magnitude of the rate coefficients. The result of calculation is shown with the open symbols. The radiation trapping of the resonance-series lines $1^1S \leftarrow n^1P$ is considered for this calculation. The $n = 3$ singlet populations are very sensitive to this effect, and the 1^1S population of 3×10^{19} m^{-3} is adopted so that they show the best agreement with the experimental data. For the $n = 3$ triplet populations the agreement is satisfactory. They are unaffected by radiation trapping for transitions terminating on the 2^3S level, since this population is rather low (4.5×10^{17} m^{-3}).

For the electron impact excitation cross sections from metastable levels we have adopted the recommended cross section by de Heer. However, as has been shown in Figs. 9–14 several theoretical and experimental data are much larger than the recommended values. The disagreements in the $2^3S \rightarrow 3^3P$ (Figs. 12, 18) and $2^3S \rightarrow 3^3D$ (Figs. 13, 19) cross sections are particularly disturbing since these upper levels are important for plasma diagnostics. Figures 45 and 46 show the de-excitation rate coefficients for these two transitions. In Fig. 12 or 13, if we connect the largest cross section values and extrapolate them down to the threshold energy, this "cross section" may be regarded as the upper bound of the true cross section. The de-excitation rate coefficient corresponding to this upper bound is also shown in Figs. 45 and 46. Substantial difference is seen in the region of the electron temperatures lower than 20–30 eV.

We replace in our CR model code the rate coefficients for transitions $2^3S \leftrightarrow 3^3P$ and $2^3S \leftrightarrow 3^3D$ with those of the upper bound. This results in an increase in the deexcitation rate by electron impacts. The calculated population distribution is given in Fig. 44b. It is seen that the singlet populations are unaffected. The $n = 3$ triplet populations are reduced substantially, and now they are underpopulated by about 30 %. These results lead to a tentative conclusion that the recommendation by de Heer gives values closer to the true cross sections.

References

[1] T. Fujimoto, J. Quant. Spectrosc. Radiat. Transfer **21**, 439(1979).

[2] T. Fujimoto, IPPJ-AM-8, Institute of Plasma Physics, Japan(1978).

[3] D. Reiter, W. Eckstein, G. Giesen and H. J. Belitz, Berichte des Forschungszentrum Jülich (KFA), Institut für Plasmaphysik, EURATOM-KFA Association, Jül-2605, April 1992.

[4] F. J. de Heer, R. Hoekstra, A. E. Kingston and H. P. Summers, Nucl. Fus. Special Supplement **3**, 19(1992).

[5] F. J. de Heer, H. O. Folkerts, F. W. Bliek, R. Hoekstra, T. Kato, A. E. Kingston, K. A. Berrington and H. P. Summers, Atomic and Plasma-Material Interaction Data for Fusion (Suppl. Journ. Nuclear Fusion), Vol. 6, IAEA, Vienna(1995).

[6] G. W. F. Drake and Zong-Chao Yan, Phys. Rev. A **46**, 2378(1992).

[7] C. E. Moore, Atomic Energy Levels, Vol. I, p. 4. U. S. Department of Commerce, Washington(1949).

[8] T. Fujimoto, A. Hirabayashi, S. Okuda, K. Shimizu and H. Takuma, J. Phys. B **19**, 571(1986).

[9] G. P. Anisimova and R. I. Semenov, Opt. Spectrosk. **54**, 41(1983)[Opt. Spectrosc. (USSR) **54**, 23(1983)]

[10] K. Sawada and T. Fujimoto, Phys. Rev. E **49**, 5565(1994).

[11] T. Kato and R. K. Janev, Nucl. Fus. Special Supplement **3**, 33(1992).

[12] V. A. Gostev, D. V. Elakhovskii, Yu. V. Zaitsev, L. A. Luizova and A. D. Khakhaev, Opt. Spectrosk. **48**, 457(1980)[Opt. Spectrosc. (USSR) **48**, 251(1980)].

[13] D. L. A. Rall, F. A. Sharpton, M. B. Schulman, L. W. Anderson, J. E. Lawler and C. C. Lin, Phys. Rev. Lett. **62**, 2253(1989).

[14] M. R. Flannery, W. F. Morrison and B. L. Richmond, J. Appl. Phys. **46**, 1186(1975).

[15] W. C. Fon, K. A. Berrington, P. G. Burke and A. E. Kingston, J. Phys. B **14**, 2921(1981).

[16] S. L. Willis, J. Hata, M. R. C. McDowell, C. J. Joachain and F. W. Byron Jr., J. Phys. B **14**, 2687(1981).

[17] E. A. Andreev and A. E. Bodrov, Chem. Phys. Lett. **109**, 450(1984).

[18] N. R. Badnell, J. Phys. B **17**, 4013(1984).

[19] K. A. Berrington, P. G. Burke, L. C. G. Freitas and A. E. Kingston, J. Phys. B **18**, 4135(1985).

[20] I. Khurana, R. Srivastava and A. N. Tripathi, J. Phys. B **20**, 3515(1987).

[21] K. C. Mathur, R. P. McEachran, L. A. Parcell and A. D. Stauffer, J. Phys. B **20**, 1599(1987).

[22] A. K. Katiyar and R. Srivastava, Phys. Rev. A **38**, 2767(1988).

[23] D. C. Cartwright and G. Csanak, Phys. Rev. A **51**, 454(1994).

[24] I. Bray and D. V. Fursa, J. Phys. B **28**, L197(1995).

[25] V. P. Shevelko and H. Tawara, NIFS-DATA-28, National Institute for Fusion Science, Japan(1995).

[26] E. T. Hudson, K. Bartschart, M. P. Scott, P. G. Burke and V. M. Burke, J. Phys. B **29**, 5513(1996).

[27] H. F. Wellenstein and W. W. Robertson, J. Chem. Phys. **56**, 1072(1972).

[28] C. F. Burrel and H. J. Kunze, Phys. Rev. A **18**, 2081(1978).

[29] N. Yasumaru, S. Oku, T. Fujimoto and K. Fukuda, J. Phys. Soc. Japan **49**, 696(1980).

[30] L. C. Johnson and E. Hinnov, Phys. Rev. **187**, 143(1969).

[31] V. P. Shevelko, A. M. Urnov and A. V. Vinogradov, J. Phys. B **9**, 2859(1976).

[32] A. S. Dickinson, Astron. Astrophys. **100**, 302(1981).

[33] D. R. Bates and A. Damgaard, Philos. Trans. Roy. Soc. London B **242**, 101(1949).

[34] G. K. Oertel and L. P. Shomo, Astrophys. J. (suppl.) **16**, 175(1968).

[35] B. Schweer, G. Mank, A. Pospieszczyk, B. Brosda and B. Pohlmeyer, J. Nucl. Mater. **196–198**, 174(1992).

[36] J. Derouard, R. Jost, M. Lombardi, T. A. Miller and R. S. Freund, Phys. Rev. A **14**, 1025(1976).

[37] H. Akatsuka and M. Suzuki, Plasma Sources Sci. Technol. **4**, 125(1995).

Table I. Coefficients of the singlet-triplet wave function mixing. Quoted from [6].

n	L	ω	n	L	ω	n	L	ω
2	1	−0.00027829						
3	1	−0.00025575	3	2	−0.01560954			
4	1	−0.00024976	4	2	−0.01139599	4	3	−0.60410243
5	1	−0.00024726	5	2	−0.01011432	5	3	−0.54992910
6	1	−0.00024597	6	2	−0.00952892	6	3	−0.51807366
7	1	−0.00024522	7	2	−0.00920674	7	3	−0.49841839
8	1	−0.00024474	8	2	−0.00900873	8	3	−0.48557680
9	1	−0.00024442	9	2	−0.00887770	9	3	−0.47676199
10	1	−0.00024419	10	2	−0.00878623	10	3	−0.47045947
5	4	−0.69347523						
6	4	−0.69319963	6	5	−0.69623846			
7	4	−0.69298889	7	5	−0.69623773	7	6	−0.69793150
8	4	−0.69283559	8	5	−0.69623716	8	6	−0.69793146
9	4	−0.69271952	9	5	−0.69623740	9	6	−0.69793155
10	4	−0.69263290	10	5	−0.69623528	10	6	−0.69793161
8	7	−0.69916705						
9	7	−0.69916705	9	8	−0.70010887			
10	7	−0.69916705	10	8	−0.70010887	10	9	−0.70085072

Table II. Fitting parameters of excitation cross sections from 1^1S. Quoted from [11].

transition	a_1	a_2	a_3
1^1S-2^1S	1.8732(−01)[a]	−2.8806(−01)	1.3589(−01)
1^1S-3^1S	4.0898(−02)	−1.3324(−01)	2.2846(−01)
1^1S-4^1S	1.5387(−02)	−4.6305(−02)	7.4398(−02)
1^1S-5^1S	7.7808(−03)	−2.6702(−02)	4.9135(−02)
1^1S-6^1S	4.2253(−03)	−1.5233(−02)	2.8548(−02)
1^1S-2^1P	1.2306(−04)	−4.9534(−01)	6.1713(−01)
1^1S-3^1P	2.3265(−02)	−1.5645(−01)	1.8723(−01)
1^1S-4^1P	4.5198(−02)	−1.1197(−01)	8.6180(−02)
1^1S-3^1D	9.4306(−03)	2.6771(−02)	−6.8326(−02)
1^1S-4^1D	5.0543(−03)	1.7876(−02)	−4.3079(−02)
1^1S-5^1D	2.8630(−03)	6.4713(−03)	−1.5538(−02)
1^1S-6^1D	1.7551(−03)	1.9242(−03)	−4.4939(−03)
1^1S-2^3S	1.6077(−03)	5.3368(−01)	0.0000(+00)
1^1S-3^3S	1.4346(−04)	1.1585(−01)	−1.6744(−01)
1^1S-4^3S	3.7705(−05)	4.6867(−02)	−5.9202(−02)
1^1S-2^3P	6.0203(−06)	−2.0588(−03)	6.7094(−01)
1^1S-3^3P	1.1608(−06)	−3.2505(−04)	1.4814(−01)
1^1S-3^3D	9.2318(−10)	−4.2120(−06)	1.9195(−02)
1^1S-4^3D	1.0935(−07)	2.1660(−05)	1.0716(−02)

transition	a_4	a_5
1^1S-2^1S	1.7397(−01)	5.4268(−01)
1^1S-3^1S	−1.1951(−01)	3.3456(−01)
1^1S-4^1S	−3.9669(−02)	1.7198(−01)
1^1S-5^1S	−2.7484(−02)	4.1853(−01)
1^1S-6^1S	−1.6014(−02)	4.4802(−01)
1^1S-2^1P	7.0850(−01)	6.0006(−01)
1^1S-3^1P	1.7360(−01)	7.9383(−01)
1^1S-4^1P	6.9230(−02)	7.7622(−01)
1^1S-3^1D	3.6579(−02)	3.6564(−02)
1^1S-4^1D	2.4534(−02)	2.1977(−01)
1^1S-5^1D	7.5518(−03)	3.4587(−02)
1^1S-6^1D	1.4452(−03)	1.7771(−03)
1^1S-2^3S	6.1023(−01)	
1^1S-3^3S	6.6875(−02)	
1^1S-4^3S	1.7539(−02)	
1^1S-2^3P	−5.7470(−01)	4.6491(−01)
1^1S-3^3P	−1.3766(−01)	1.3179(−01)
1^1S-3^3D	−1.2276(−02)	3.0710(−01)
1^1S-4^3D	−3.9355(−03)	5.4484(−01)

[a] $p(q)$ means $p \times 10^q$.

Table III. Fitting parameters of de-excitation rate coefficients for $1^1S - n^1L$.

transition	b_0	b_1	b_2
$1^1S - 2^1S$	$-1.984916(+01)^a$	$-1.303465(-01)$	$-6.627066(-02)$
$1^1S - 3^1S$	$-2.153638(+01)$	$-1.238957(-01)$	$-2.217281(-02)$
$1^1S - 4^1S$	$-2.238702(+01)$	$-2.239600(-01)$	$1.133684(-03)$
$1^1S - 5^1S$	$-2.356223(+01)$	$1.027186(-02)$	$-1.669309(-02)$
$1^1S - 6^1S$	$-2.424079(+01)$	$4.062789(-02)$	$-2.011313(-02)$
$1^1S - 2^1P$	$-2.150398(+01)$	$1.330463(-01)$	$7.495941(-02)$
$1^1S - 3^1P$	$-2.300797(+01)$	$2.319997(-01)$	$2.698392(-02)$
$1^1S - 4^1P$	$-2.391053(+01)$	$3.108091(-01)$	$5.426116(-02)$
$1^1S - 3^1D$	$-2.347836(+01)$	$-4.282777(-01)$	$4.885311(-02)$
$1^1S - 4^1D$	$-2.421538(+01)$	$-3.166936(-01)$	$1.722734(-02)$
$1^1S - 5^1D$	$-2.462440(+01)$	$-4.003402(-01)$	$4.541288(-02)$
$1^1S - 6^1D$	$-2.517510(+01)$	$-3.666263(-01)$	$5.107732(-02)$

transition	b_3	b_4	b_5
$1^1S - 2^1S$	$2.252300(-03)$	$5.173040(-03)$	$-5.529607(-04)$
$1^1S - 3^1S$	$-2.068328(-02)$	$4.028275(-03)$	$1.697833(-03)$
$1^1S - 4^1S$	$-1.577502(-02)$	$2.750694(-03)$	$1.326404(-03)$
$1^1S - 5^1S$	$-2.796032(-02)$	$3.444244(-03)$	$2.257574(-03)$
$1^1S - 6^1S$	$-3.116243(-02)$	$3.790588(-03)$	$2.533678(-03)$
$1^1S - 2^1P$	$2.926147(-02)$	$-7.618363(-03)$	$-2.047379(-03)$
$1^1S - 3^1P$	$2.990058(-02)$	$-4.218964(-03)$	$-2.518005(-03)$
$1^1S - 4^1P$	$1.948737(-02)$	$-6.123304(-03)$	$-1.494422(-03)$
$1^1S - 3^1D$	$2.032843(-02)$	$-4.922154(-03)$	$-1.551338(-03)$
$1^1S - 4^1D$	$1.882597(-02)$	$-3.015048(-03)$	$-1.651427(-03)$
$1^1S - 5^1D$	$1.322500(-02)$	$-4.193208(-03)$	$-1.012932(-03)$
$1^1S - 6^1D$	$3.938573(-03)$	$-3.927187(-03)$	$-2.620147(-04)$

transition	b_6	b_7	b_8
$1^1S - 2^1S$	$-1.375703(-04)$	$2.593347(-05)$	$-1.161637(-06)$
$1^1S - 3^1S$	$-5.822274(-04)$	$6.074336(-05)$	$-2.145306(-06)$
$1^1S - 4^1S$	$-4.524860(-04)$	$4.767726(-05)$	$-1.699981(-06)$
$1^1S - 5^1S$	$-6.643838(-04)$	$6.527043(-05)$	$-2.219568(-06)$
$1^1S - 6^1S$	$-7.386579(-04)$	$7.214274(-05)$	$-2.441880(-06)$
$1^1S - 2^1P$	$7.259827(-04)$	$-7.337404(-05)$	$2.515892(-06)$
$1^1S - 3^1P$	$6.940663(-04)$	$-6.418789(-05)$	$2.077929(-06)$
$1^1S - 4^1P$	$5.552810(-04)$	$-5.657446(-05)$	$1.941658(-06)$
$1^1S - 3^1D$	$5.257894(-04)$	$-5.229616(-05)$	$1.767167(-06)$
$1^1S - 4^1D$	$4.729529(-04)$	$-4.418491(-05)$	$1.429251(-06)$
$1^1S - 5^1D$	$3.822996(-04)$	$-3.903685(-05)$	$1.335502(-06)$
$1^1S - 6^1D$	$2.156178(-04)$	$-2.514788(-05)$	$9.201934(-07)$

[a] $p(q)$ means $p \times 10^q$.

Table IV. Fitting parameters of de-excitation rate coefficients for $1^1S - n^3L$.

transition	b_0	b_1	b_2
$1^1S - 2^3S$	$-2.005136(+01)^a$	$-6.255068(-01)$	$-2.253667(-02)$
$1^1S - 3^3S$	$-2.160351(+01)$	$-4.917069(-01)$	$6.331211(-03)$
$1^1S - 4^3S$	$-2.260697(+01)$	$-4.327300(-01)$	$1.755672(-02)$
$1^1S - 2^3P$	$-2.229190(+01)$	$4.598996(-02)$	$-1.220724(-02)$
$1^1S - 3^3P$	$-2.325245(+01)$	$-1.378579(-01)$	$2.266333(-02)$
$1^1S - 3^3D$	$-2.425732(+01)$	$-2.975323(-01)$	$-4.608692(-02)$
$1^1S - 4^3D$	$-2.600235(+01)$	$-6.392955(-02)$	$-4.951564(-02)$

	b_3	b_4	b_5
$1^1S - 2^3S$	$9.860191(-03)$	$-1.361735(-03)$	$-1.173059(-03)$
$1^1S - 3^3S$	$-1.822835(-03)$	$-3.210948(-03)$	$-1.926423(-04)$
$1^1S - 4^3S$	$-6.253646(-03)$	$-3.826624(-03)$	$1.500895(-04)$
$1^1S - 2^3P$	$-2.332892(-02)$	$-2.818469(-03)$	$1.114157(-03)$
$1^1S - 3^3P$	$-2.380728(-02)$	$-3.604769(-03)$	$1.212955(-03)$
$1^1S - 3^3D$	$-1.276539(-02)$	$-7.915249(-04)$	$4.230522(-04)$
$1^1S - 4^3D$	$-1.490643(-02)$	$-1.192482(-03)$	$5.003489(-04)$

	b_6	b_7	b_8
$1^1S - 2^3S$	$3.061146(-04)$	$-2.715230(-05)$	$8.408049(-07)$
$1^1S - 3^3S$	$1.858219(-04)$	$-2.186202(-05)$	$7.981227(-07)$
$1^1S - 4^3S$	$1.423412(-04)$	$-1.976673(-05)$	$7.715483(-07)$
$1^1S - 2^3P$	$-7.016463(-05)$	$-2.389134(-06)$	$2.562882(-07)$
$1^1S - 3^3P$	$-6.991154(-05)$	$-3.110345(-06)$	$2.907516(-07)$
$1^1S - 3^3D$	$-1.453074(-05)$	$-2.754938(-06)$	$1.720104(-07)$
$1^1S - 4^3D$	$-9.083025(-06)$	$-4.227792(-06)$	$2.386132(-07)$

[a] $p(q)$ means $p \times 10^q$.

Table V. Fitting parameters of excitation cross sections from 2^1S.

transition	a_1	a_2	a_3
2^1S-3^1S	3.8637(+00)[a]	8.3634(+00)	−2.7395(+01)
2^1S-4^1S	1.2325(+00)	2.6351(+00)	−8.6806(+00)
2^1S-2^1P	5.6412(+01)	−1.7252(+02)	3.0455(+02)
2^1S-3^1P	−3.3889(+00)	5.4638(+00)	4.3526(+00)
2^1S-4^1P	−5.5502(−01)	4.8965(−01)	3.7628(+00)
2^1S-3^1D	1.0352(+01)	5.3916(+01)	−7.5355(+01)
2^1S-4^1D	1.8936(+00)	5.0062(+00)	−1.6888(+01)
2^1S-4^1F	4.9058(−01)	2.5493(+00)	−3.5637(+00)
2^1S-2^3P	8.0686(+02)	−2.7011(+03)	6.2231(+02)
2^1S-3^3S	1.1548(+00)	1.2906(+00)	−2.8368(+00)
2^1S-4^3S	3.1166(−01)	9.7477(−01)	−1.7726(+00)
2^1S-3^3P	1.8690(+00)	3.4409(+00)	2.0998(+01)
2^1S-4^3P	6.2644(−01)	1.1023(+00)	5.5614(+00)
2^1S-3^3D	3.9992(+00)	1.6159(+01)	−3.8675(+01)
2^1S-4^3D	1.2182(+00)	6.9497(+00)	−1.4648(+01)
2^1S-4^3F	1.9545(−01)	8.7282(−01)	−1.8326(+00)

	a_4	a_5	a_6
2^1S-3^1S	2.2357(+01)	1.0000(+00)	1.3103(+00)
2^1S-4^1S	7.0629(+00)	1.0000(+00)	1.3009(+00)
2^1S-2^1P	3.4864(+01)	1.0000(+00)	2.4891(+00)
2^1S-3^1P	3.3679(+00)	7.8354(−01)	2.5824(+00)
2^1S-4^1P	8.6999(−01)	6.4493(−01)	4.4316(+00)
2^1S-3^1D	1.0162(+02)	1.0000(+00)	2.4794(+00)
2^1S-4^1D	1.1263(+01)	1.0000(+00)	6.7418(−01)
2^1S-4^1F	4.7950(+00)	1.0000(+00)	2.4756(+00)
2^1S-2^3P	1.1182(+04)	3.0950(−01)	2.9408(+01)
2^1S-3^3S	2.4943(+00)	4.6530(−01)	9.8036(−01)
2^1S-4^3S	1.6342(+00)	4.1481(−01)	2.4537(+00)
2^1S-3^3P	−6.6085(+00)	3.3424(−01)	8.5777(+00)
2^1S-4^3P	−2.1730(+00)	3.9002(−01)	6.6056(+00)
2^1S-3^3D	3.1806(+01)	1.0000(+00)	1.5482(+00)
2^1S-4^3D	9.1219(+00)	1.0000(+00)	1.4076(+00)
2^1S-4^3F	1.1169(+00)	1.0000(+00)	1.3756(+00)

[a] $p(q)$ means $p \times 10^q$.

Table VI. Fitting parameters of the excitation cross sections from 2^3S.

transition	a_1	a_2	a_3
2^3S-2^1S	9.5187(+01)[a]	1.5303(+03)	−6.7565(+03)
2^3S-3^1S	8.9640(−01)	6.1588(−01)	1.2506(+00)
2^3S-4^1S	2.1579(−01)	4.7134(+00)	−1.3416(+01)
2^3S-2^1P	4.8193(+01)	7.0681(+02)	−3.2657(+03)
2^3S-3^1P	7.9460(−01)	2.2962(+00)	−1.8739(+00)
2^3S-4^1P	1.8457(−01)	1.1635(+00)	−3.5622(+00)
2^3S-3^1D	1.5560(+00)	3.0215(+00)	−6.9190(+00)
2^3S-4^1D	4.3568(−01)	9.9997(−01)	−1.7892(+00)
2^3S-4^1F	6.4055(−02)	1.5546(−01)	−2.9447(−01)
2^3S-3^3S	8.5433(+00)	−3.9664(+00)	2.1007(+01)
2^3S-4^3S	1.7349(+00)	−5.2800(−02)	5.2179(+00)
2^3S-2^3P	1.2079(+02)	−7.6398(+01)	1.8329(+03)
2^3S-3^3P	−3.5825(+00)	4.9905(+00)	9.5894(−01)
2^3S-4^3P	−1.3062(+00)	1.9126(+00)	−2.9875(−02)
2^3S-3^3D	1.6388(+01)	5.6270(+01)	−1.5613(+02)
2^3S-4^3D	4.0104(+00)	1.4042(+01)	−3.8542(+01)
2^3S-4^3F	5.9323(−01)	2.0806(+00)	−5.7209(+00)

	a_4	a_5	a_6
2^3S-2^1S	1.3144(+04)	5.6207(−02)	1.4932(+02)
2^3S-3^1S	−9.8095(−01)	6.2646(−01)	1.2715(+00)
2^3S-4^1S	3.5523(+01)	9.1839(−02)	5.1700(+01)
2^3S-2^1P	4.6163(+03)	6.9042(−01)	8.1351(+00)
2^3S-3^1P	1.7584(+01)	9.2610(−01)	2.4463(+00)
2^3S-4^1P	1.0312(+01)	9.0477(−01)	2.9167(+00)
2^3S-3^1D	4.9172(+00)	1.0000(+00)	6.9103(−01)
2^3S-4^1D	7.4003(−01)	1.0000(+00)	5.4408(−01)
2^3S-4^1F	1.3571(−01)	1.0000(+00)	5.6055(−01)
2^3S-3^3S	−8.5587(+00)	4.1201(−01)	4.0770(+00)
2^3S-4^3S	−1.2652(+00)	2.7818(−01)	8.0080(+00)
2^3S-2^3P	7.7594(+01)	5.8110(−01)	8.2826(+00)
2^3S-3^3P	3.3639(+00)	3.8228(−02)	7.0982(+00)
2^3S-4^3P	1.1122(+00)	3.6148(−03)	2.2218(−01)
2^3S-3^3D	1.0751(+02)	1.0000(+00)	1.1336(+00)
2^3S-4^3D	2.6868(+01)	1.0000(+00)	1.1764(+00)
2^3S-4^3F	3.9821(+00)	1.0000(+00)	1.1703(+00)

[a] $p(q)$ means $p \times 10^q$.

Table VII. Fitting parameters of de-excitation rate coefficients for $2^1S - n^1L$.

transition	b_0	b_1	b_2
$2^1S - 3^1S$	$-1.661342(+01)^a$	$2.786089(-01)$	$-6.374324(-02)$
$2^1S - 4^1S$	$-1.798026(+01)$	$3.104588(-01)$	$-5.087710(-02)$
$2^1S - 2^1P$	$-1.440885(+01)$	$4.496497(-01)$	$-1.004429(-01)$
$2^1S - 3^1P$	$-1.830419(+01)$	$5.176017(-02)$	$6.517655(-02)$
$2^1S - 4^1P$	$-1.969738(+01)$	$1.791818(-02)$	$6.553520(-02)$
$2^1S - 3^1D$	$-1.723823(+01)$	$5.338751(-01)$	$-2.083460(-01)$
$2^1S - 4^1D$	$-1.896339(+01)$	$2.573627(-01)$	$2.094426(-02)$
$2^1S - 4^1F$	$-2.088162(+01)$	$6.337583(-01)$	$-2.141008(-01)$

	b_4	b_5	b_6
$2^1S - 3^1S$	$-2.011202(-02)$	$2.309213(-04)$	$1.670936(-03)$
$2^1S - 4^1S$	$-1.824779(-02)$	$-1.460173(-03)$	$1.763308(-03)$
$2^1S - 2^1P$	$-1.009030(-02)$	$1.180146(-03)$	$9.839128(-04)$
$2^1S - 3^1P$	$3.363705(-03)$	$-3.775721(-03)$	$-8.102613(-04)$
$2^1S - 4^1P$	$6.114056(-03)$	$-2.672857(-03)$	$-1.354705(-03)$
$2^1S - 3^1D$	$8.217787(-03)$	$1.882660(-03)$	$-1.006448(-04)$
$2^1S - 4^1D$	$-5.094130(-02)$	$2.002846(-04)$	$3.574182(-03)$
$2^1S - 4^1F$	$6.590542(-03)$	$2.154179(-03)$	$-1.731374(-04)$

	b_7	b_8	b_9
$2^1S - 3^1S$	$-3.465936(-04)$	$2.814507(-05)$	$-8.400606(-07)$
$2^1S - 4^1S$	$-3.028439(-04)$	$2.148198(-05)$	$-5.660465(-07)$
$2^1S - 2^1P$	$-2.509543(-04)$	$2.290054(-05)$	$-7.476769(-07)$
$2^1S - 3^1P$	$3.595857(-04)$	$-3.939492(-05)$	$1.421593(-06)$
$2^1S - 4^1P$	$4.327060(-04)$	$-4.308677(-05)$	$1.469006(-06)$
$2^1S - 3^1D$	$-2.267058(-05)$	$2.445832(-06)$	$-6.620935(-08)$
$2^1S - 4^1D$	$-7.462842(-04)$	$6.190292(-05)$	$-1.894656(-06)$
$2^1S - 4^1F$	$-4.325535(-06)$	$5.031709(-07)$	$4.714461(-09)$

[a] $p(q)$ means $p \times 10^q$.

Table VIII. Fitting parameters of de-excitation rate coefficients for $2^1S - n^3L$.

transition	b_0	b_1	b_2
$2^1S - 3^3S$	$-1.793938(+01)^a$	$-8.896477(-01)$	$-8.347472(-02)$
$2^1S - 4^3S$	$-1.908740(+01)$	$-8.195725(-01)$	$-7.892384(-02)$
$2^1S - 2^3P$	$-1.796241(+01)$	$-3.358538(-01)$	$-1.295956(-01)$
$2^1S - 3^3P$	$-1.907974(+01)$	$-6.678234(-01)$	$-1.035515(-01)$
$2^1S - 4^3P$	$-2.015856(+01)$	$-6.156972(-01)$	$-9.203520(-02)$
$2^1S - 3^3D$	$-1.998833(+01)$	$-2.329699(-01)$	$-1.973993(-01)$
$2^1S - 4^3D$	$-2.117507(+01)$	$-7.226693(-02)$	$-1.977569(-01)$
$2^1S - 4^3F$	$-2.341913(+01)$	$-7.502819(-02)$	$-1.988570(-01)$

	b_3	b_4	b_5
$2^1S - 3^3S$	$-3.098982(-03)$	$1.428353(-03)$	$7.244689(-05)$
$2^1S - 4^3S$	$-5.352113(-03)$	$1.237213(-03)$	$1.551125(-04)$
$2^1S - 2^3P$	$-2.273255(-02)$	$3.059424(-03)$	$1.531414(-03)$
$2^1S - 3^3P$	$-1.323526(-02)$	$3.724737(-03)$	$2.092280(-04)$
$2^1S - 4^3P$	$-1.694819(-02)$	$3.305269(-03)$	$4.688476(-04)$
$2^1S - 3^3D$	$7.244063(-04)$	$2.224279(-03)$	$1.347863(-04)$
$2^1S - 4^3D$	$-9.806004(-03)$	$3.686201(-03)$	$3.795414(-04)$
$2^1S - 4^3F$	$-9.457498(-03)$	$3.864573(-03)$	$3.003899(-04)$

	b_6	b_7	b_8
$2^1S - 3^3S$	$-4.355252(-05)$	$4.218296(-06)$	$-1.348031(-07)$
$2^1S - 4^3S$	$-4.712223(-05)$	$3.754246(-06)$	$-1.025022(-07)$
$2^1S - 2^3P$	$-4.202826(-04)$	$3.934499(-05)$	$-1.305593(-06)$
$2^1S - 3^3P$	$-1.329287(-04)$	$1.403402(-05)$	$-4.860831(-07)$
$2^1S - 4^3P$	$-1.699857(-04)$	$1.630257(-05)$	$-5.372345(-07)$
$2^1S - 3^3D$	$-7.958523(-05)$	$7.771841(-06)$	$-2.485152(-07)$
$2^1S - 4^3D$	$-1.628599(-04)$	$1.580369(-05)$	$-5.169111(-07)$
$2^1S - 4^3F$	$-1.509811(-04)$	$1.499923(-05)$	$-4.960284(-07)$

[a] $p(q)$ means $p \times 10^q$.

Table IX. Fitting parameters of de-excitation rate coefficients for $2^3S - n^1L$.

transition	b_0	b_1	b_2
$2^3S - 2^1S$	$-1.543987(+01)^a$	$-5.882079(-01)$	$-1.055397(-01)$
$2^3S - 3^1S$	$-1.720465(+01)$	$-7.196601(-01)$	$-9.243111(-02)$
$2^3S - 4^1S$	$-1.814838(+01)$	$-6.739987(-01)$	$-8.825198(-02)$
$2^3S - 2^1P$	$-1.744044(+01)$	$-2.669145(-01)$	$-1.332375(-01)$
$2^3S - 3^1P$	$-1.910760(+01)$	$-2.986581(-01)$	$-2.015318(-01)$
$2^3S - 4^1P$	$-2.053274(+01)$	$-2.194298(-01)$	$-1.973528(-01)$
$2^3S - 3^1D$	$-1.899243(+01)$	$-4.617791(-01)$	$-1.365826(-01)$
$2^3S - 4^1D$	$-2.024829(+01)$	$-3.543689(-01)$	$-1.342850(-01)$
$2^3S - 4^1F$	$-2.251818(+01)$	$-3.569640(-01)$	$-1.320051(-01)$

	b_3	b_4	b_5
$2^3S - 2^1S$	$-7.637681(-03)$	$1.541379(-03)$	$2.048899(-04)$
$2^3S - 3^1S$	$-1.020319(-02)$	$2.672337(-03)$	$1.913968(-04)$
$2^3S - 4^1S$	$-1.249816(-02)$	$2.771263(-03)$	$2.632931(-04)$
$2^3S - 2^1P$	$-5.597472(-03)$	$7.025263(-04)$	$-2.572109(-05)$
$2^3S - 3^1P$	$-8.046812(-03)$	$8.229090(-03)$	$-1.188128(-03)$
$2^3S - 4^1P$	$-1.608932(-02)$	$9.718466(-03)$	$-1.102028(-03)$
$2^3S - 3^1D$	$-5.682201(-03)$	$2.157598(-03)$	$1.821764(-04)$
$2^3S - 4^1D$	$-1.434858(-02)$	$3.418733(-03)$	$3.722792(-04)$
$2^3S - 4^1F$	$-1.423464(-02)$	$3.182674(-03)$	$4.165759(-04)$

	b_6	b_7	b_8
$2^3S - 2^1S$	$-4.798693(-05)$	$2.628181(-06)$	$-2.955397(-08)$
$2^3S - 3^1S$	$-9.720699(-05)$	$9.717845(-06)$	$-3.246808(-07)$
$2^3S - 4^1S$	$-1.143767(-04)$	$1.135765(-05)$	$-3.830127(-07)$
$2^3S - 2^1P$	$6.648135(-05)$	$-1.122509(-05)$	$5.115955(-07)$
$2^3S - 3^1P$	$5.180370(-05)$	$2.149676(-06)$	$-1.829335(-07)$
$2^3S - 4^1P$	$-5.840264(-06)$	$8.649812(-06)$	$-4.216917(-07)$
$2^3S - 3^1D$	$-7.719496(-05)$	$7.016555(-06)$	$-2.146917(-07)$
$2^3S - 4^1D$	$-1.466955(-04)$	$1.391234(-05)$	$-4.497146(-07)$
$2^3S - 4^1F$	$-1.490357(-04)$	$1.381609(-05)$	$-4.403635(-07)$

[a] $p(q)$ means $p \times 10^q$.

Table X. Fitting parameters of de-excitation rate coefficients for $2^3S - n^3L$.

transition	b_0	b_1	b_2
$2^3S - 3^3S$	$-1.636783(+01)^a$	$-2.712662(-01)$	$2.641262(-02)$
$2^3S - 4^3S$	$-1.799936(+01)$	$-2.948790(-01)$	$3.210884(-02)$
$2^3S - 2^3P$	$-1.521105(+01)$	$4.246033(-01)$	$-7.452294(-02)$
$2^3S - 3^3P$	$-1.815731(+01)$	$-5.833802(-01)$	$6.960187(-02)$
$2^3S - 4^3P$	$-1.928328(+01)$	$-6.083723(-01)$	$4.865539(-02)$
$2^3S - 3^3D$	$-1.795322(+01)$	$3.323052(-01)$	$-4.430282(-02)$
$2^3S - 4^3D$	$-1.951990(+01)$	$3.530513(-01)$	$-3.814093(-02)$
$2^3S - 4^3F$	$-2.176618(+01)$	$3.519445(-01)$	$-3.706029(-02)$

	b_3	b_4	b_5
$2^3S - 3^3S$	$-7.542254(-03)$	$-7.275337(-04)$	$2.620161(-04)$
$2^3S - 4^3S$	$-6.572373(-03)$	$-1.064291(-03)$	$2.981719(-04)$
$2^3S - 2^3P$	$-7.630836(-03)$	$4.262193(-03)$	$-1.278114(-03)$
$2^3S - 3^3P$	$4.327626(-02)$	$-6.375701(-03)$	$-2.776179(-03)$
$2^3S - 4^3P$	$4.593114(-02)$	$-4.315137(-03)$	$-3.219225(-03)$
$2^3S - 3^3D$	$-2.851896(-02)$	$-2.075106(-04)$	$2.160701(-03)$
$2^3S - 4^3D$	$-2.475428(-02)$	$-1.644289(-03)$	$2.090355(-03)$
$2^3S - 4^3F$	$-2.506725(-02)$	$-1.667246(-03)$	$2.118286(-03)$

	b_3	b_4	b_5
$2^3S - 3^3S$	$-1.541241(-05)$	$-4.598216(-07)$	$4.787360(-08)$
$2^3S - 4^3S$	$-1.908820(-05)$	$-8.083830(-08)$	$3.150486(-08)$
$2^3S - 2^3P$	$2.226108(-04)$	$-1.900172(-05)$	$6.196188(-07)$
$2^3S - 3^3P$	$8.099950(-04)$	$-7.708995(-05)$	$2.560787(-06)$
$2^3S - 4^3P$	$8.168392(-04)$	$-7.309551(-05)$	$2.325137(-06)$
$2^3S - 3^3D$	$-4.198754(-04)$	$3.255007(-05)$	$-9.333818(-07)$
$2^3S - 4^3D$	$-3.510650(-04)$	$2.422335(-05)$	$-6.182127(-07)$
$2^3S - 4^3F$	$-3.566250(-04)$	$2.469232(-05)$	$-6.330256(-07)$

[a] $p(q)$ means $p \times 10^q$.

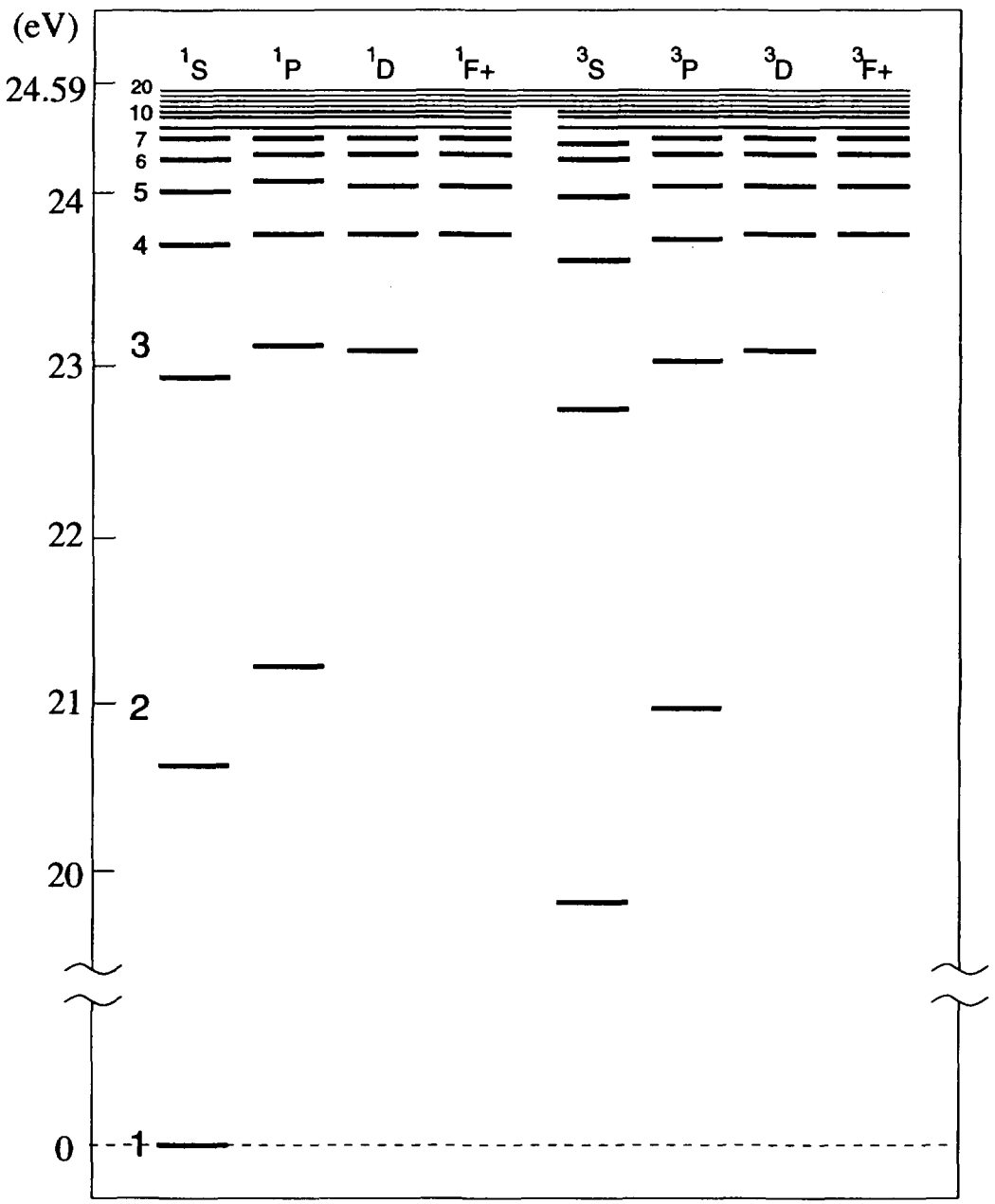

FIG. 1. Energy level diagram of helium as considered in the calculation. "$^{1,3}F+$" denote the levels which represent all the levels with $l \geq 3$.

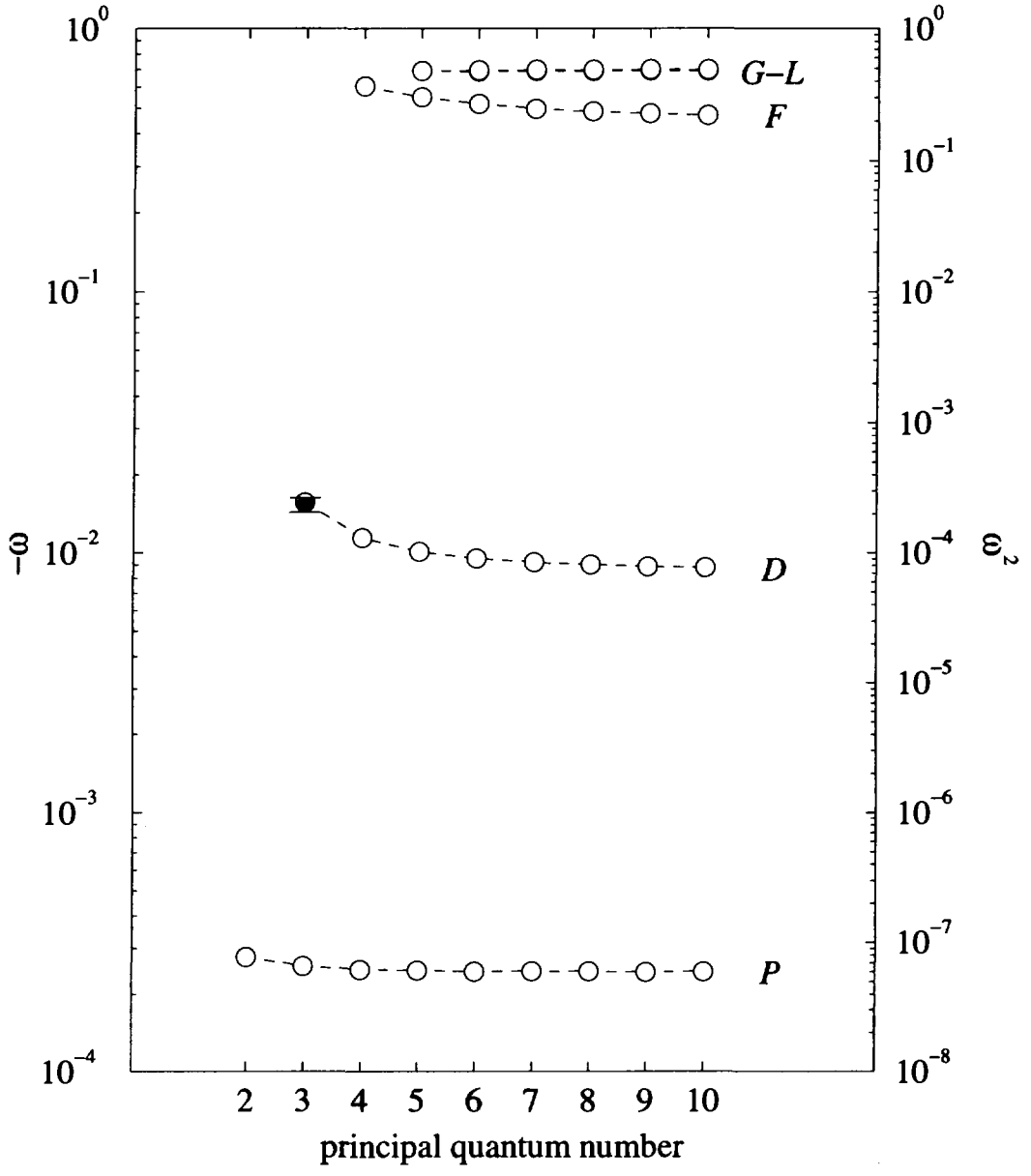

FIG. 2. Coefficient for wavefunction mixing between singlet and triplet levels. ○: [6], ●: experiment [8].

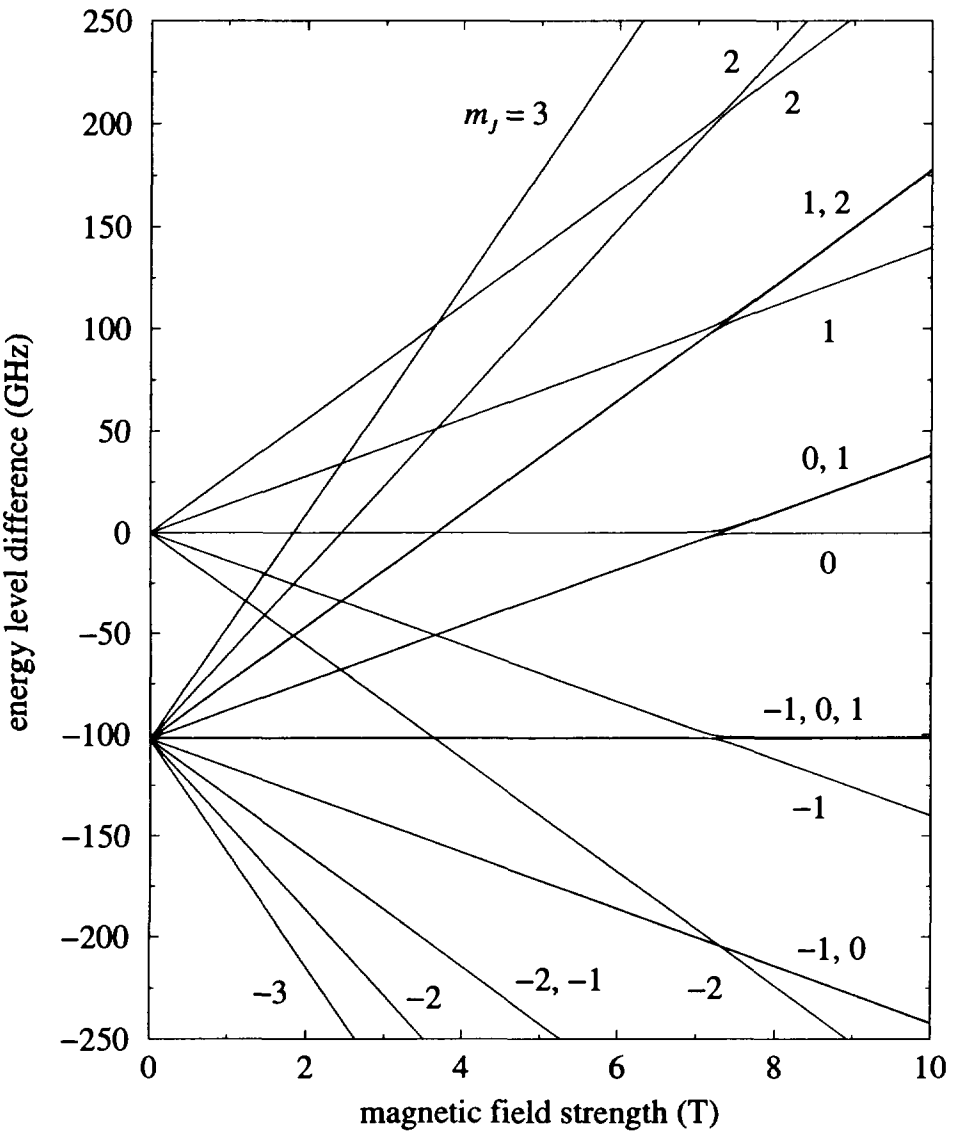

FIG. 3. The magnetic field dependence of the Zeeman shifts for $3^{1,3}D$ states. E shows the energy with respect to the 3^1D level position when no magnetic field is present.

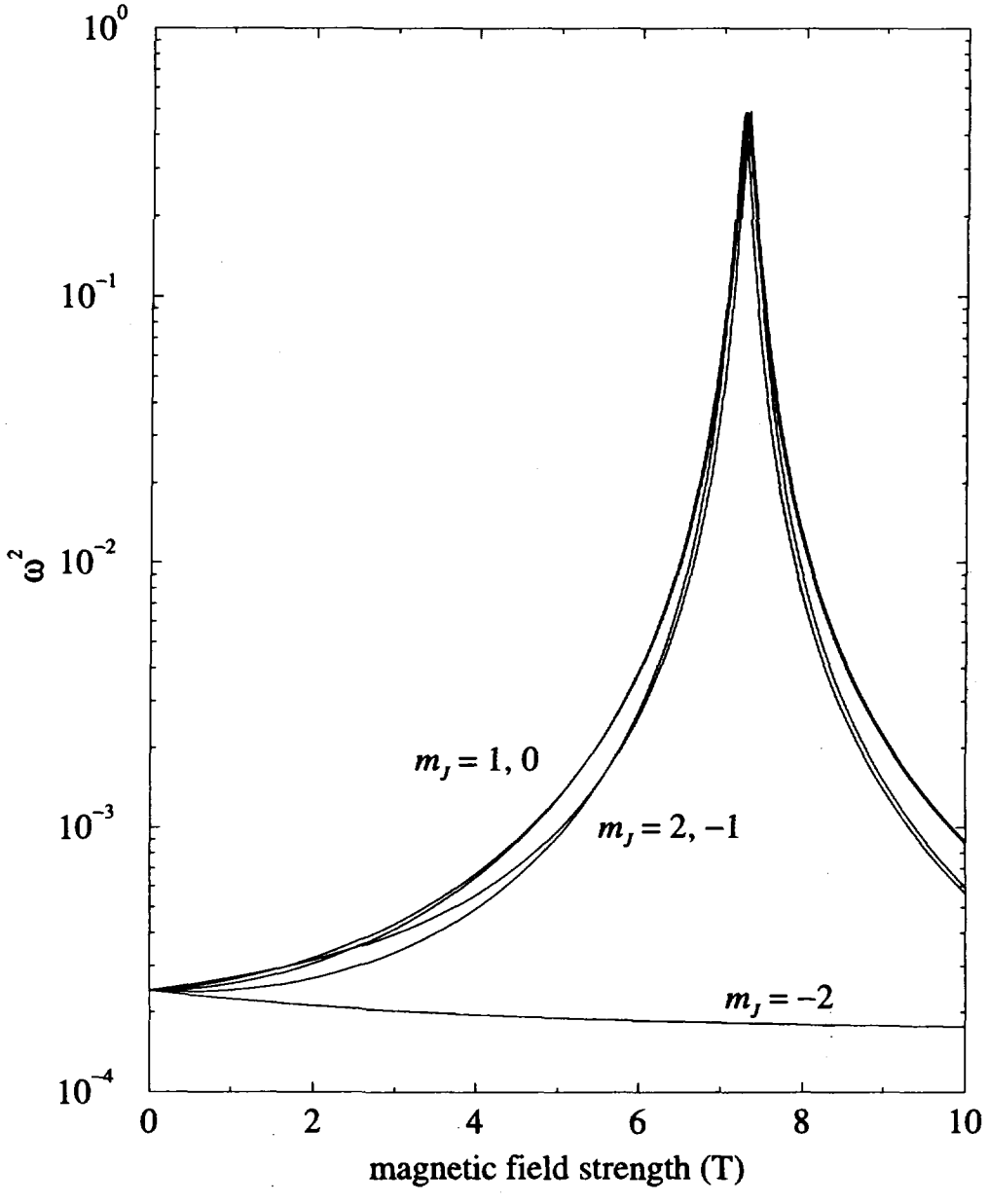

FIG. 4. The magnetic field dependence of the mixing coefficients.

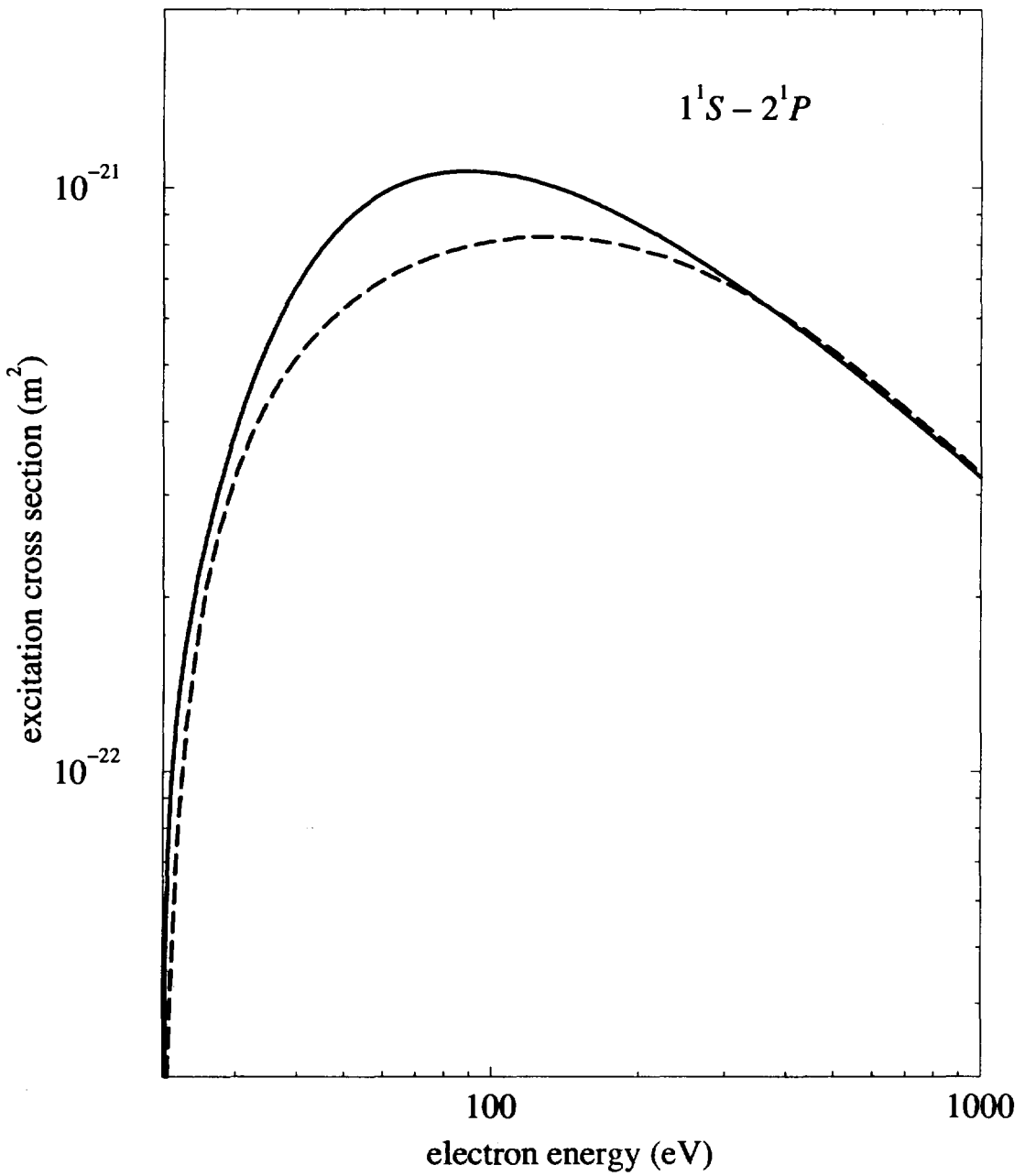

FIG. 5. Excitation cross section for $1^1S \rightarrow 2^1P$. – – – : original [2], —— : Kato and Janev [11].

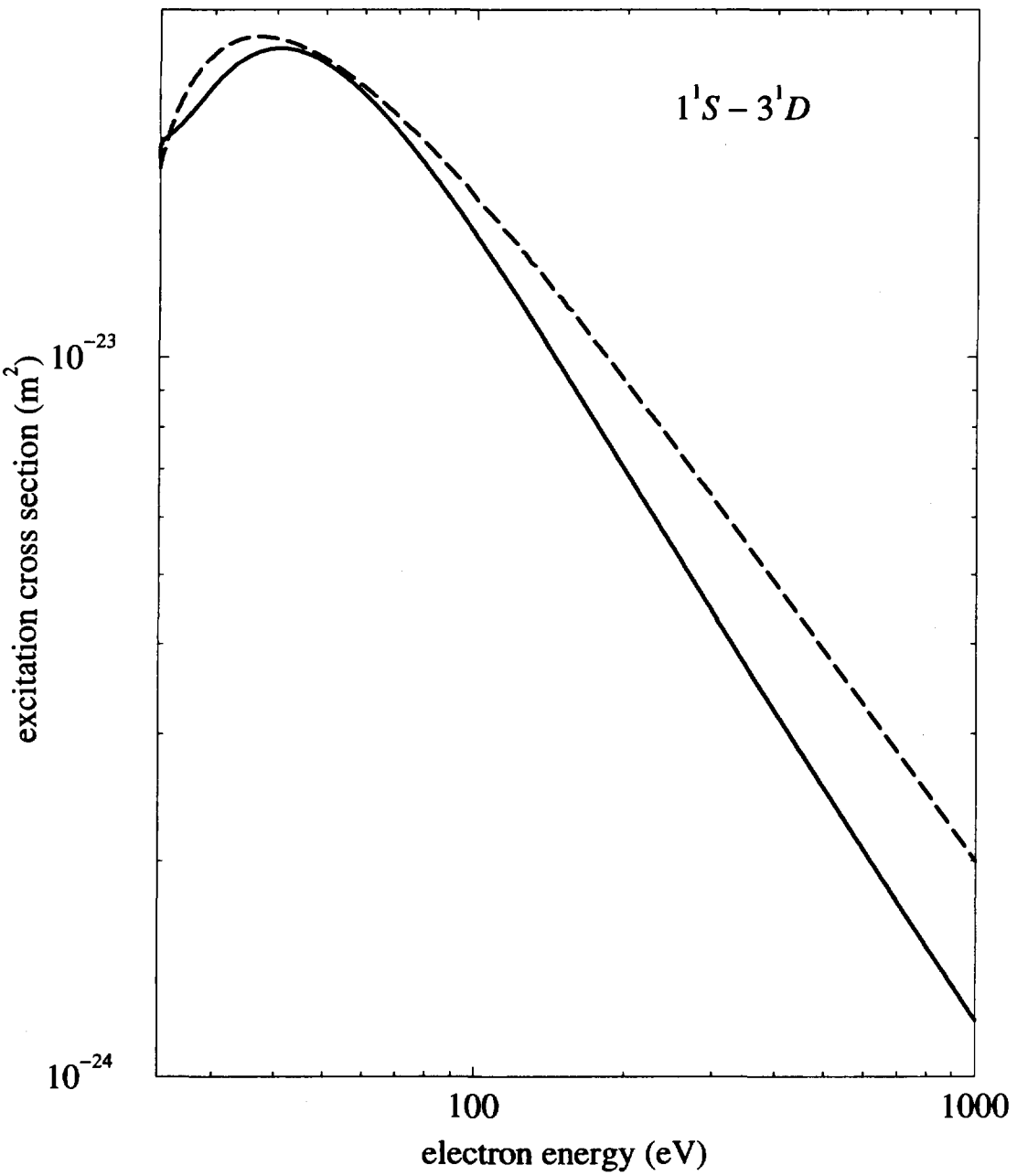

FIG. 6. Similar figure to Fig. 5 except that transition is $1^1S \rightarrow 3^1D$.

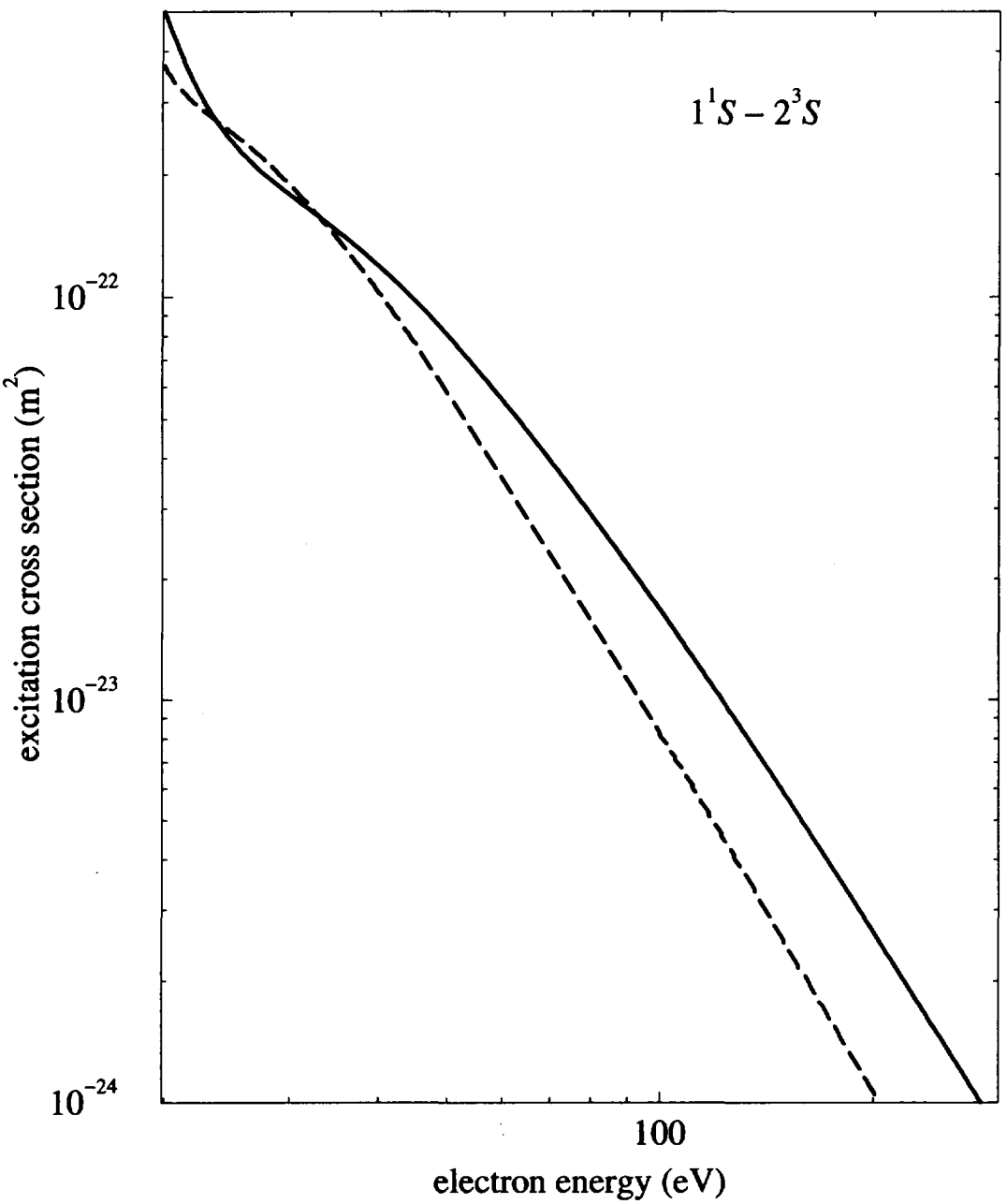

FIG. 7. Similar figure to Fig. 5 except that transition is $1^1S \rightarrow 2^3S$.

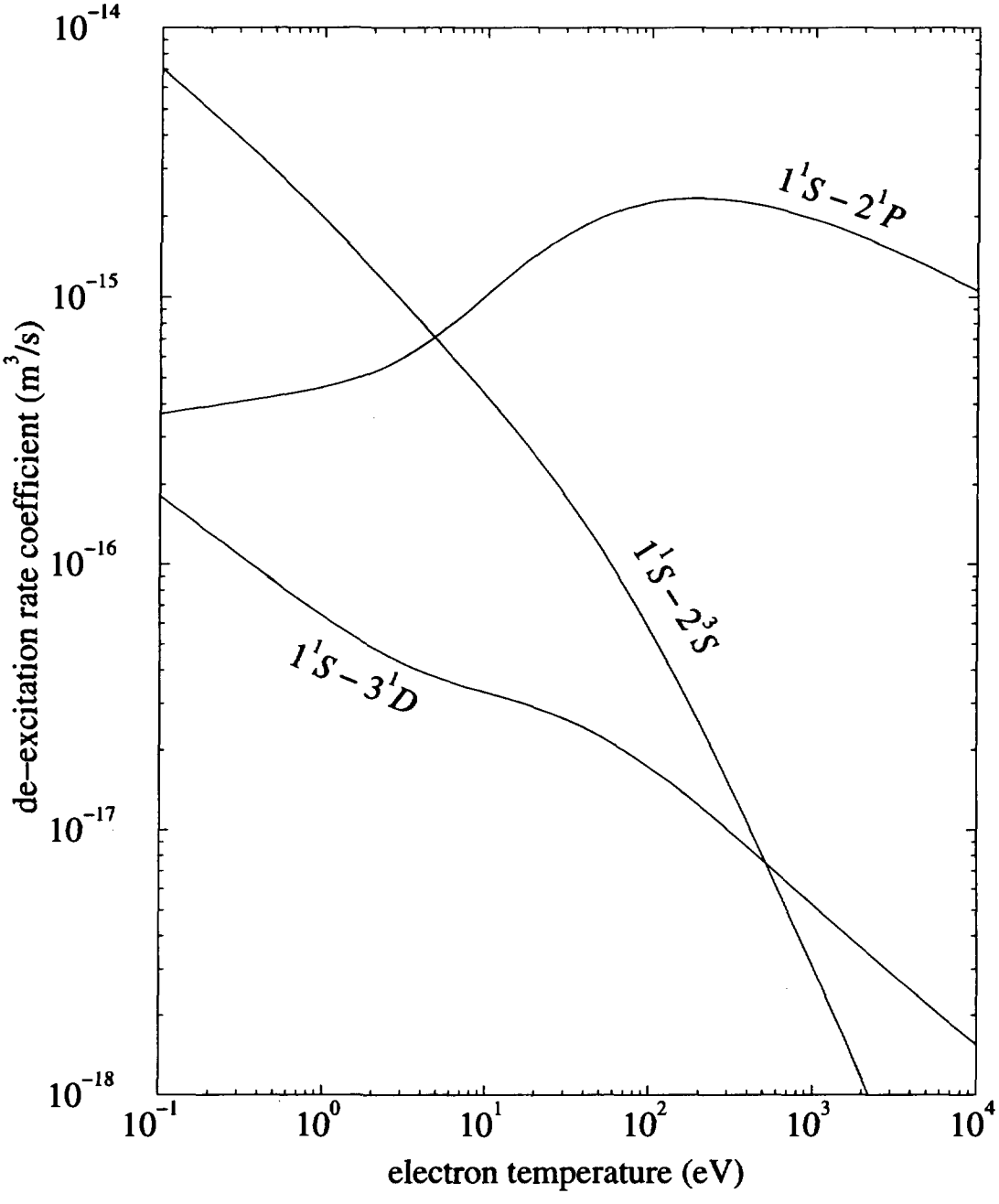

FIG. 8. De-excitation rate coefficient for $1^1S \leftarrow 2^1P, 3^1D, 2^3S$.

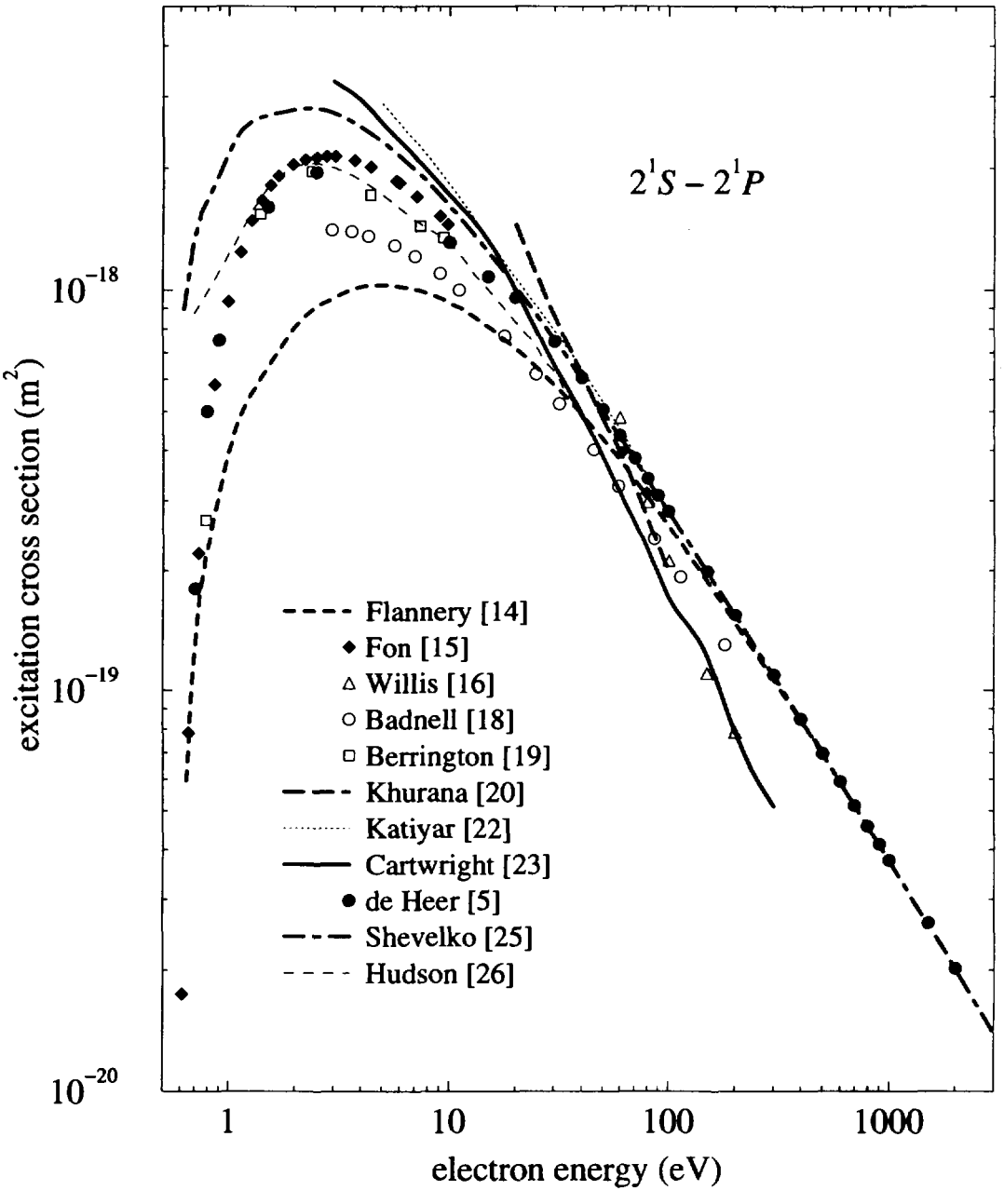

FIG. 9. Excitation cross section for $2^1S \rightarrow 2^1P$.

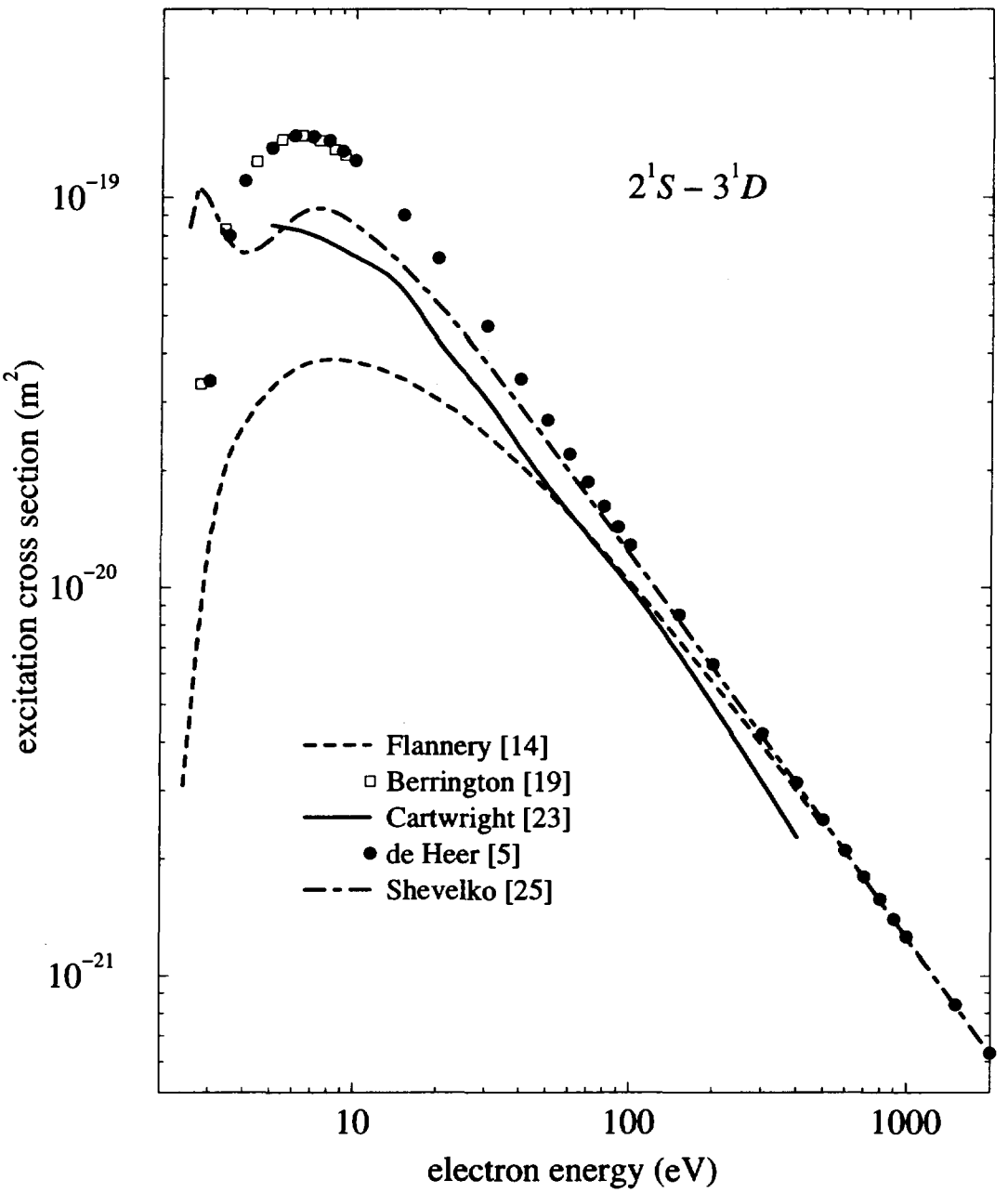

FIG. 10. Excitation cross section for $2^1S \rightarrow 3^1D$.

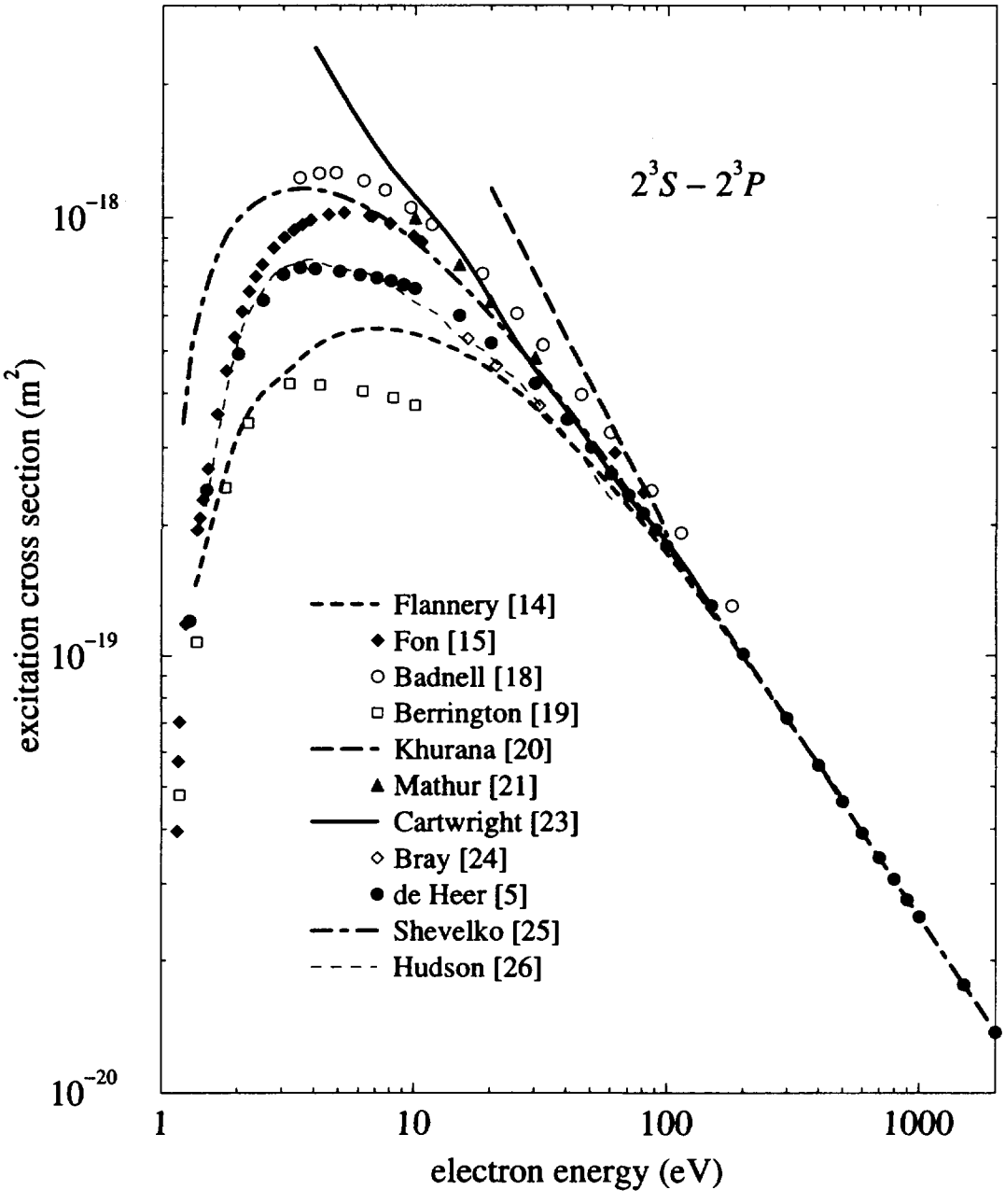

FIG. 11. Excitation cross section for $2^3S \rightarrow 2^3P$.

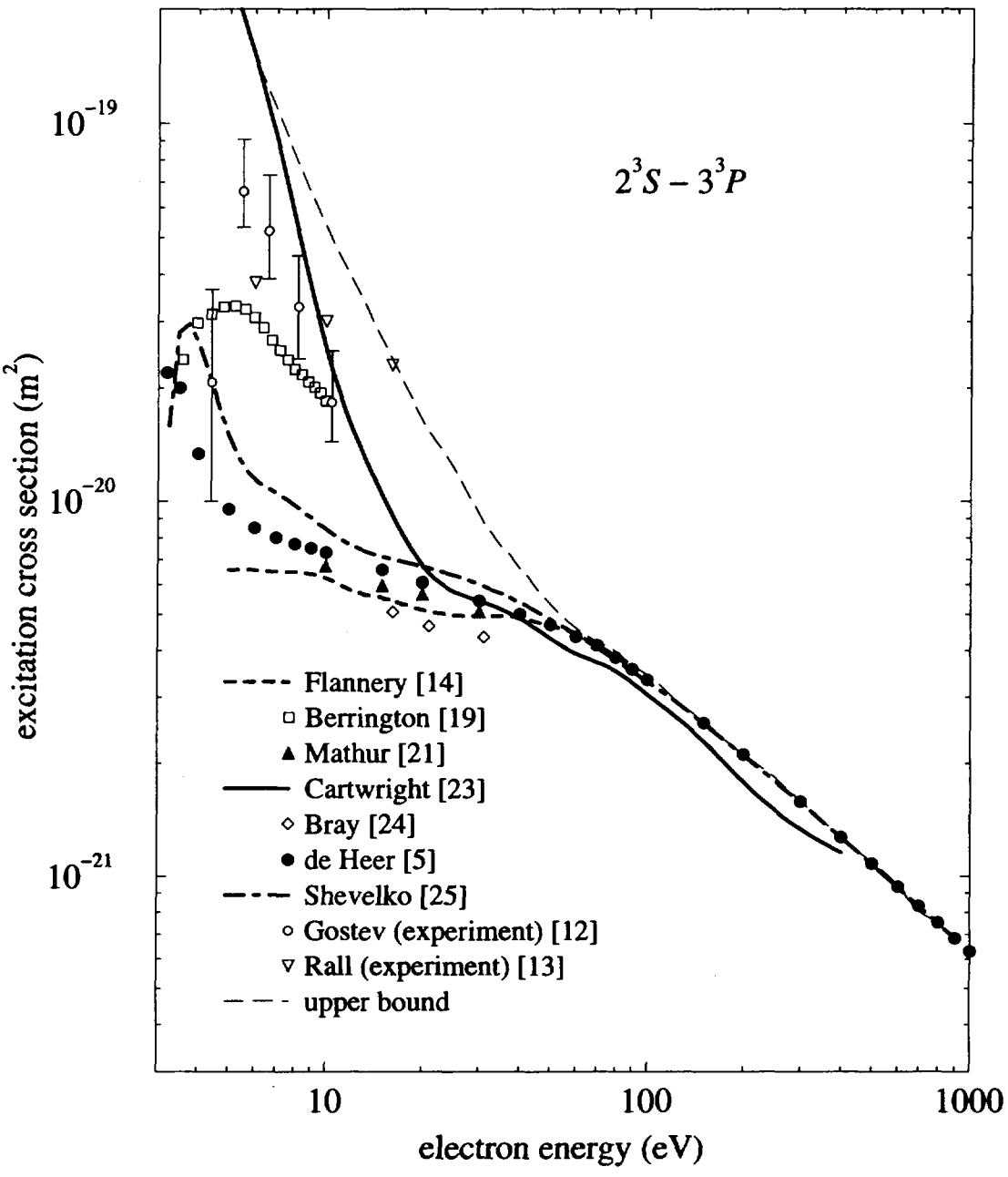

FIG. 12. Excitation cross section for $2^3S \rightarrow 3^3P$.

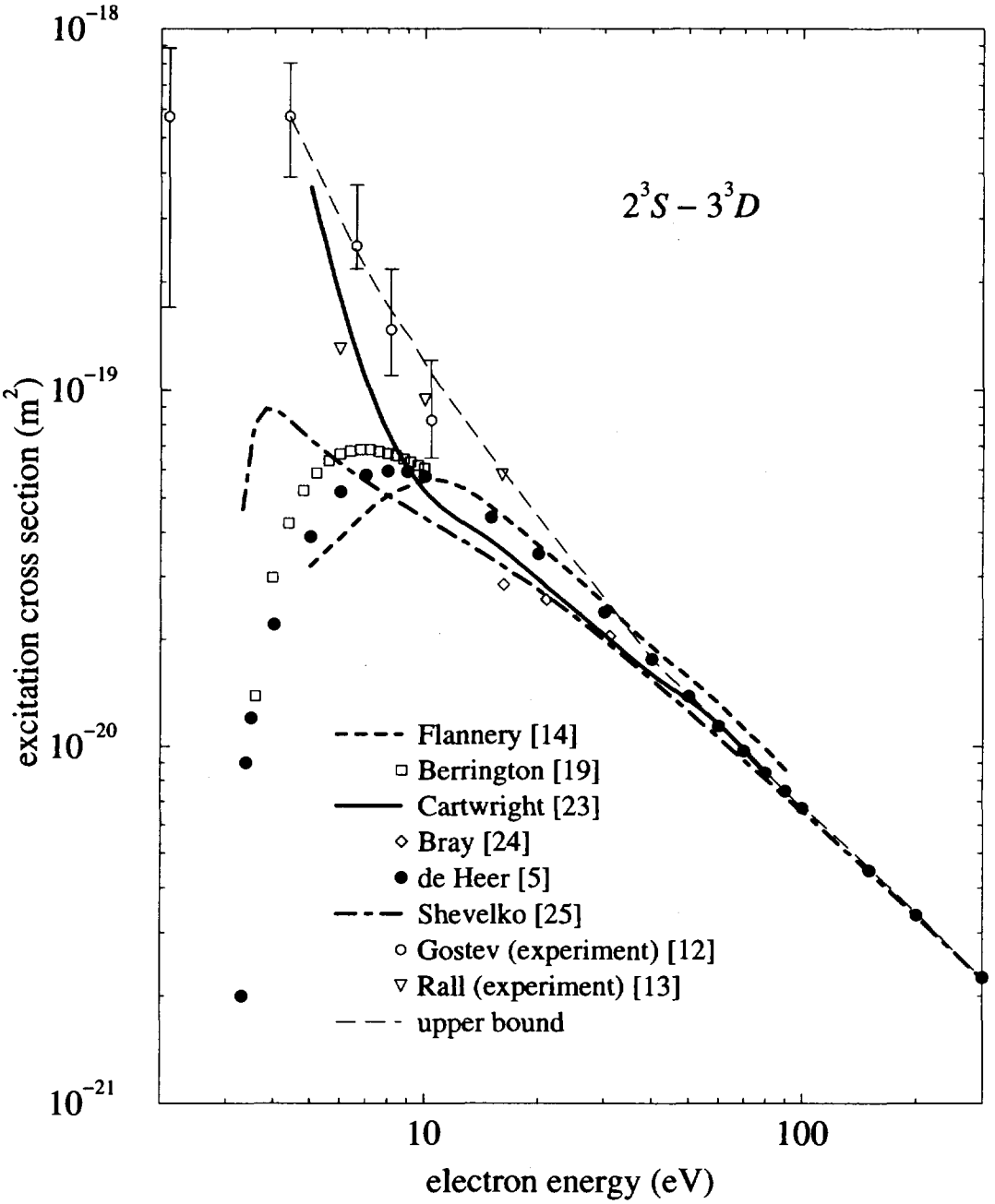

FIG. 13. Excitation cross section for $2^3S \rightarrow 3^3D$.

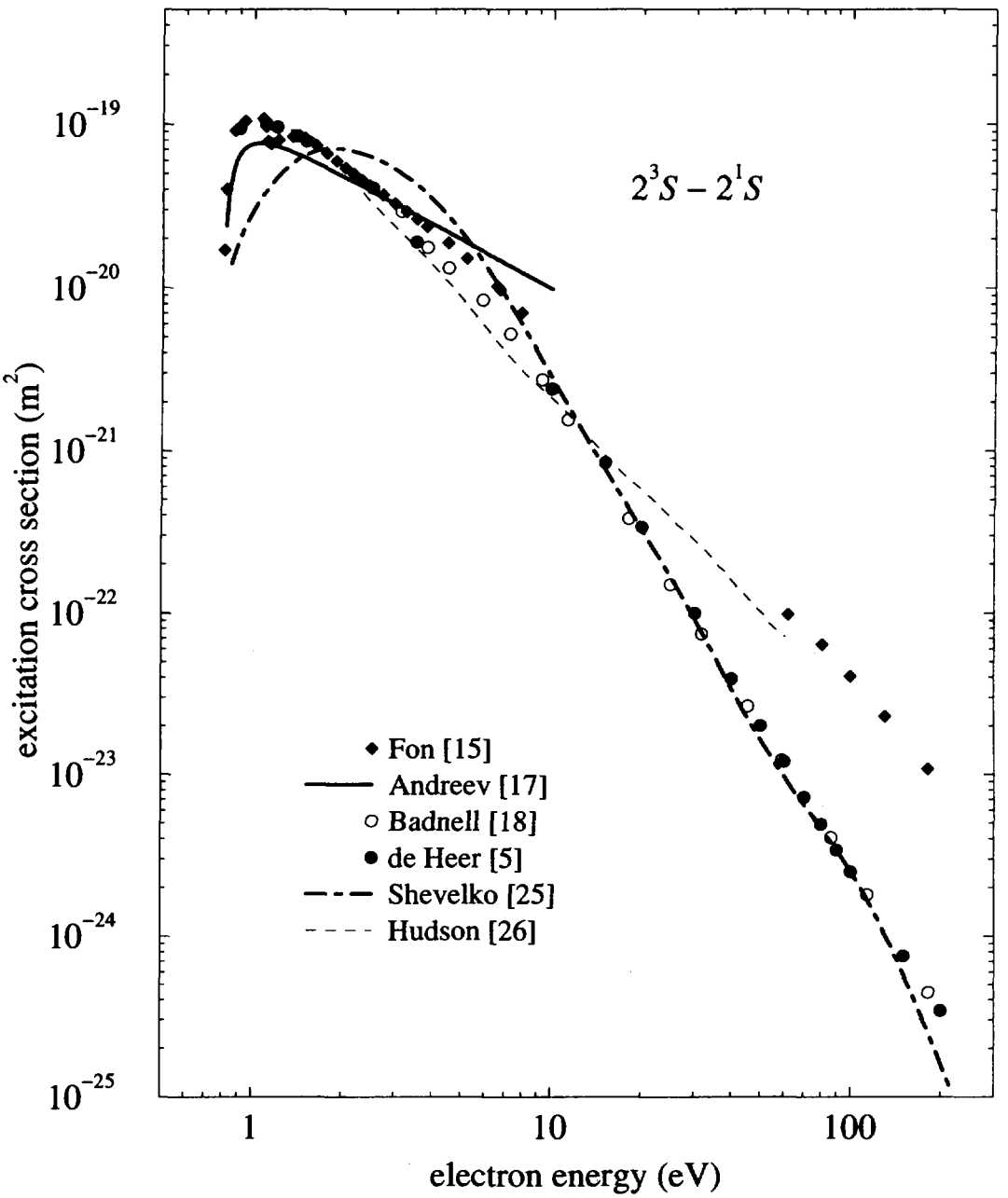

FIG. 14. Excitation cross section for $2^3S \rightarrow 2^1S$.

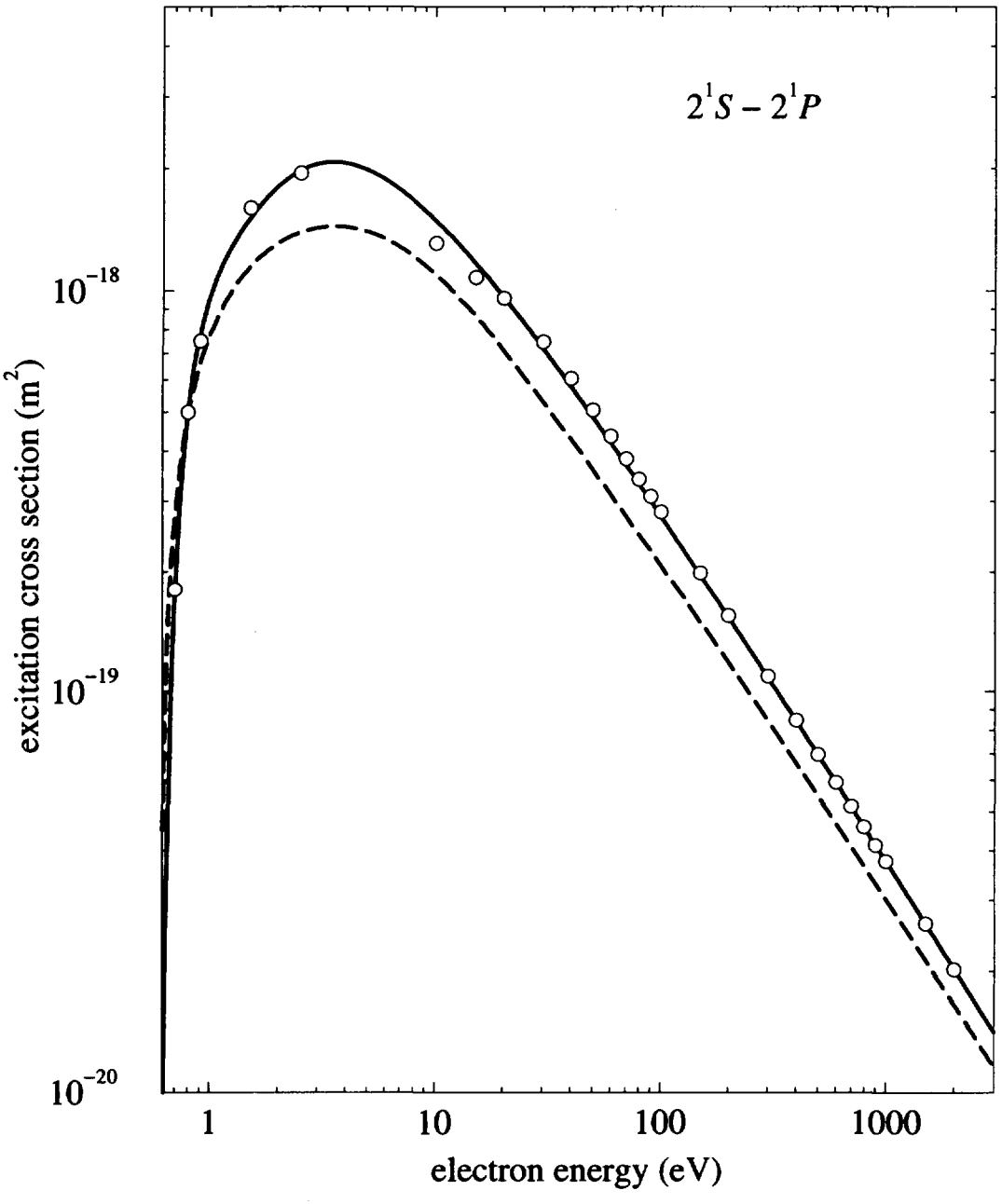

FIG. 15. Excitation cross section for $2^1S \rightarrow 2^1P$. – – – : original [2], ○: de Heer [5], —— : fitting of [5].

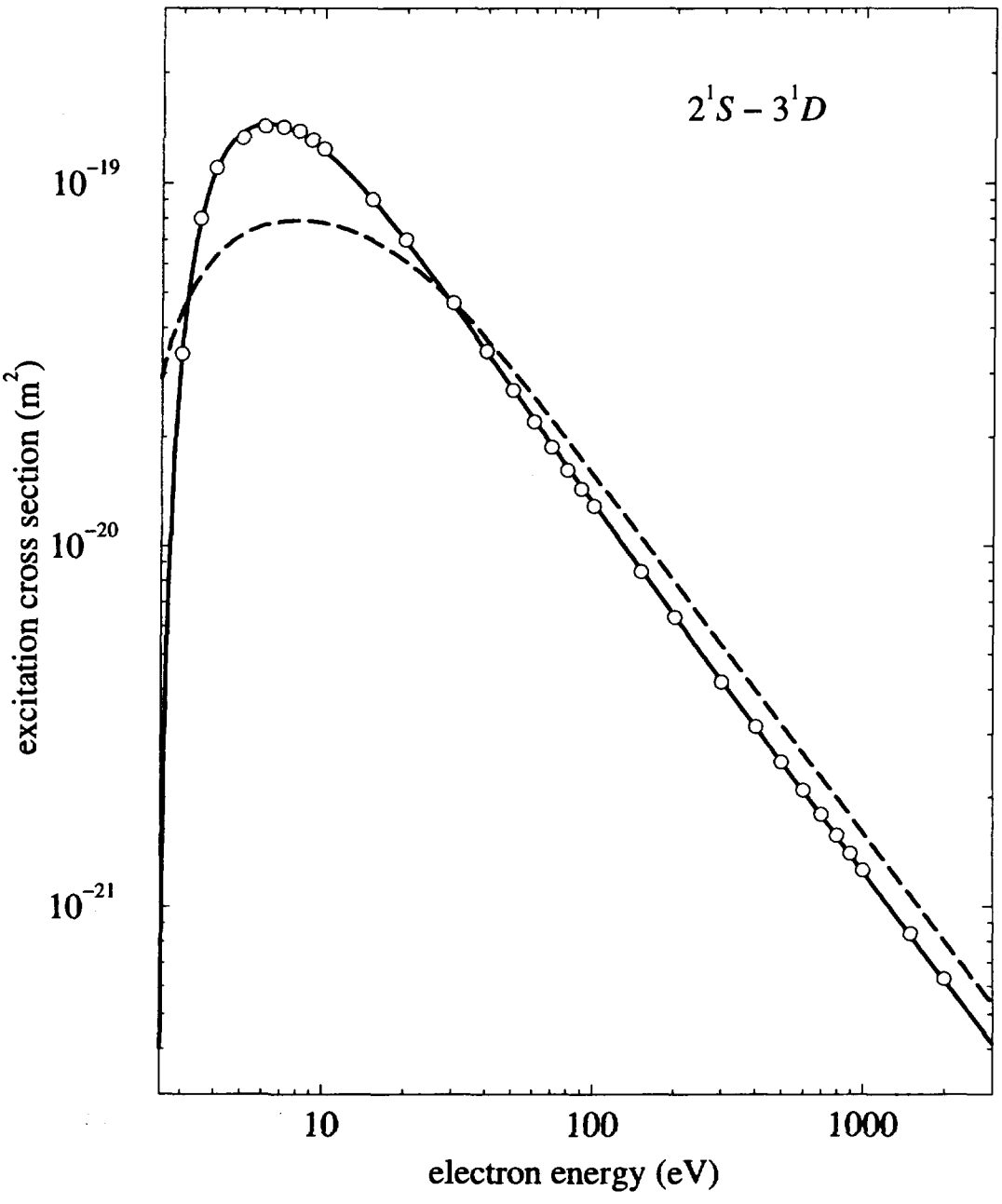

FIG. 16. Similar figure to Fig. 15 except that transition is $2^1S \rightarrow 3^1D$.

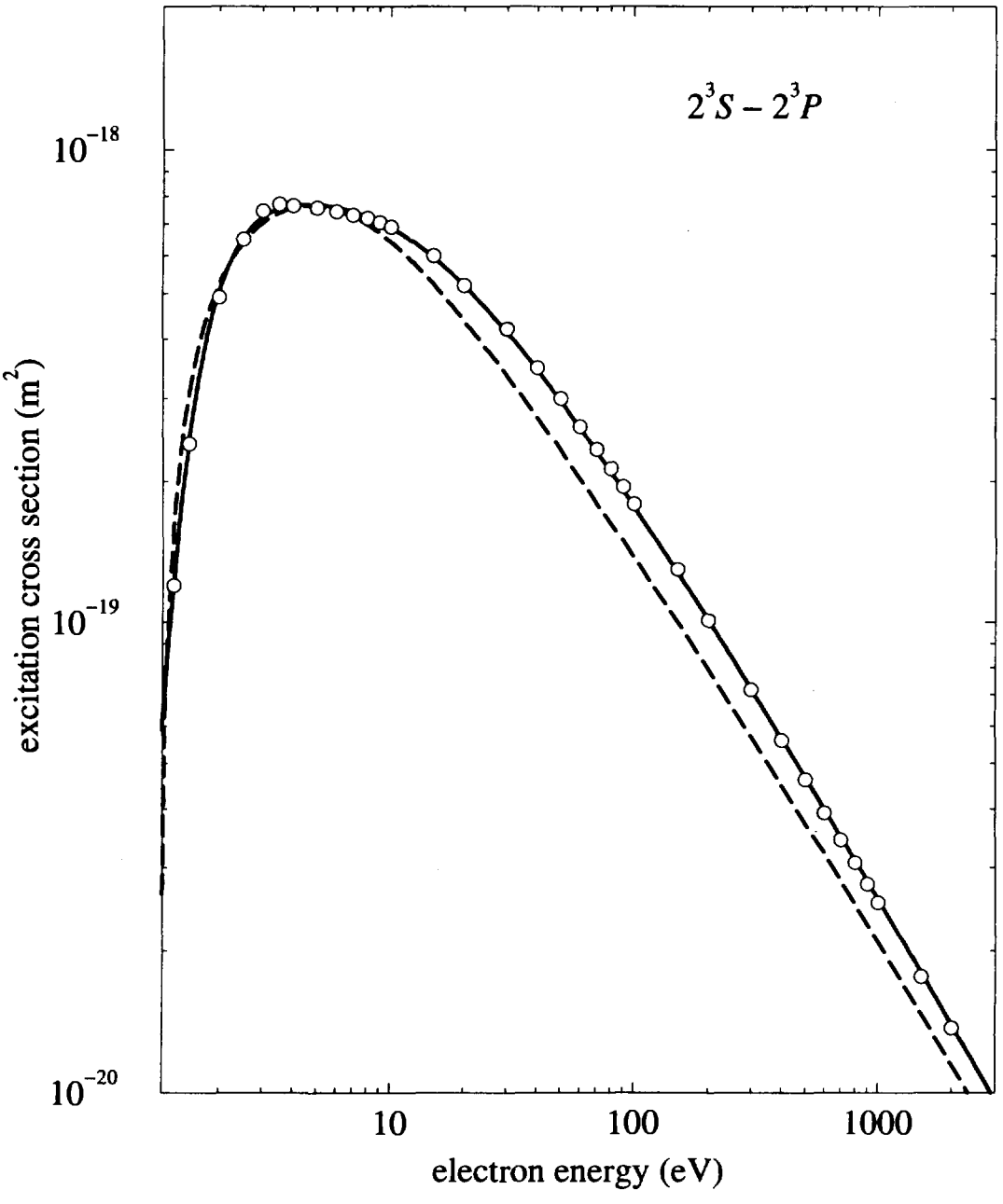

FIG. 17. Similar figure to Fig. 15 except that transition is $2^3S \rightarrow 2^3P$.

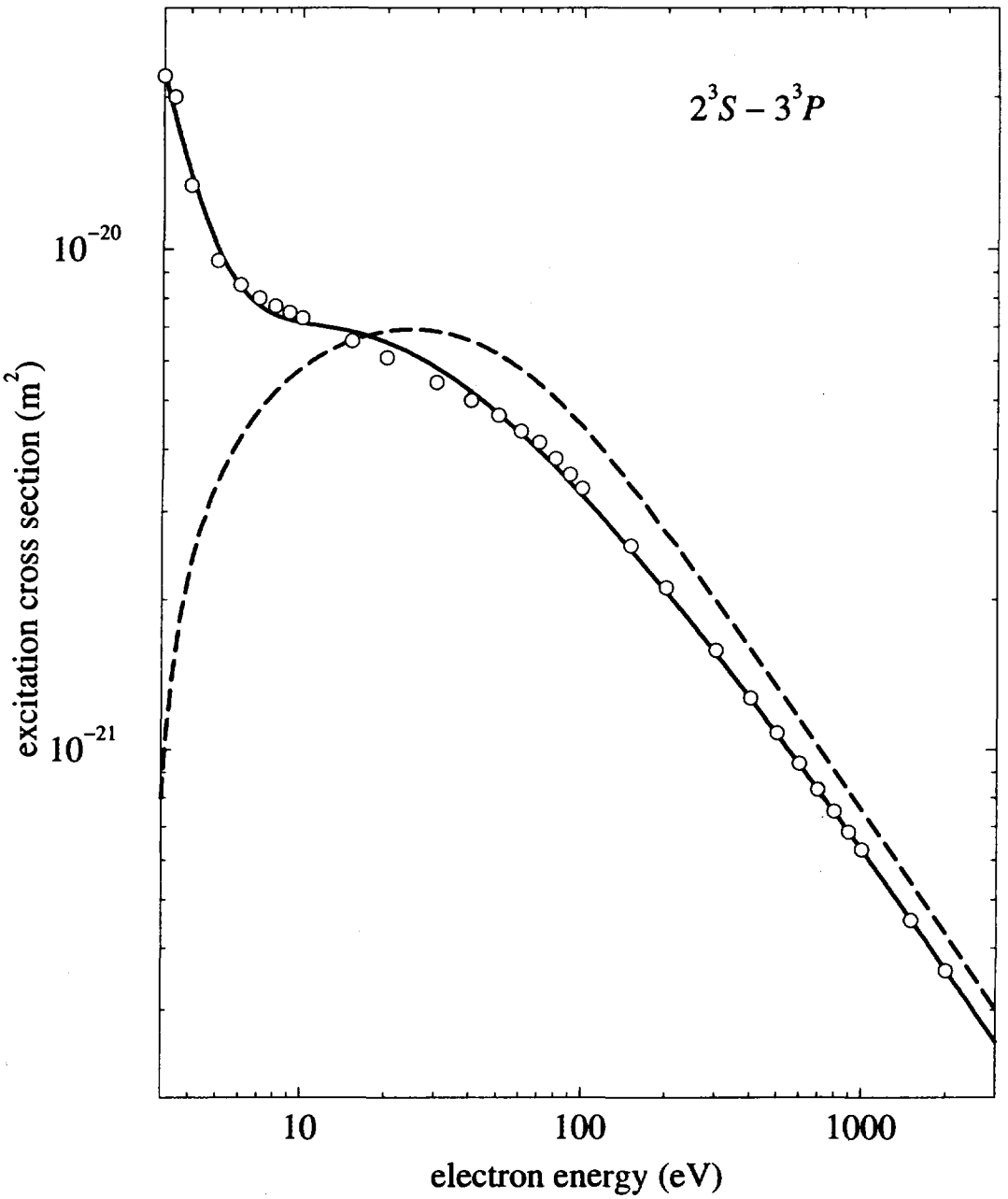

FIG. 18. Similar figure to Fig. 15 except that transition is $2^3S \rightarrow 3^3P$.

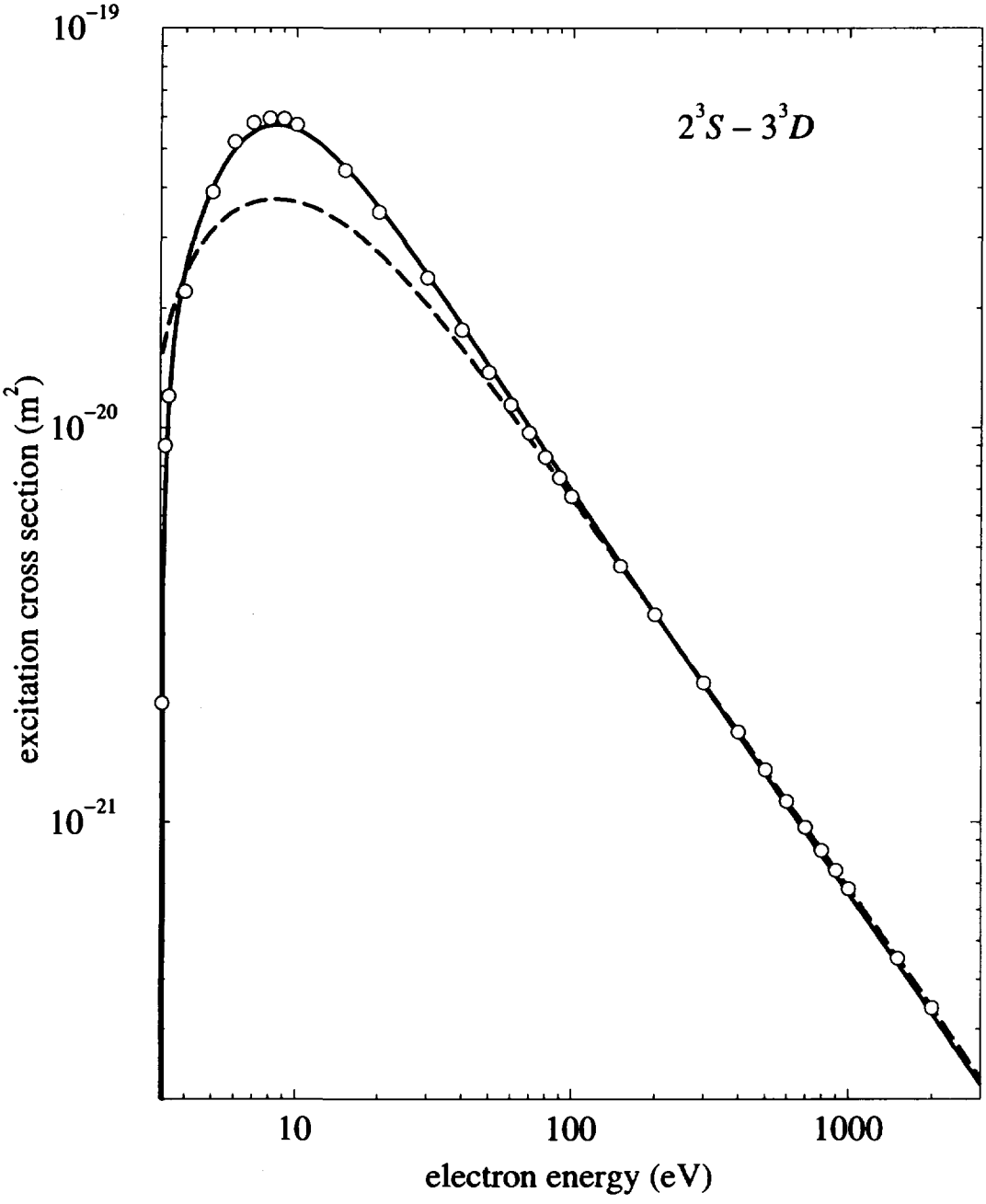

FIG. 19. Similar figure to Fig. 15 except that transition is $2^3S \rightarrow 3^3D$.

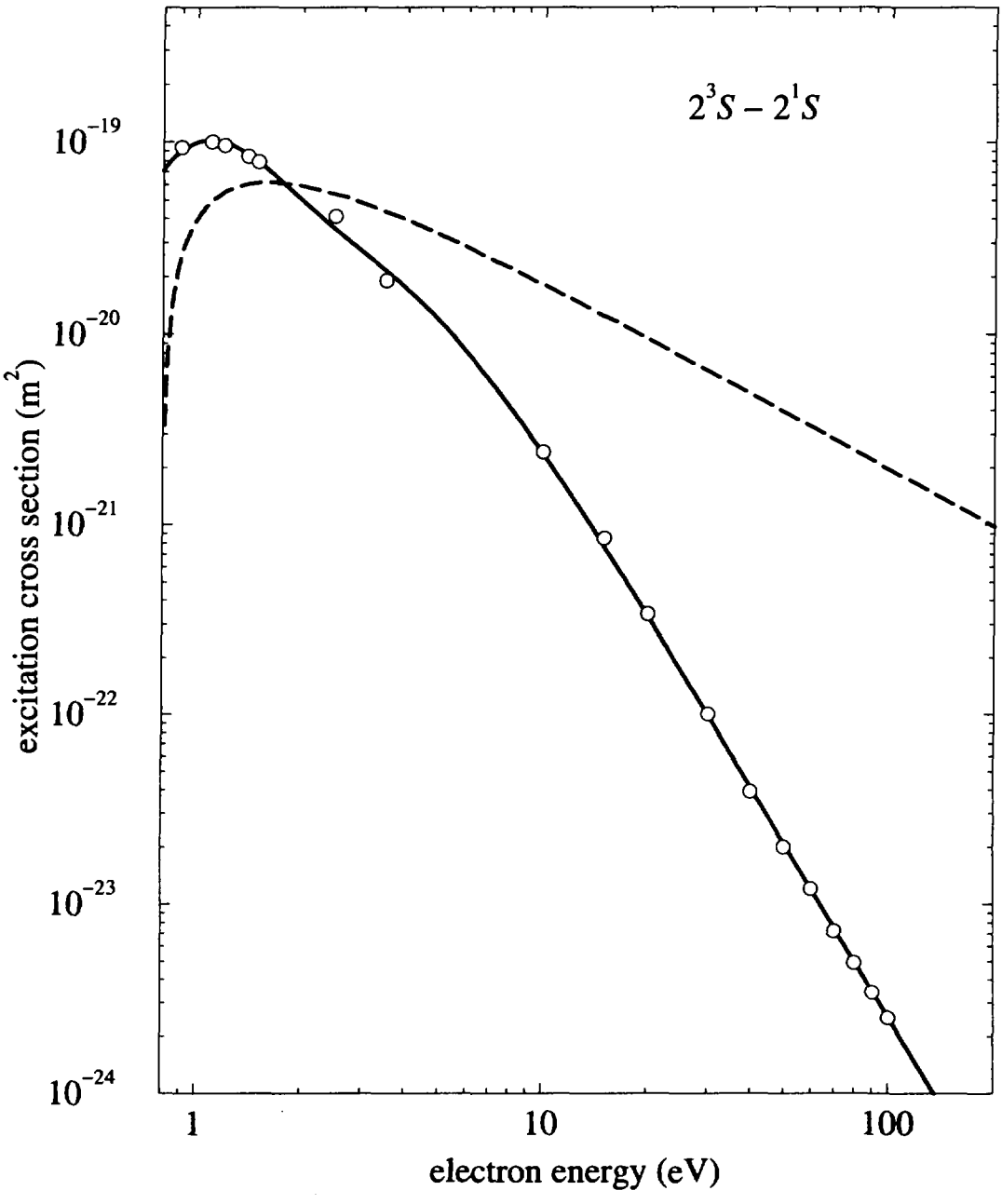

FIG. 20. Similar figure to Fig. 15 except that transition is $2^3S \rightarrow 2^1S$.

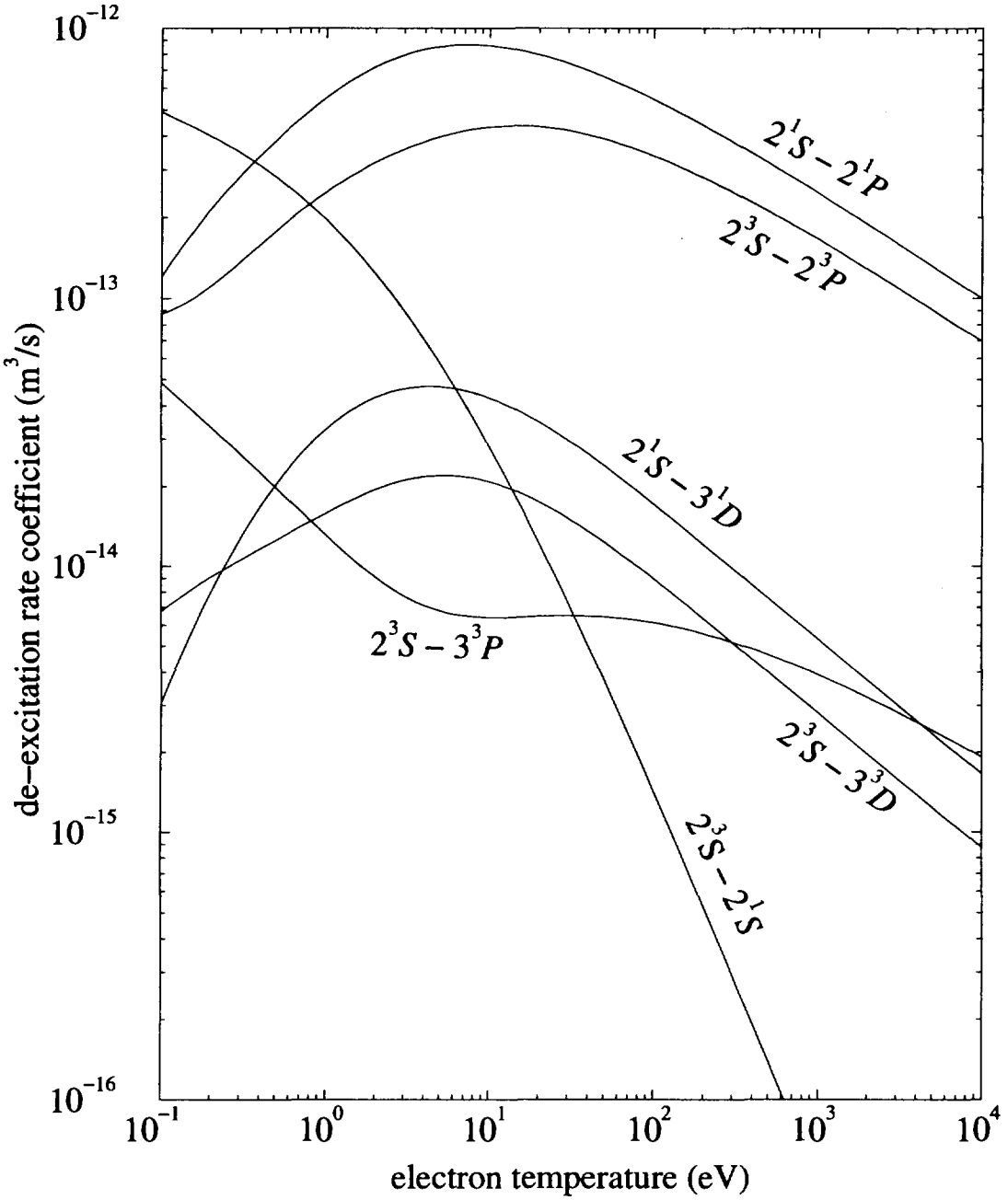

FIG. 21. De-excitation rate coefficient for $2^1S \leftarrow 2^1P, 3^1D, 2^3P, 3^3P, 3^3D$.

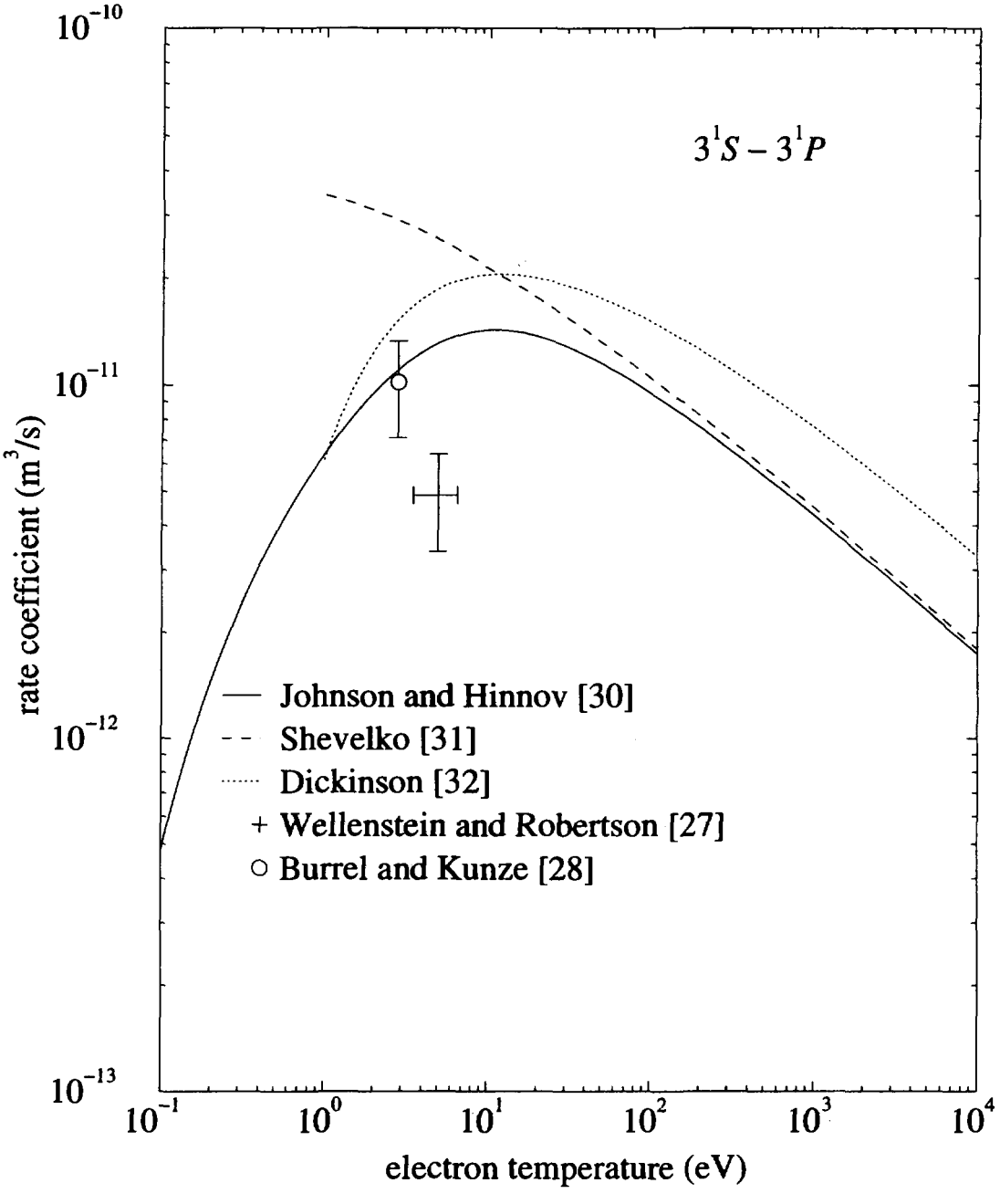

FIG. 22. Transition rate coefficient for $3^1S \rightarrow 3^1P$.

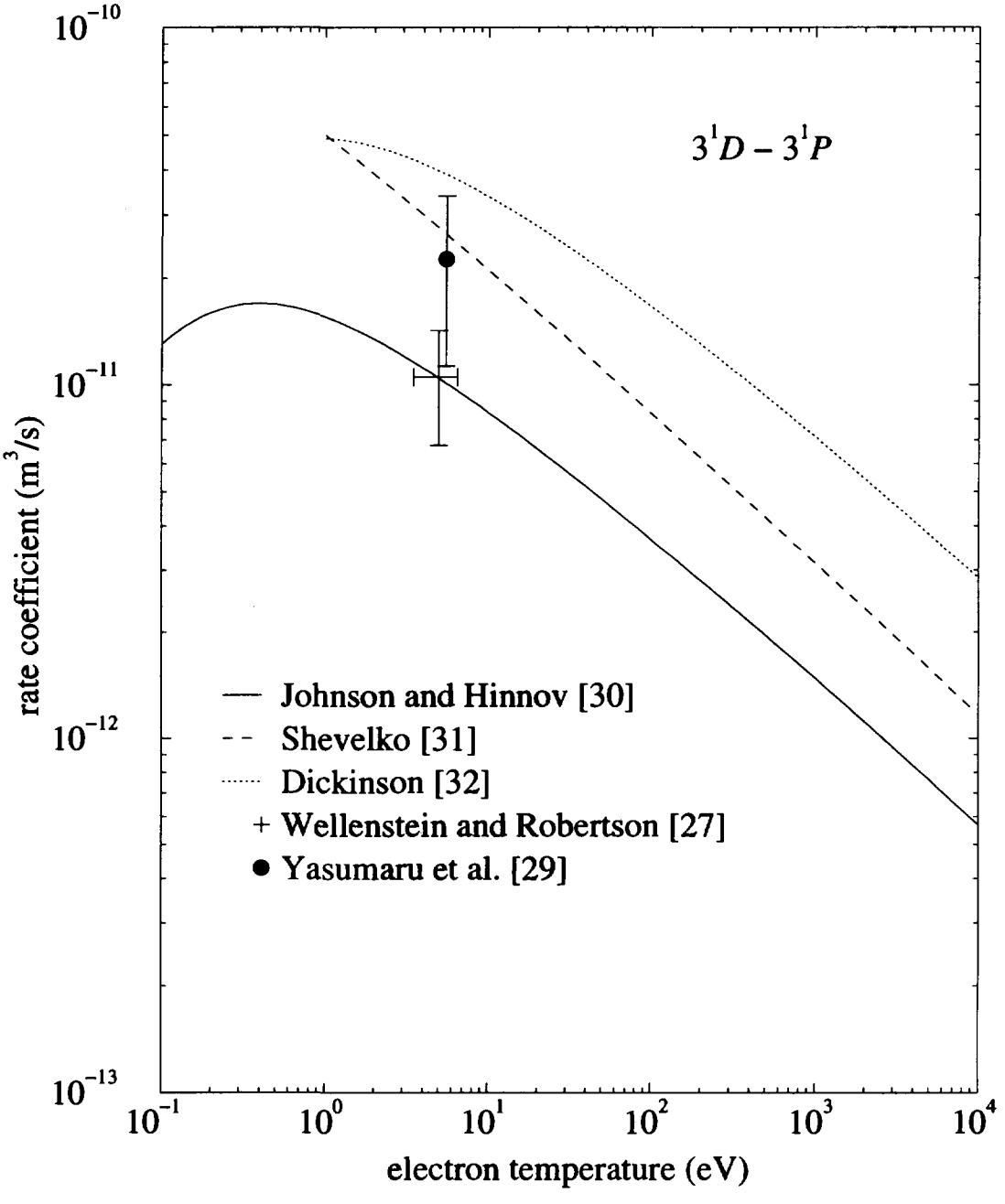

FIG. 23. Transition rate coefficient for $3^1D \rightarrow 3^1P$.

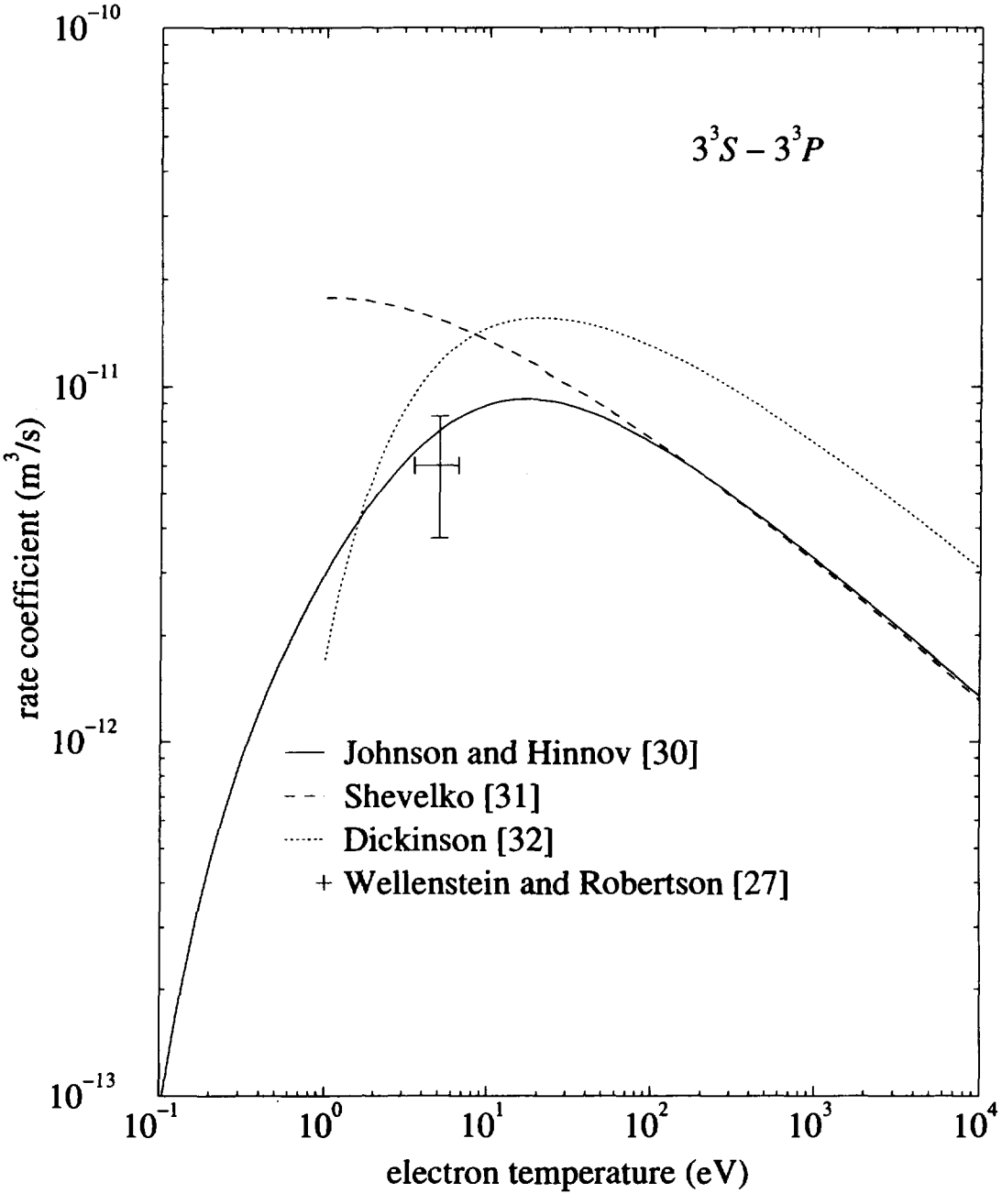

FIG. 24. Transition rate coefficient for $3^3S \rightarrow 3^3P$.

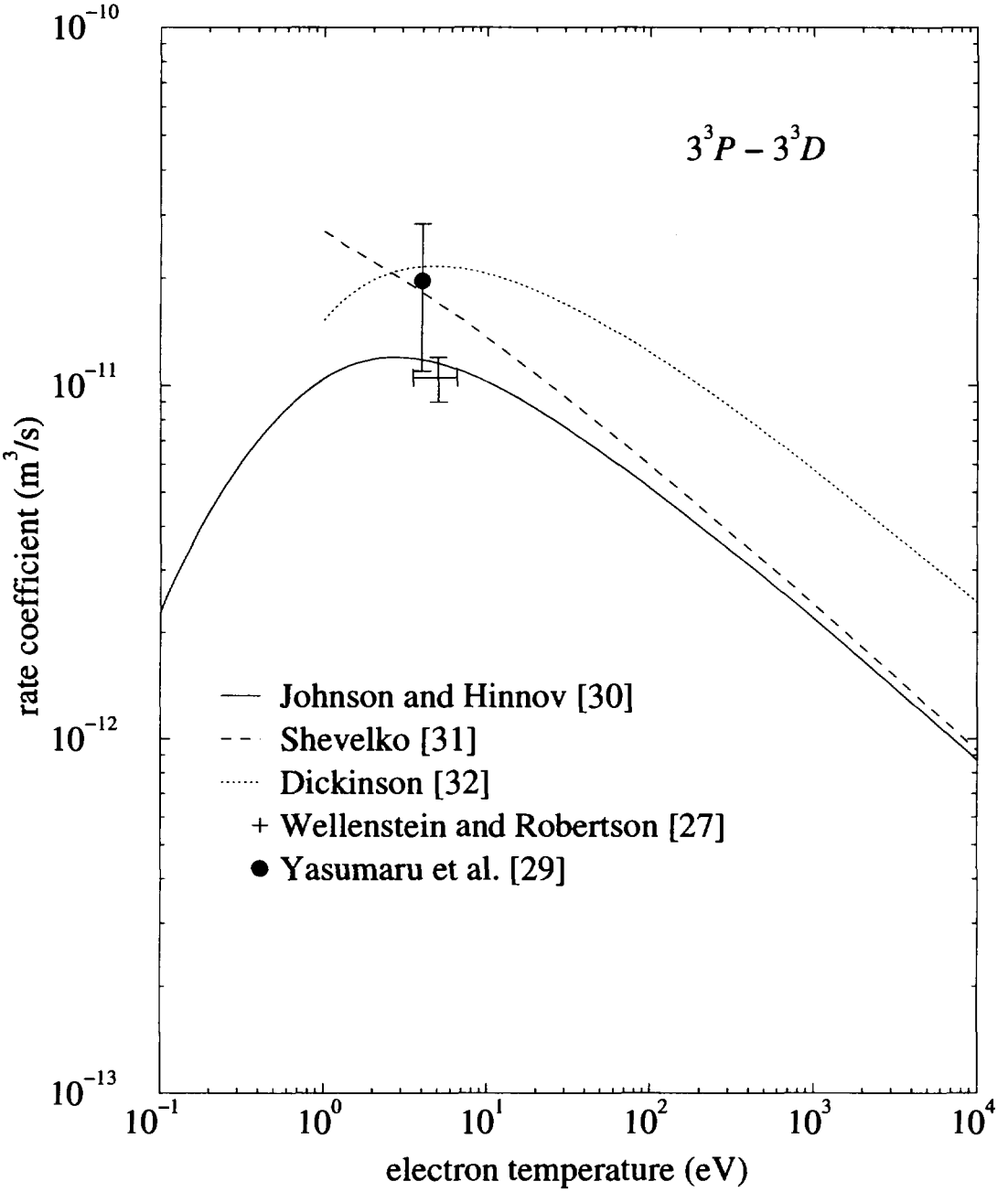

FIG. 25. Transition rate coefficient for $3^3P \rightarrow 3^3D$.

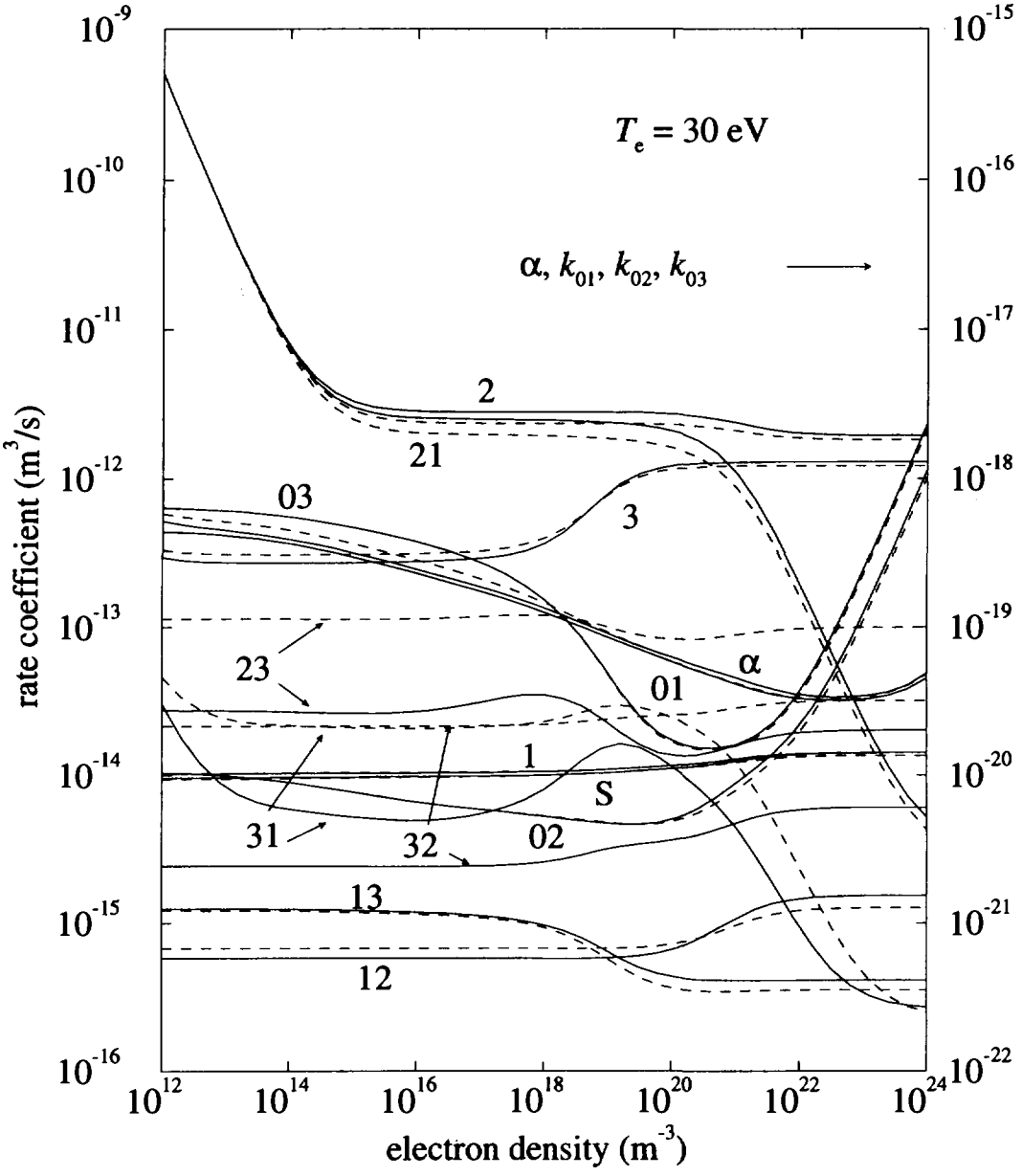

FIG. 26. Collisional-radiative coupling coefficients k's for T_e = 30 eV. Also shown are the collisional-radiative ionization rate coefficient S and the recombination rate coefficient α in formulation II. Dotted lines are from [1].

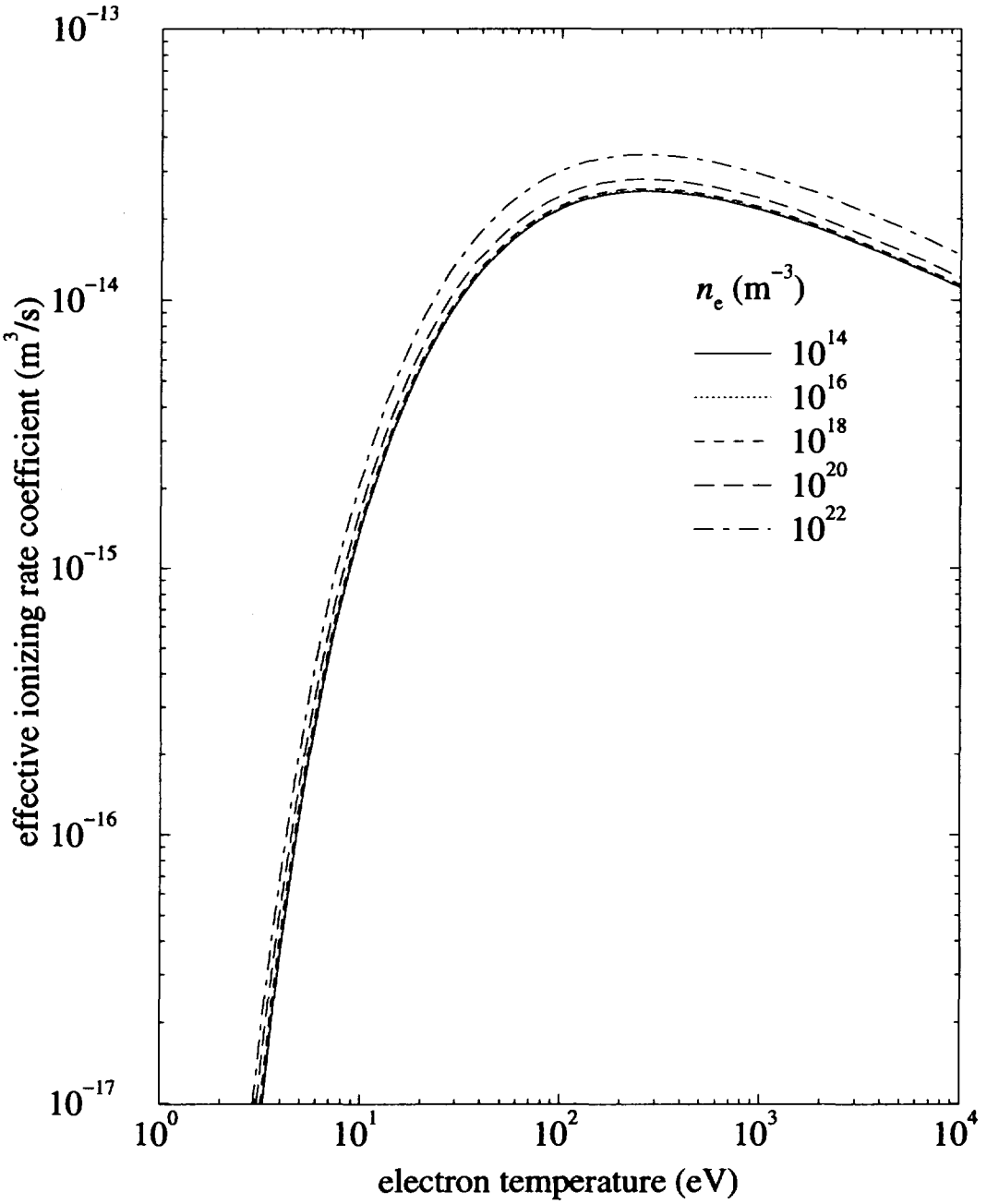

FIG. 27. Collisional-radiative ionization rate coefficient.

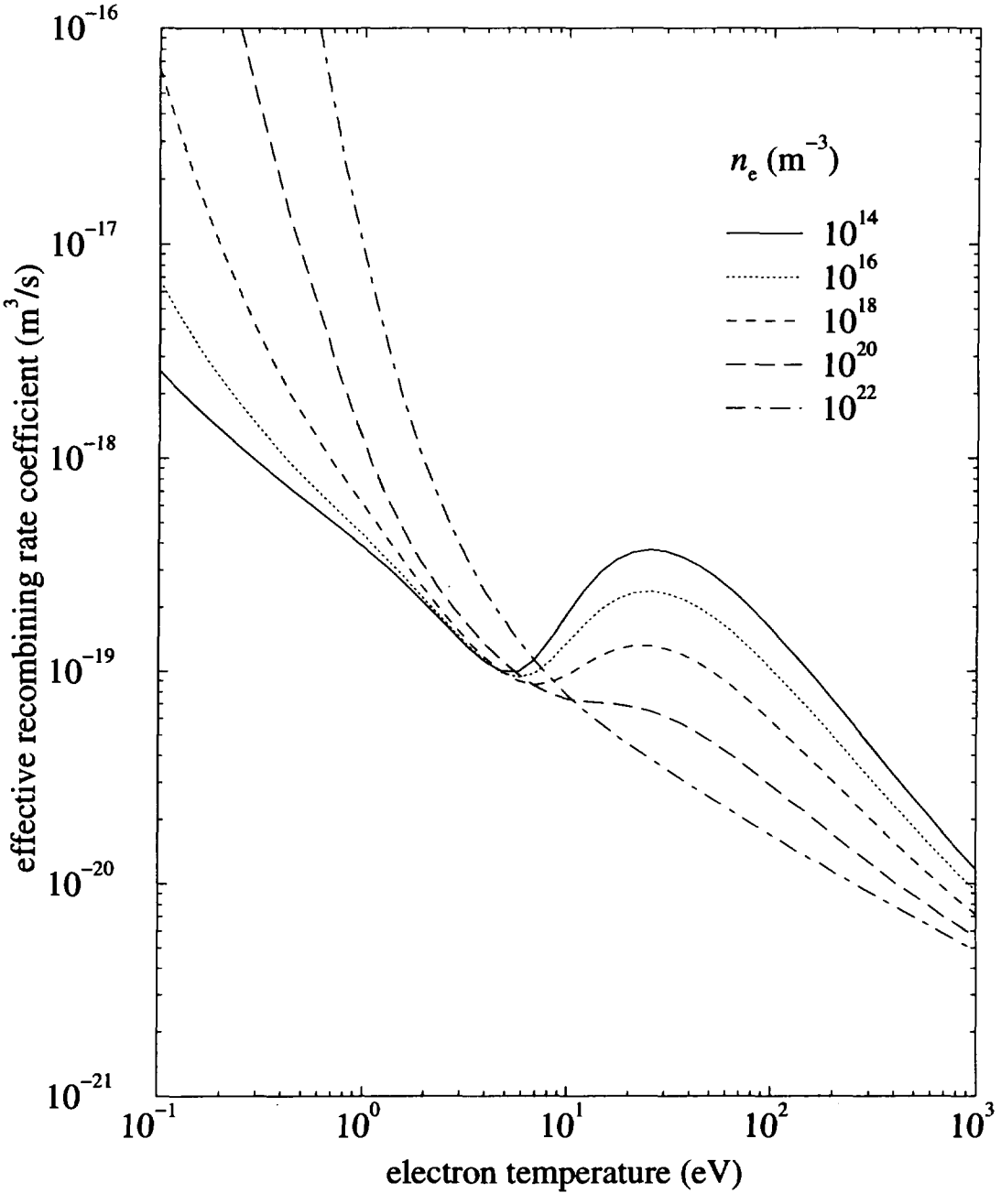

FIG. 28. Collisional-radiative recombining rate coefficient.

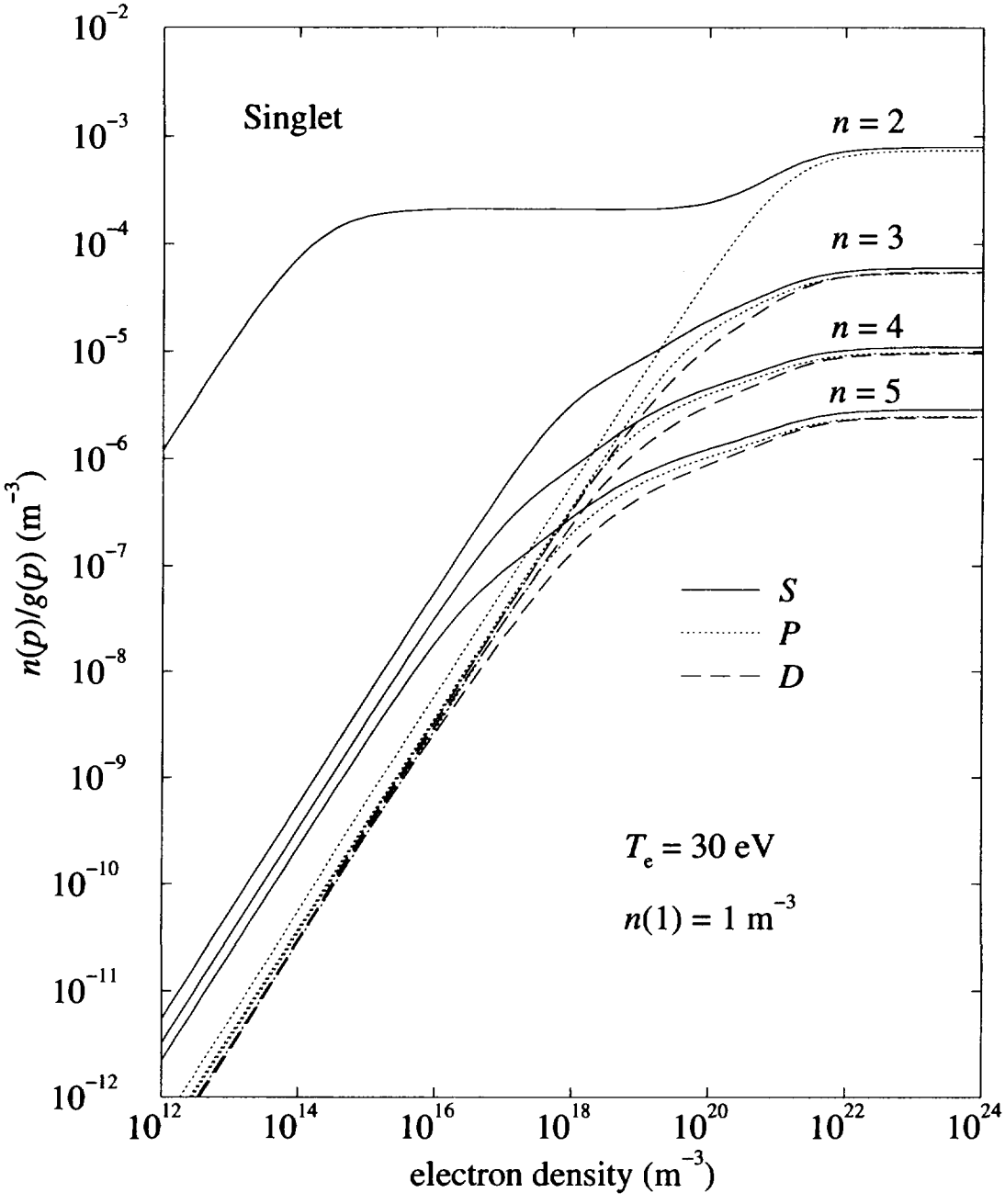

FIG. 29. The ionizing plasma component of the singlet excited level populations calculated in formulation II. $n(1^1S)$ and T_e are assumed to be 1 m^{-3} and 30 eV, respectively.

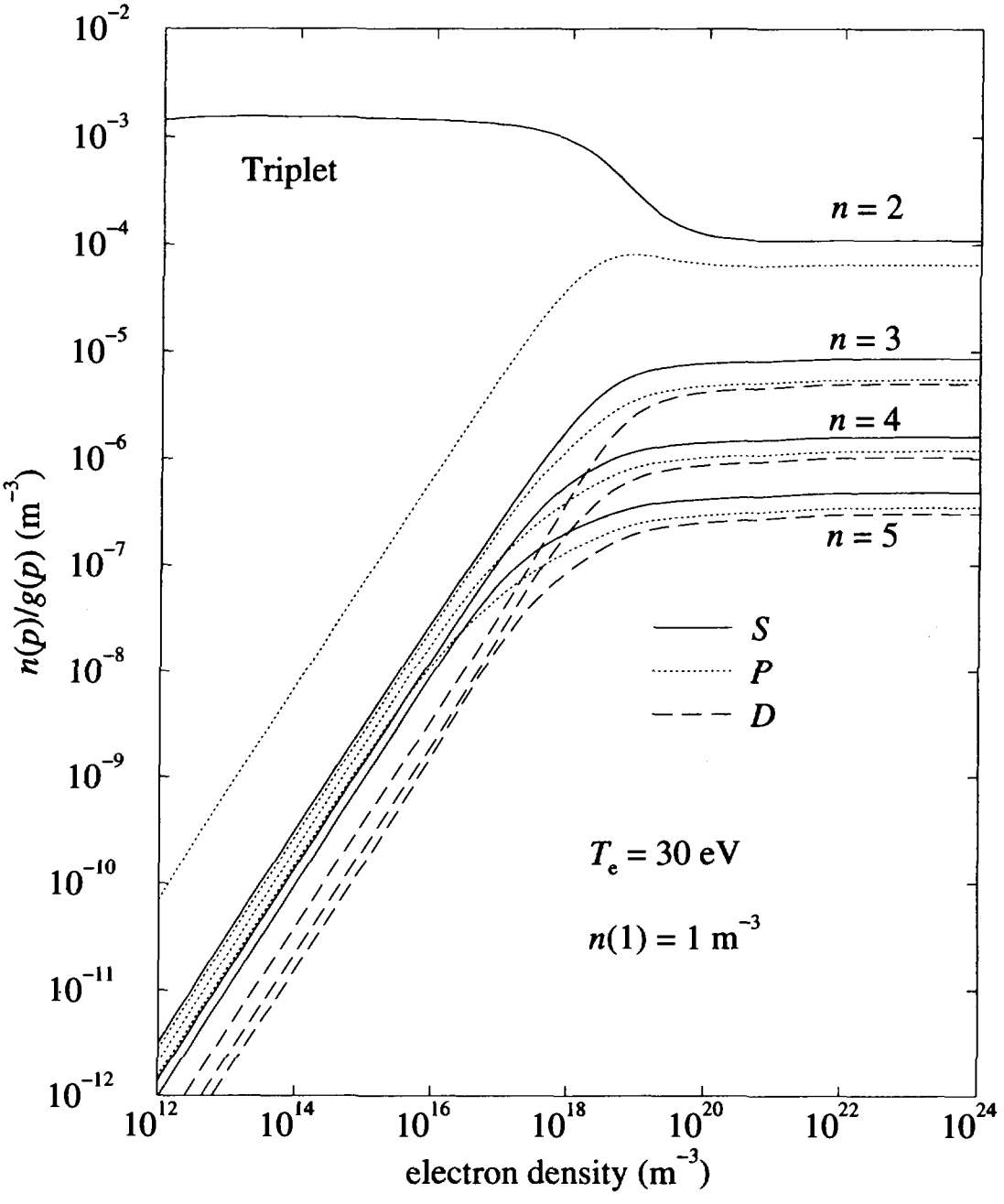

FIG. 30. The ionizing plasma component of the triplet excited level populations calculated in formulation I. $n(1^1S)$ and T_e are assumed to be 1 m^{-3} and 30 eV, respectively.

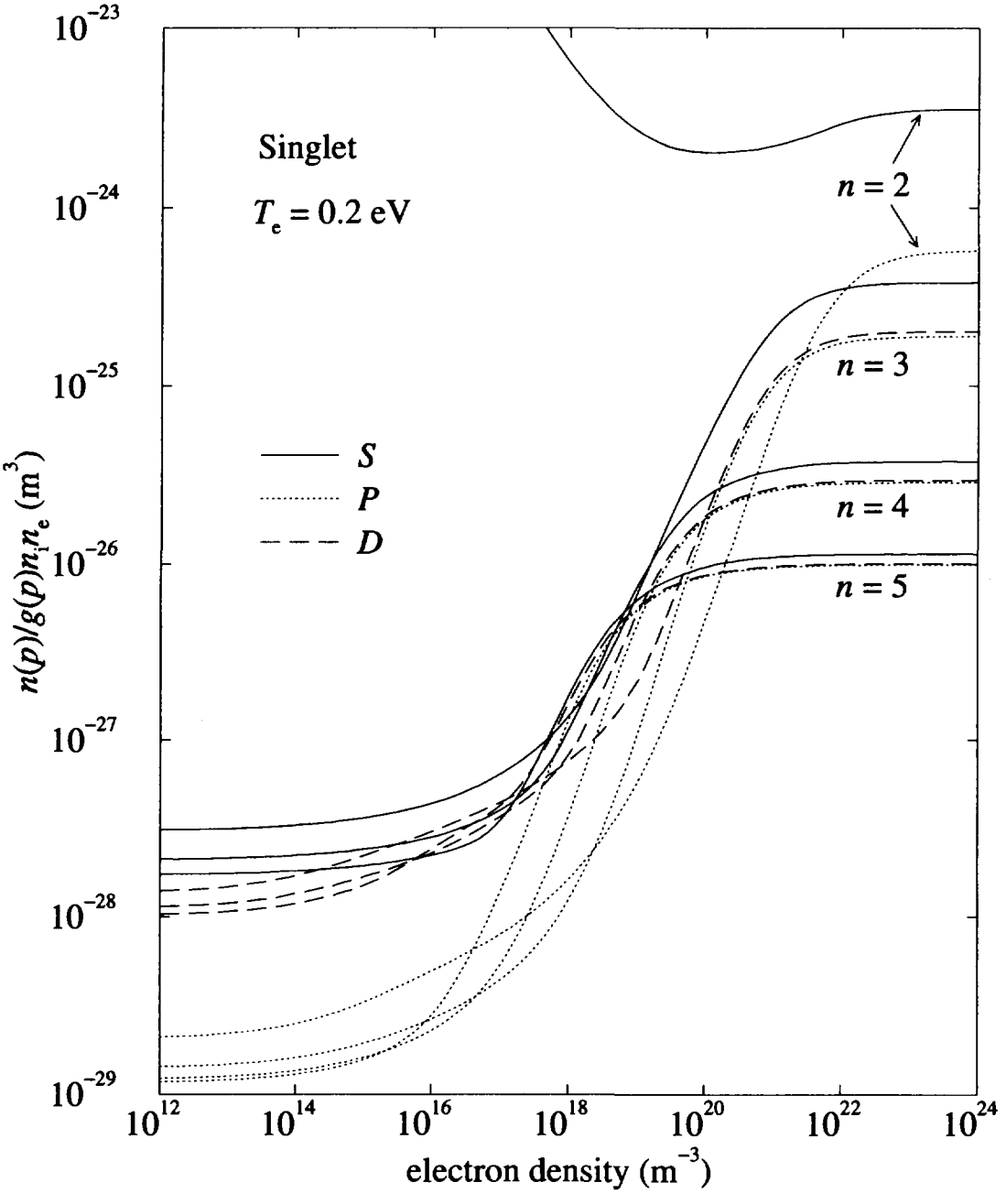

FIG. 31. The recombining plasma component of the singlet excited level populations calculated in formulation II. T_e is assumed to be 0.2 eV.

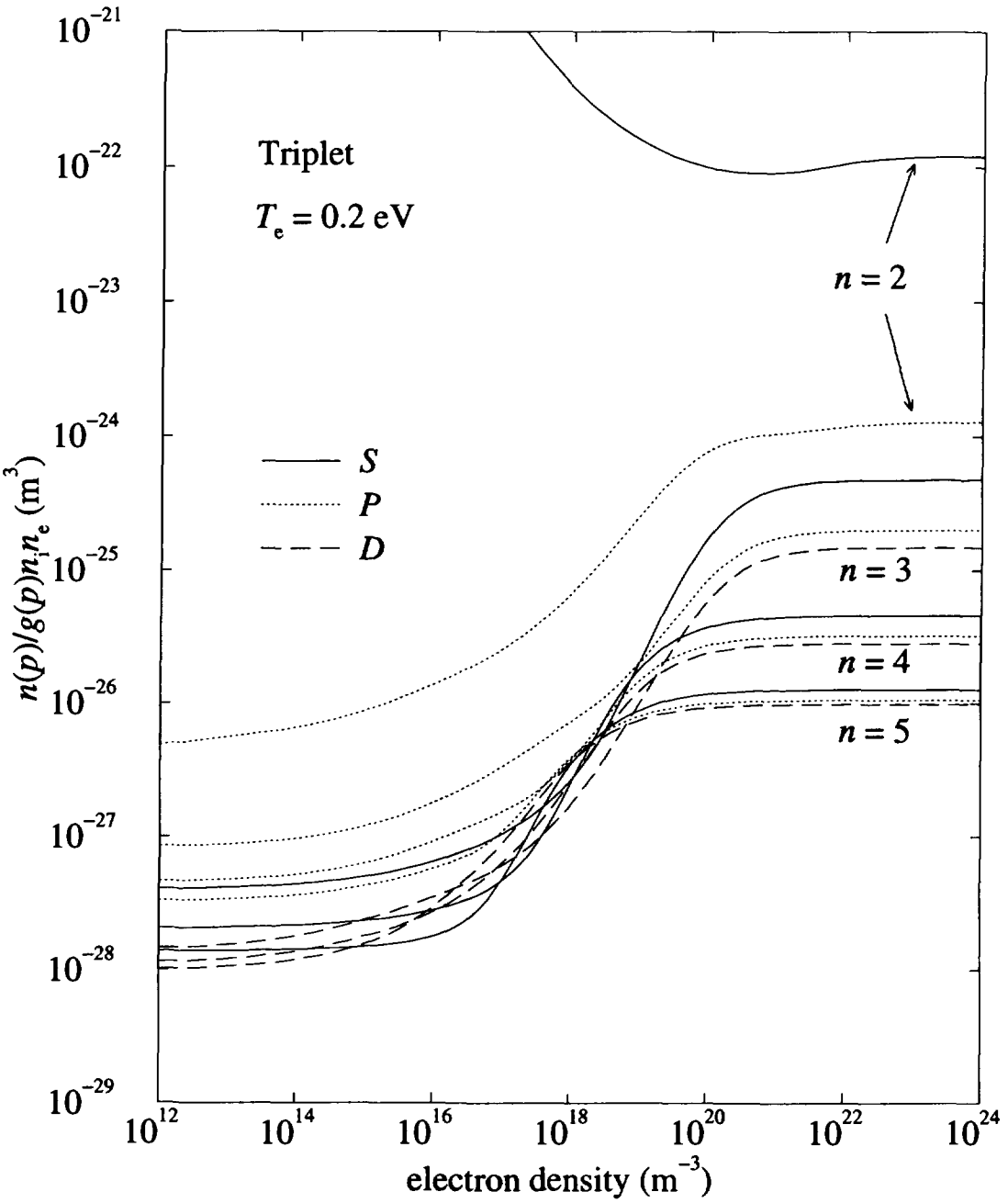

FIG. 32. The recombining plasma component of the triplet excited level populations calculated in formulation II. T_e is assumed to be 0.2 eV.

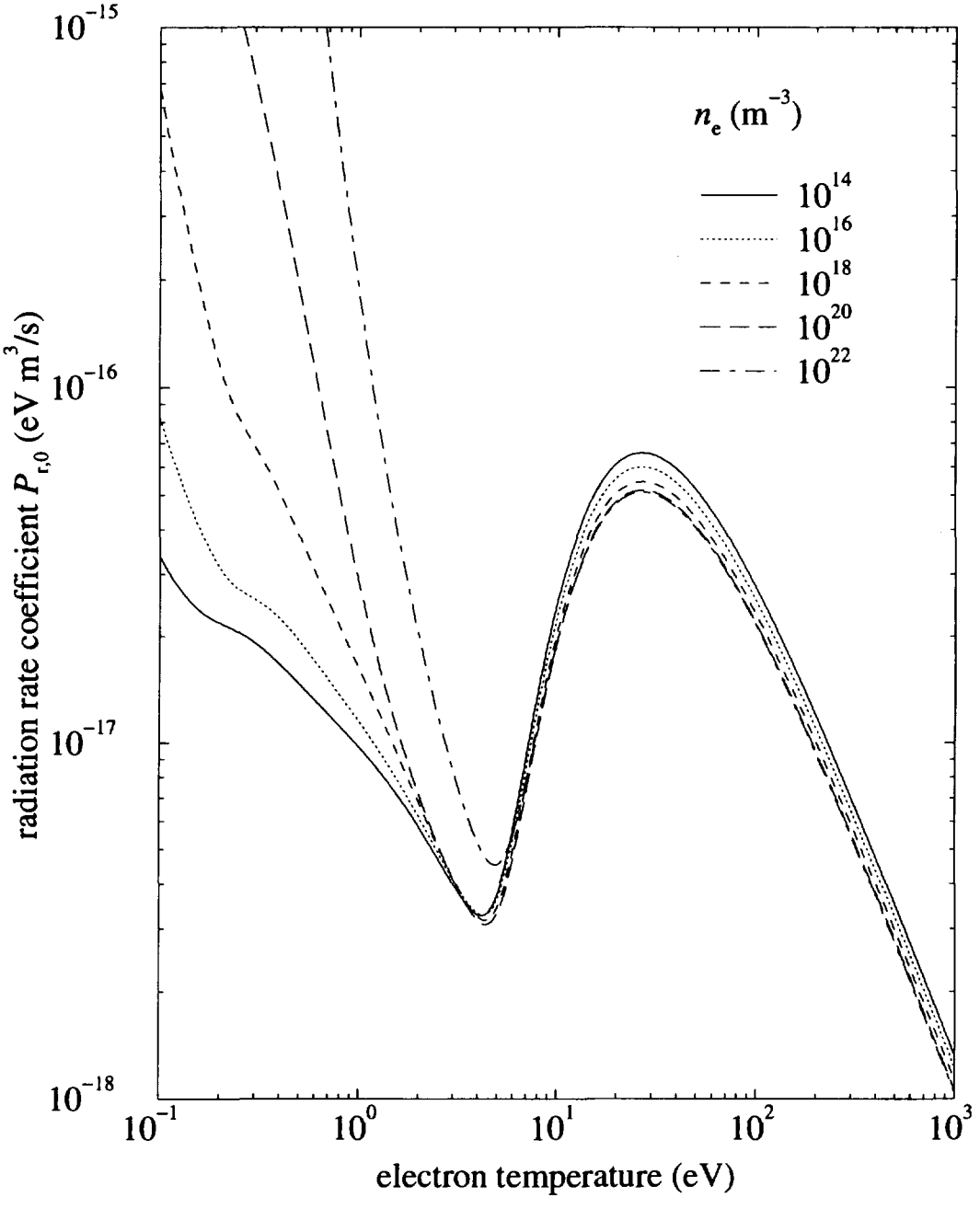

FIG. 33. Radiation loss rate coefficient (eV·m^3/s) for the recombining plasma component.

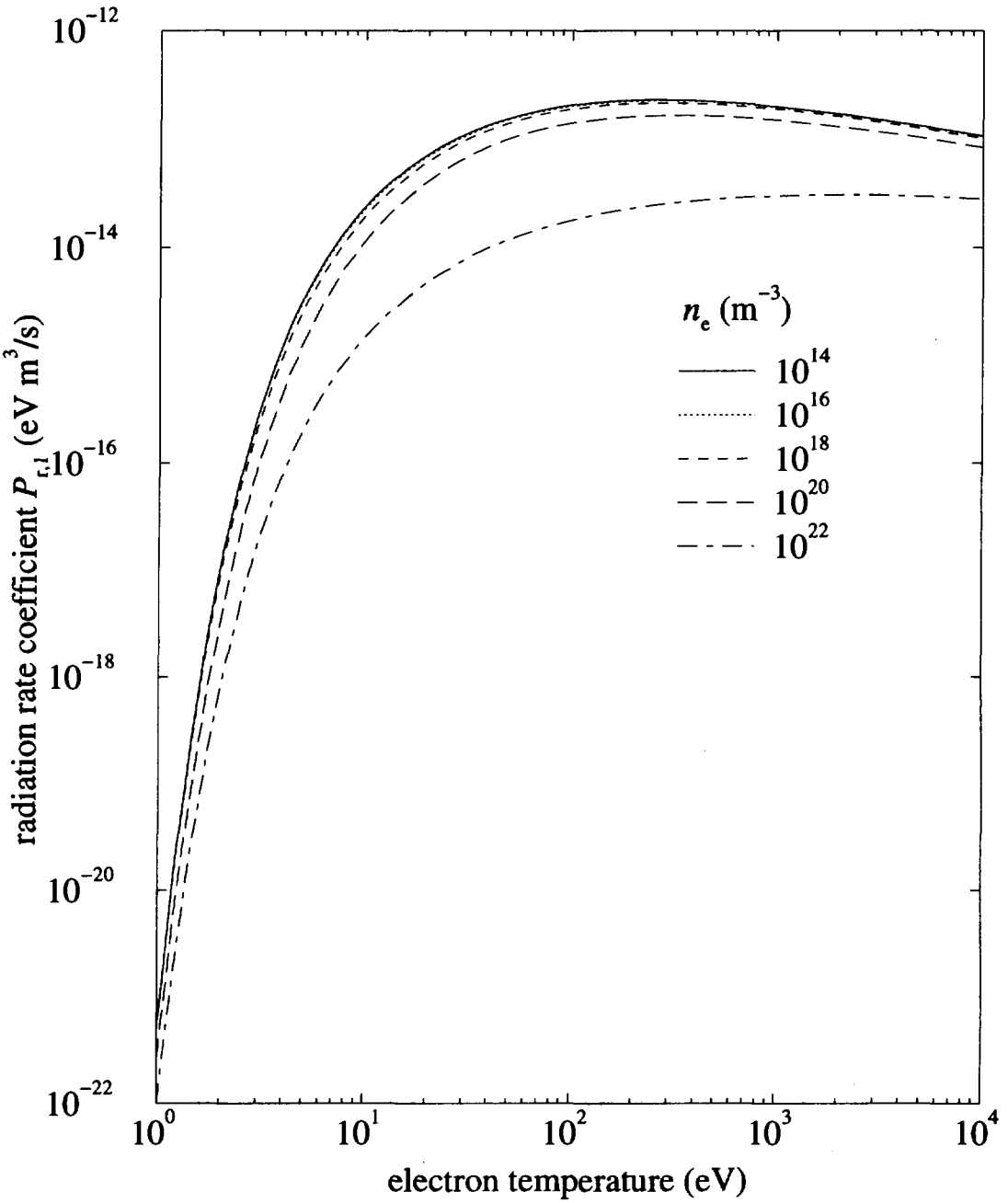

FIG. 34. Radiation loss rate coefficient (eV·m^3/s) for the ionizing plasma component.

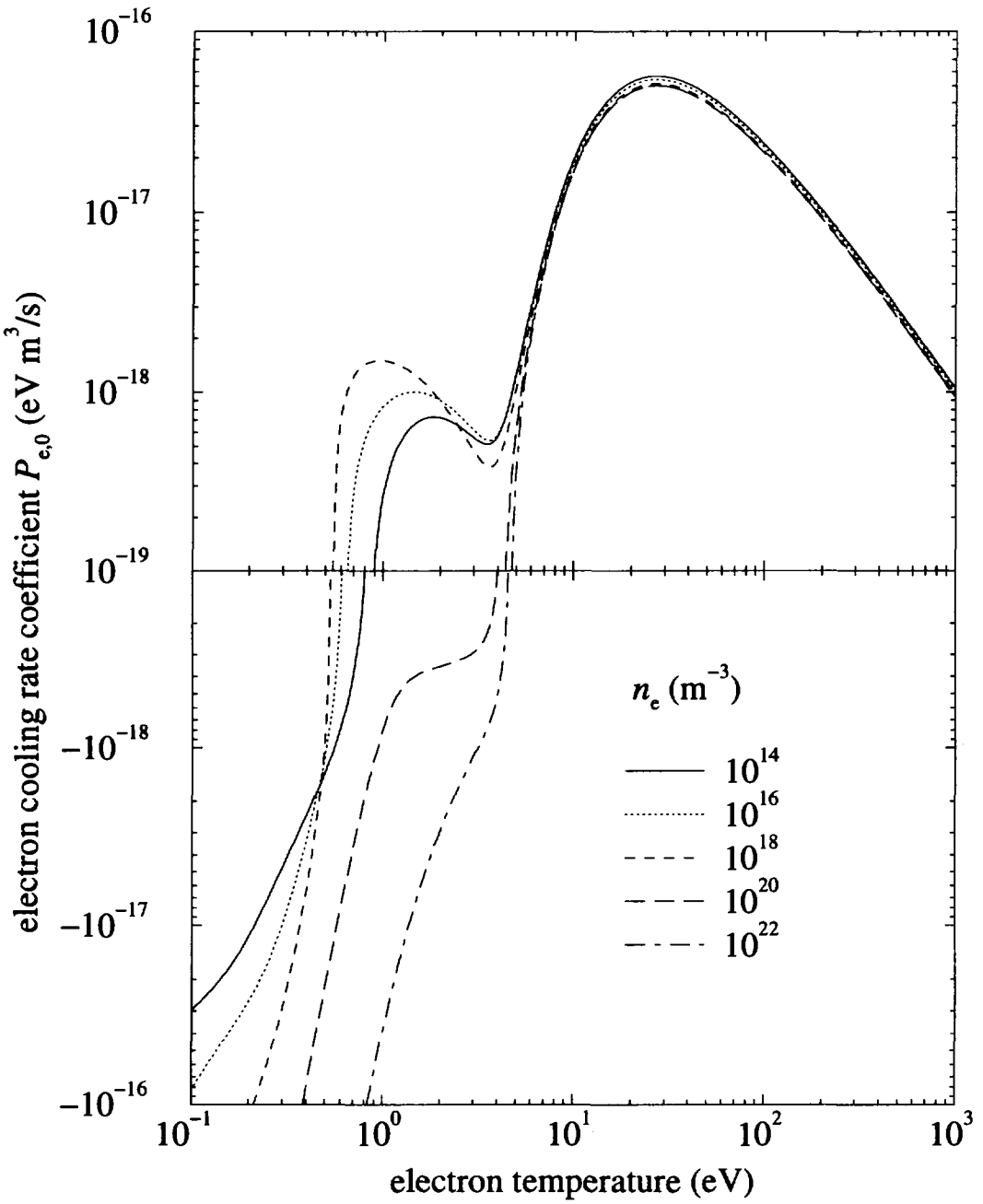

FIG. 35. Electron cooling rate coefficient (eV · m^3/s) for the recombining plasma component. The negative value means the electron heating due to the electron impact de-excitation and three-body recombination.

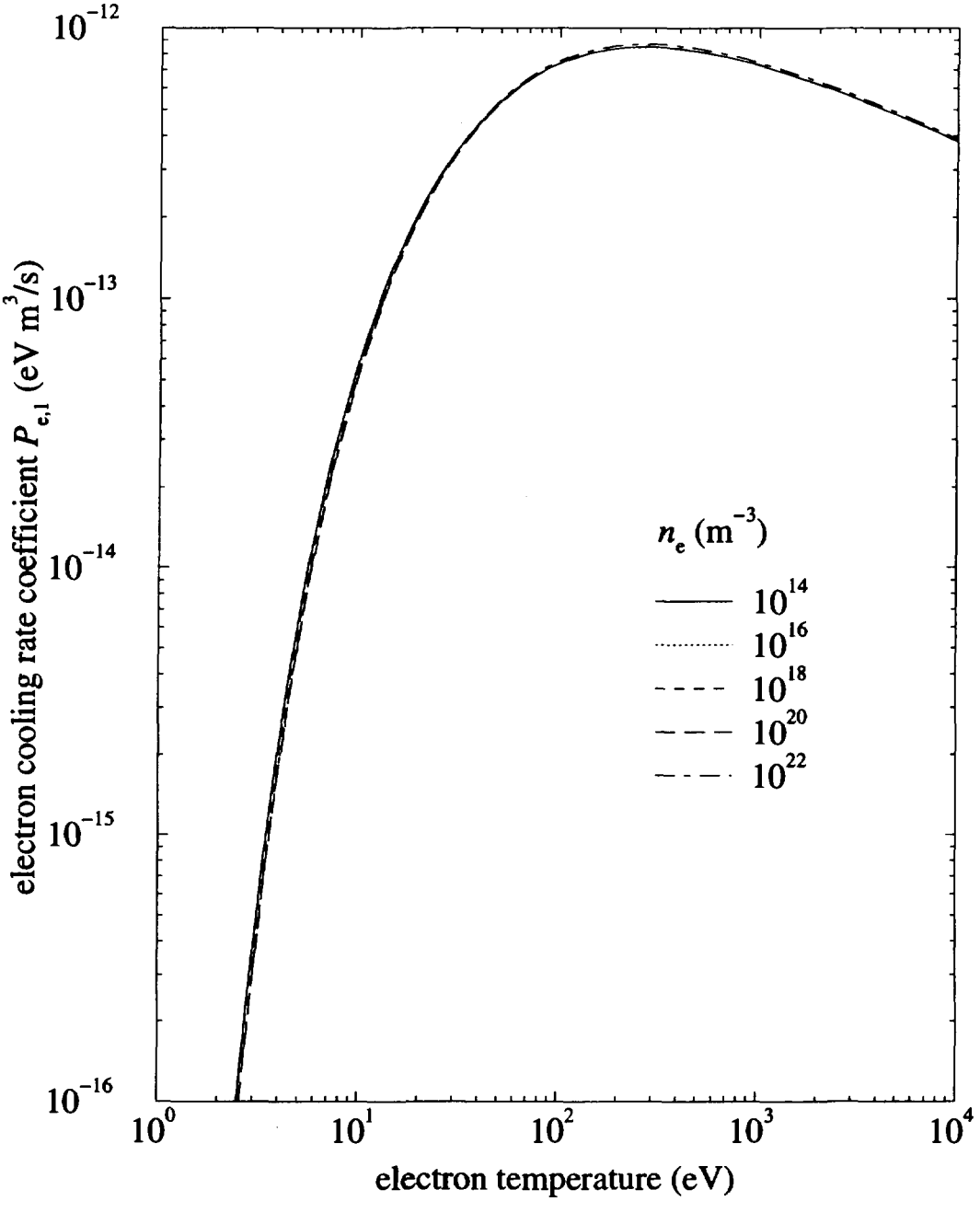

FIG. 36. Electron cooling rate coefficient (eV · m^3/s) for the ionizing plasma component.

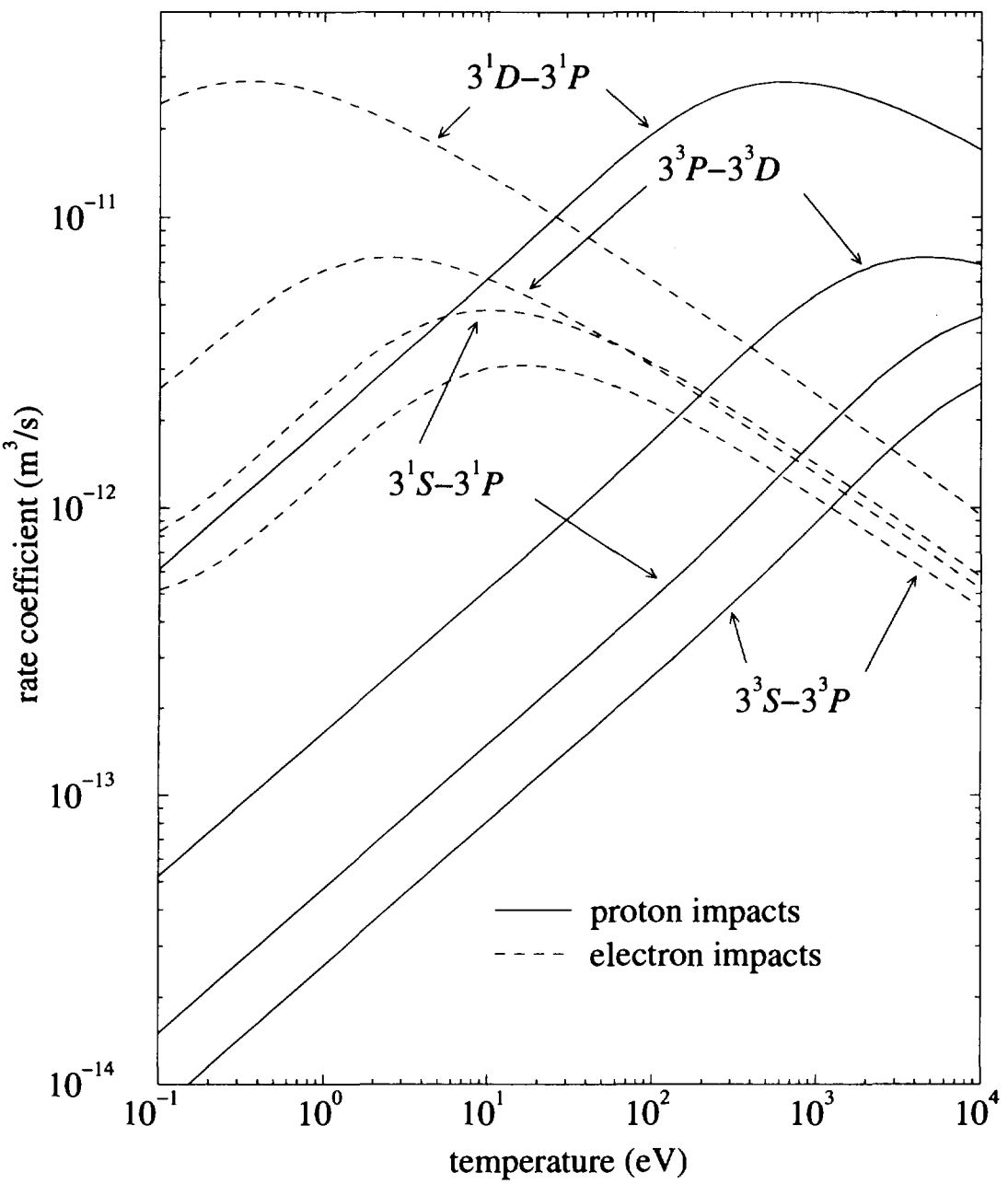

FIG. 37. Rate coefficient for $3^1S \leftarrow 3^1P$, $3^1D \leftarrow 3^1P$, $3^3S \leftarrow 3^3P$ and $3^3P \leftarrow 3^3D$ transitions.

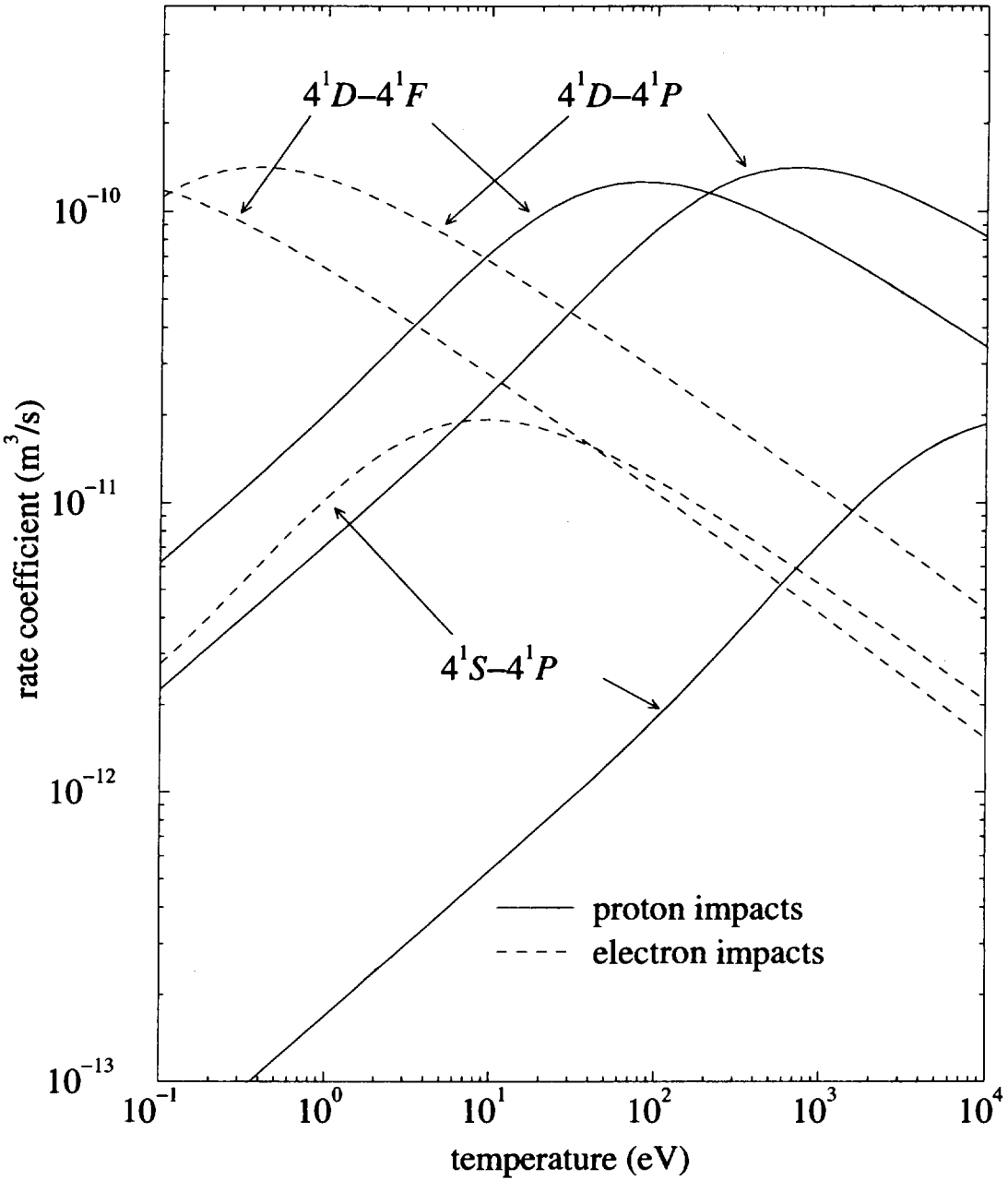

FIG. 38. Rate coefficient for $4^1S \leftarrow 4^1P$, $4^1D \leftarrow 4^1P$ and $4^1D \leftarrow 4^1F$ transitions.

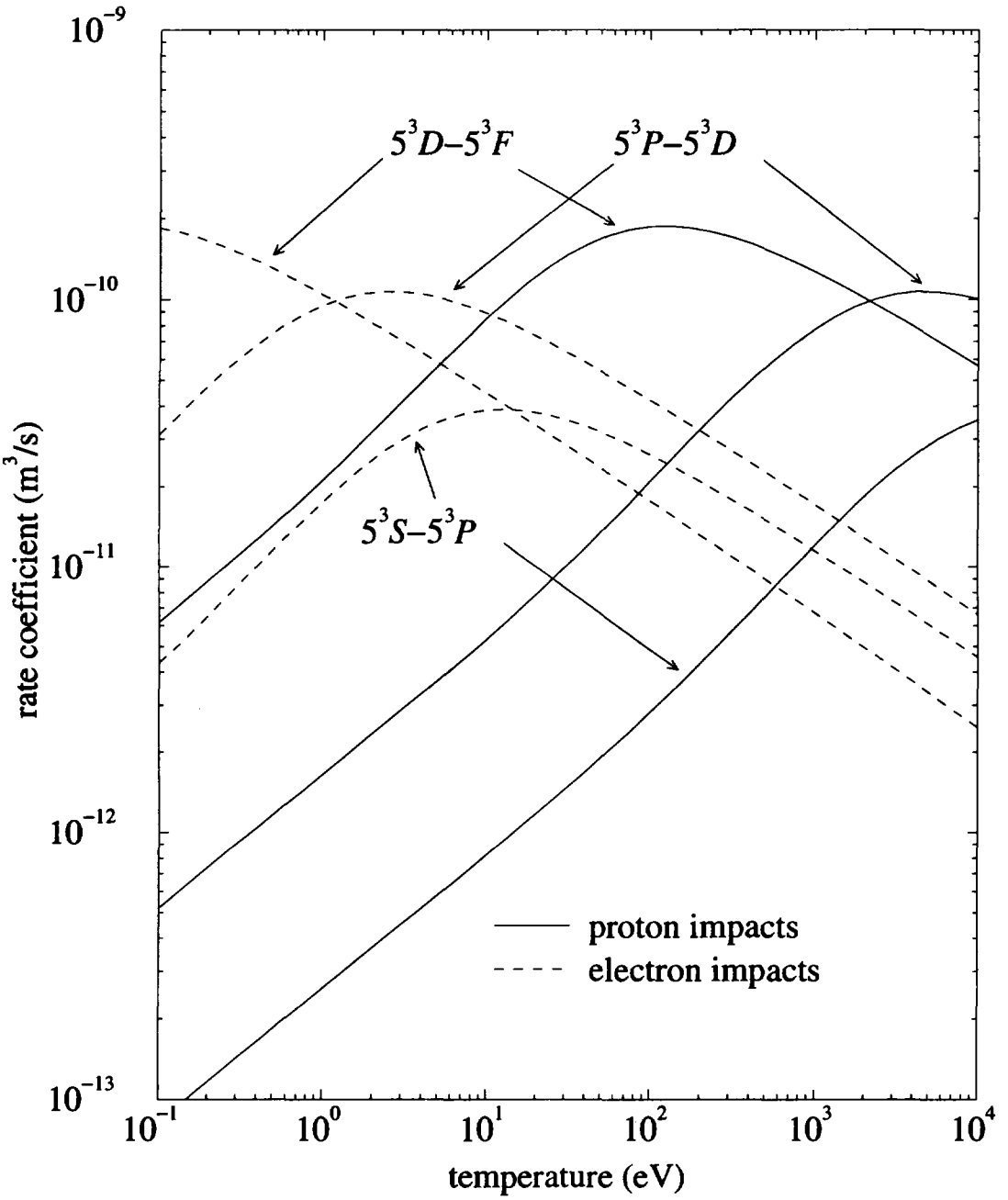

FIG. 39. Rate coefficient for $5^3S \leftarrow 5^3P$, $5^3P \leftarrow 5^3D$ and $5^3D \leftarrow 5^3F$ transitions.

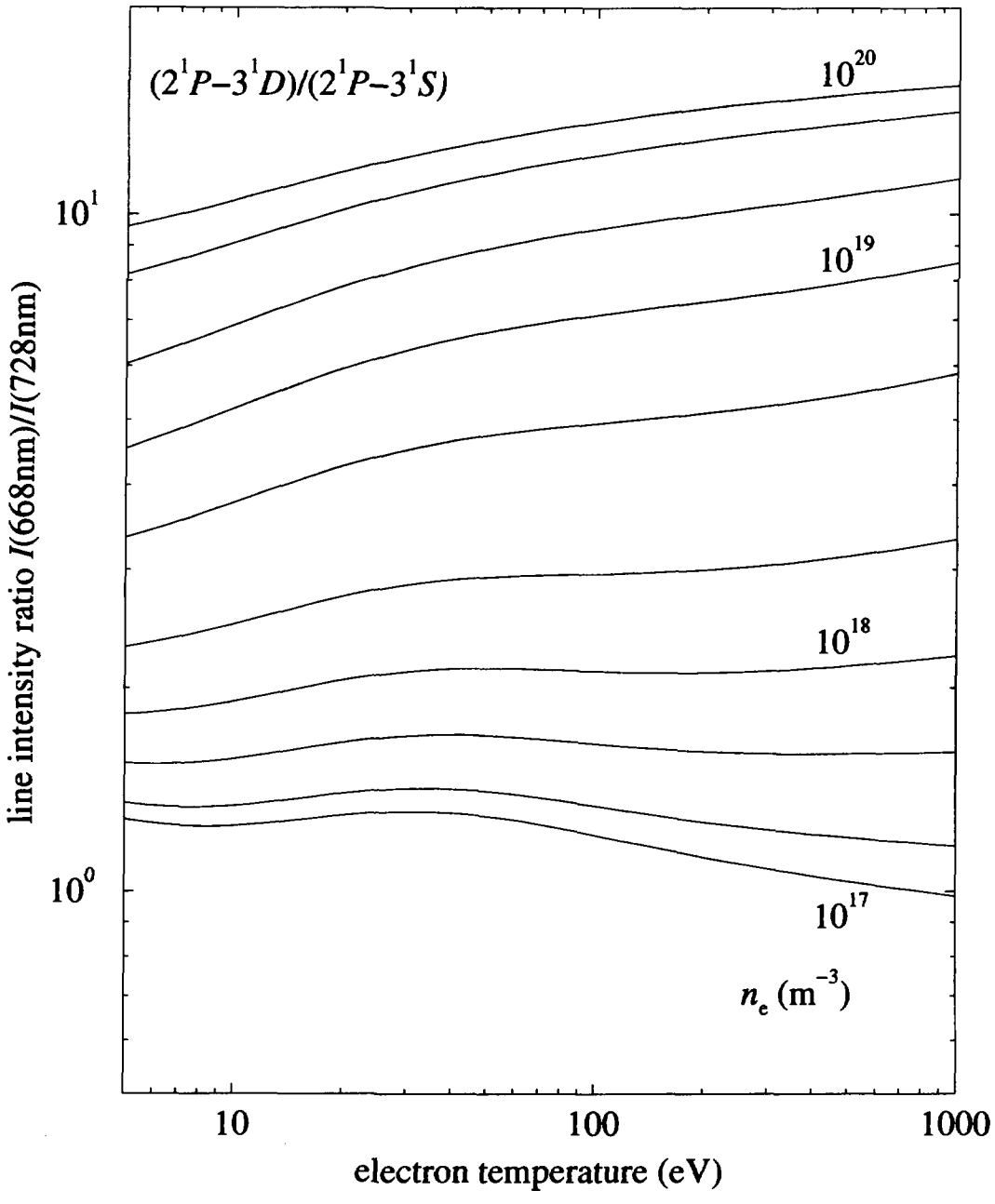

FIG. 40. The line intensity ratio of the transitions, $2^1P \leftarrow 3^1D$ to $2^1P \leftarrow 3^1S$ for the measurment of the electron density. The density is changed by 1, 2, 5, 10 steps. They are calculated in formulation II.

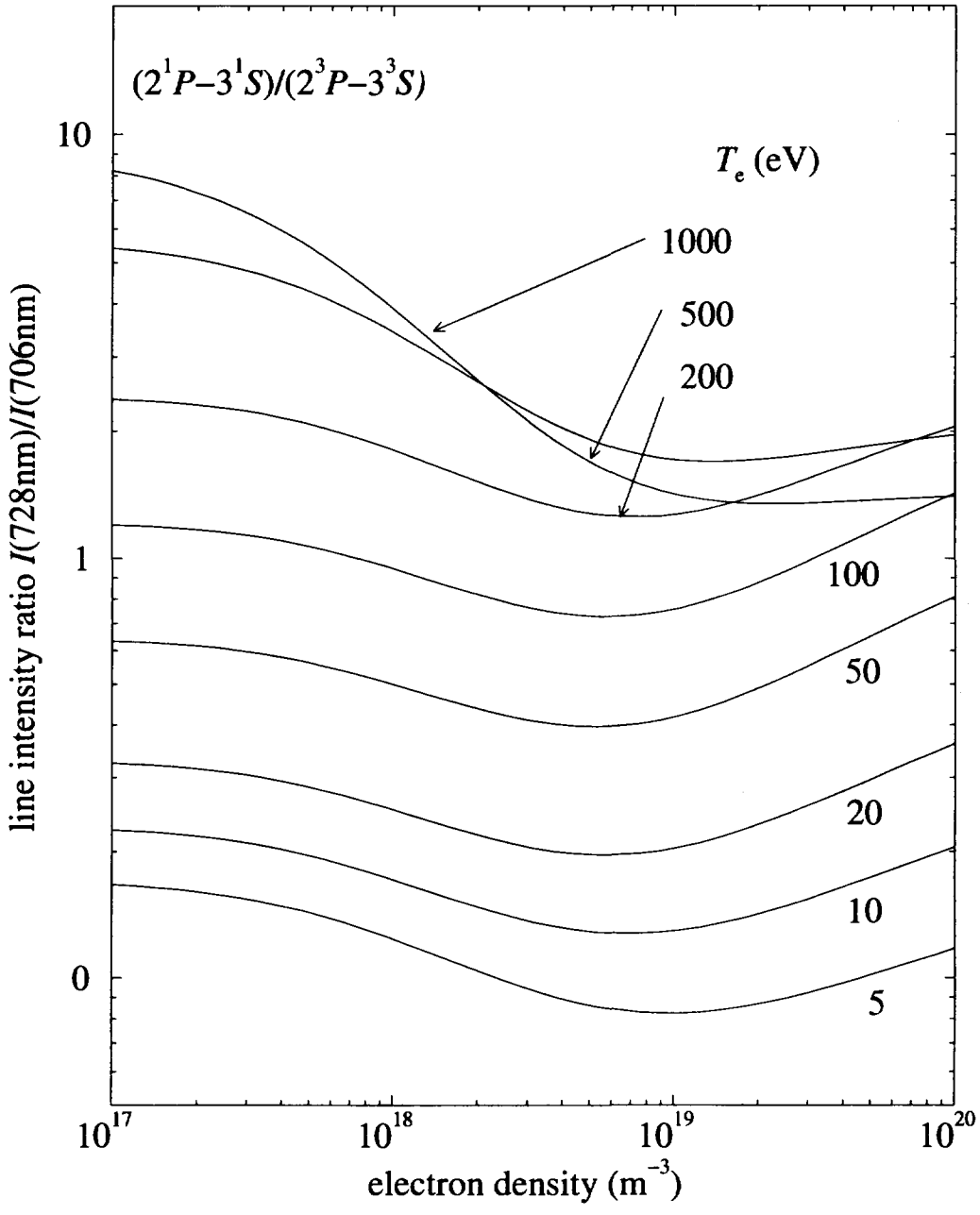

FIG. 41. The line intensity ratio of the transitions, $2^1P \leftarrow 3^1S$ to $2^3P \leftarrow 3^3S$ for the measurment of the electron temperature. They are calculated in formulation II.

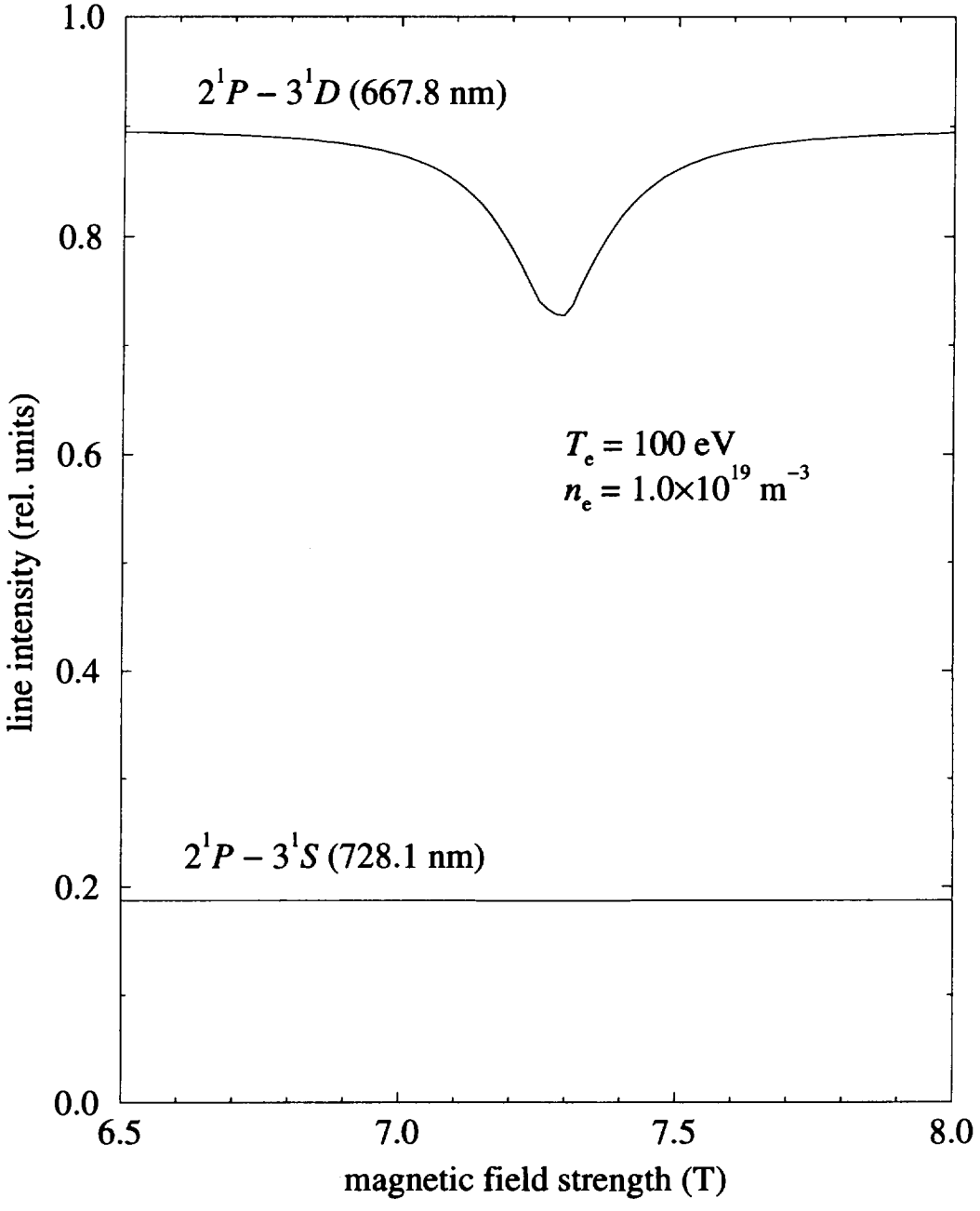

FIG. 42. The magnetic field dependence of the line intensities for the transitions, $2^1P \leftarrow 3^1D$ and $2^1P \leftarrow 3^1S$. This ratio is sometimes adopted for the electron density measurement.

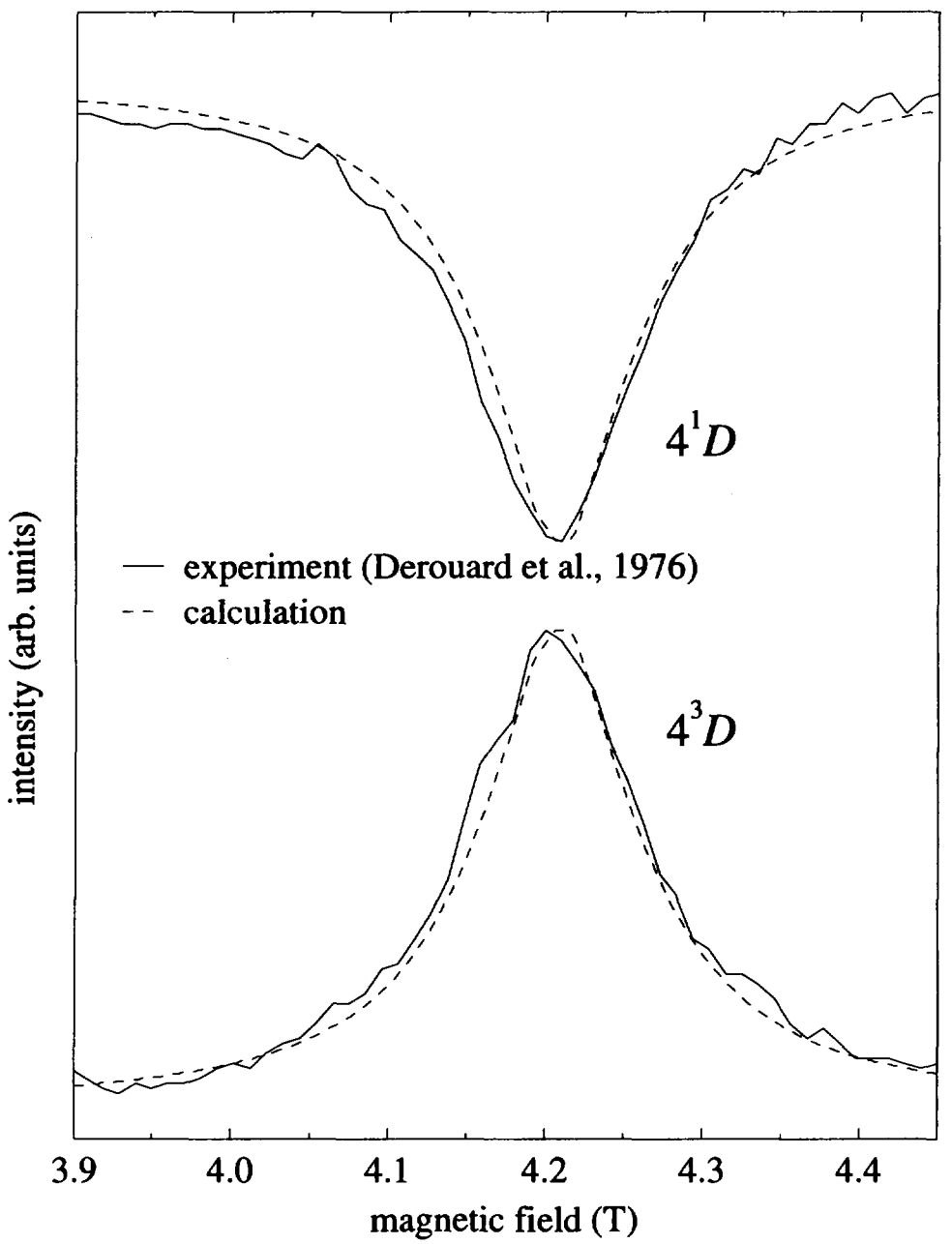

FIG. 43. The magnetic field dependence of the line intensities for the transitions, $2^1P \leftarrow 4^1D$ and $2^3P \leftarrow 4^3D$. —— : experiment [36].

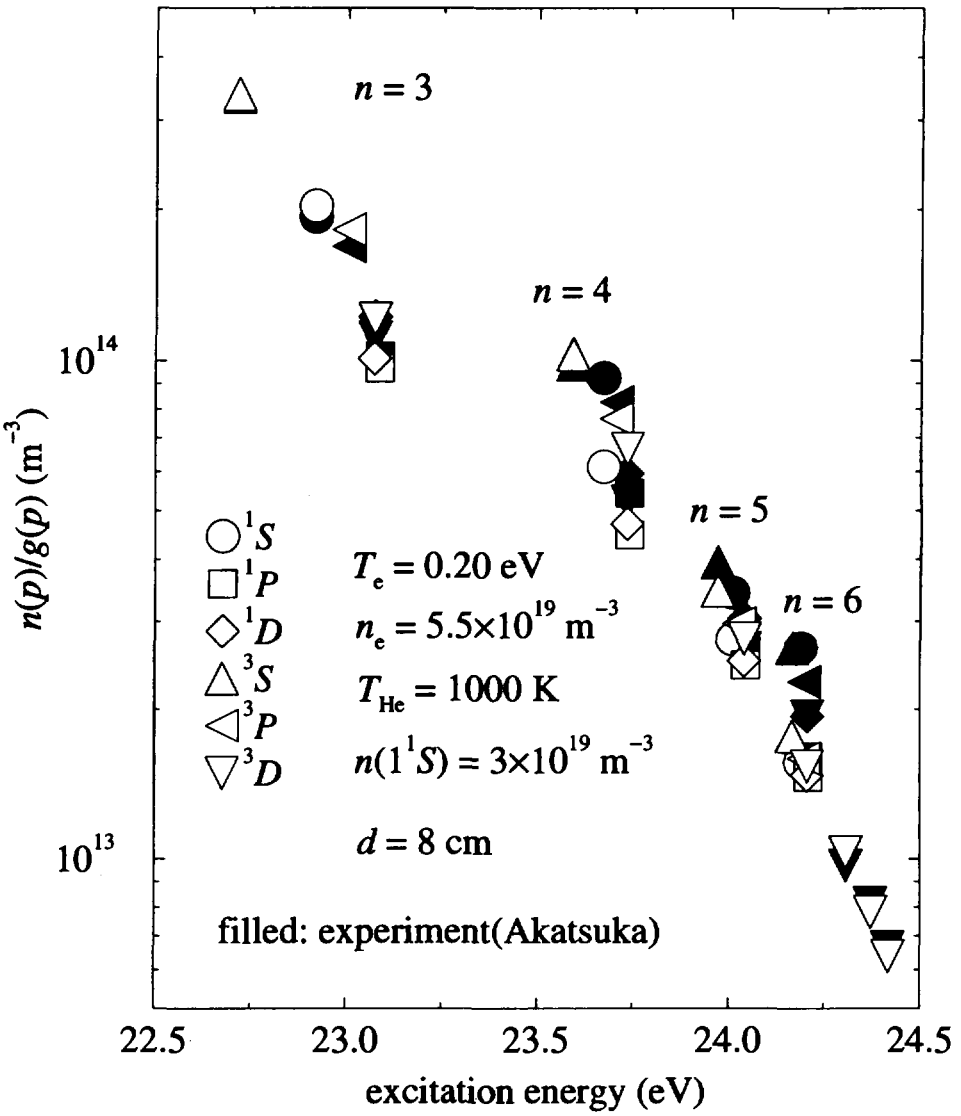

FIG. 44a. The excited level populations obtained from the afterglow plasma experiment [37]. They are compared with the present CR model calculation. The calculated results are shown with the open symbols.

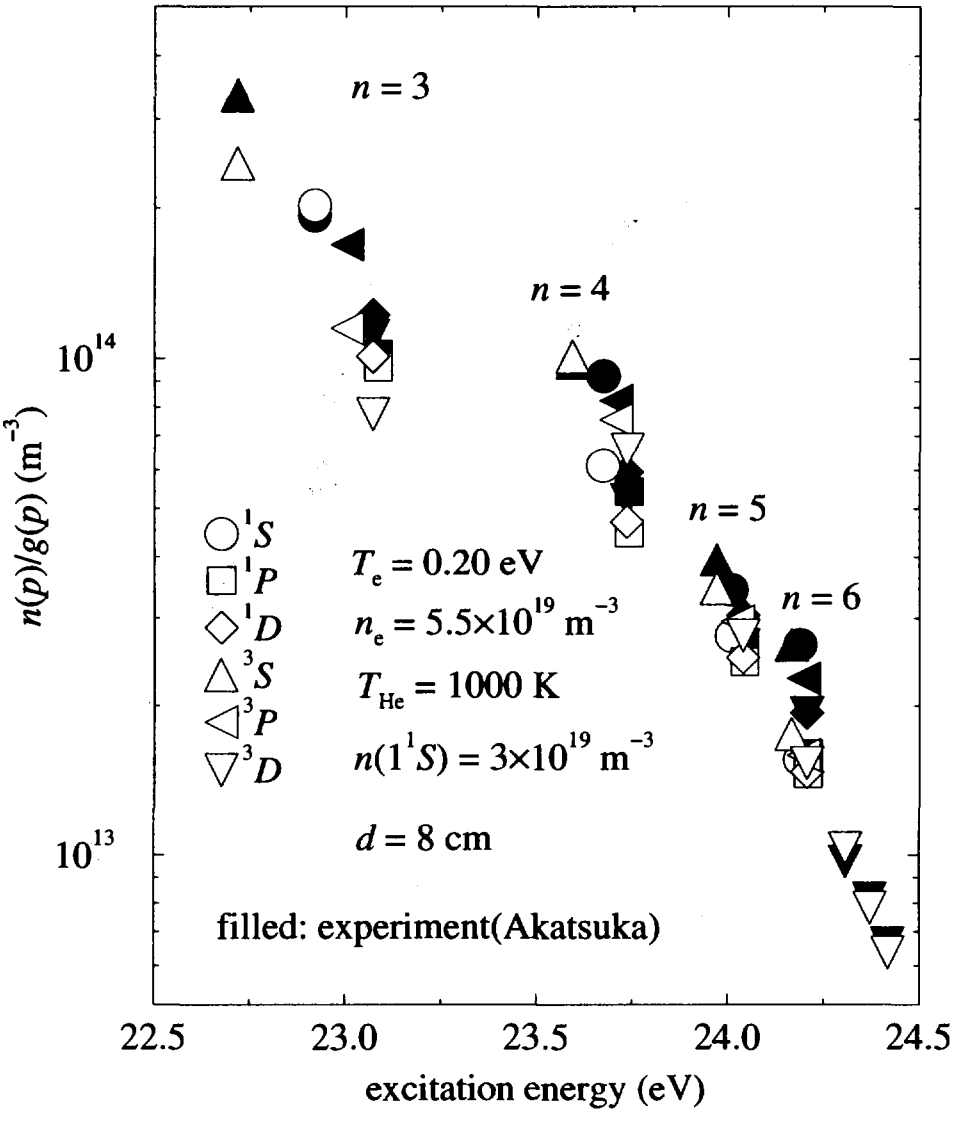

FIG. 44b. The experimental results are the same as the previous one. The calculation is done with the upper bound cross section for the $2^3S \rightarrow 3^3P$ (Fig. 12) and $2^3S \rightarrow 3^3D$ (Fig. 13) transitions.

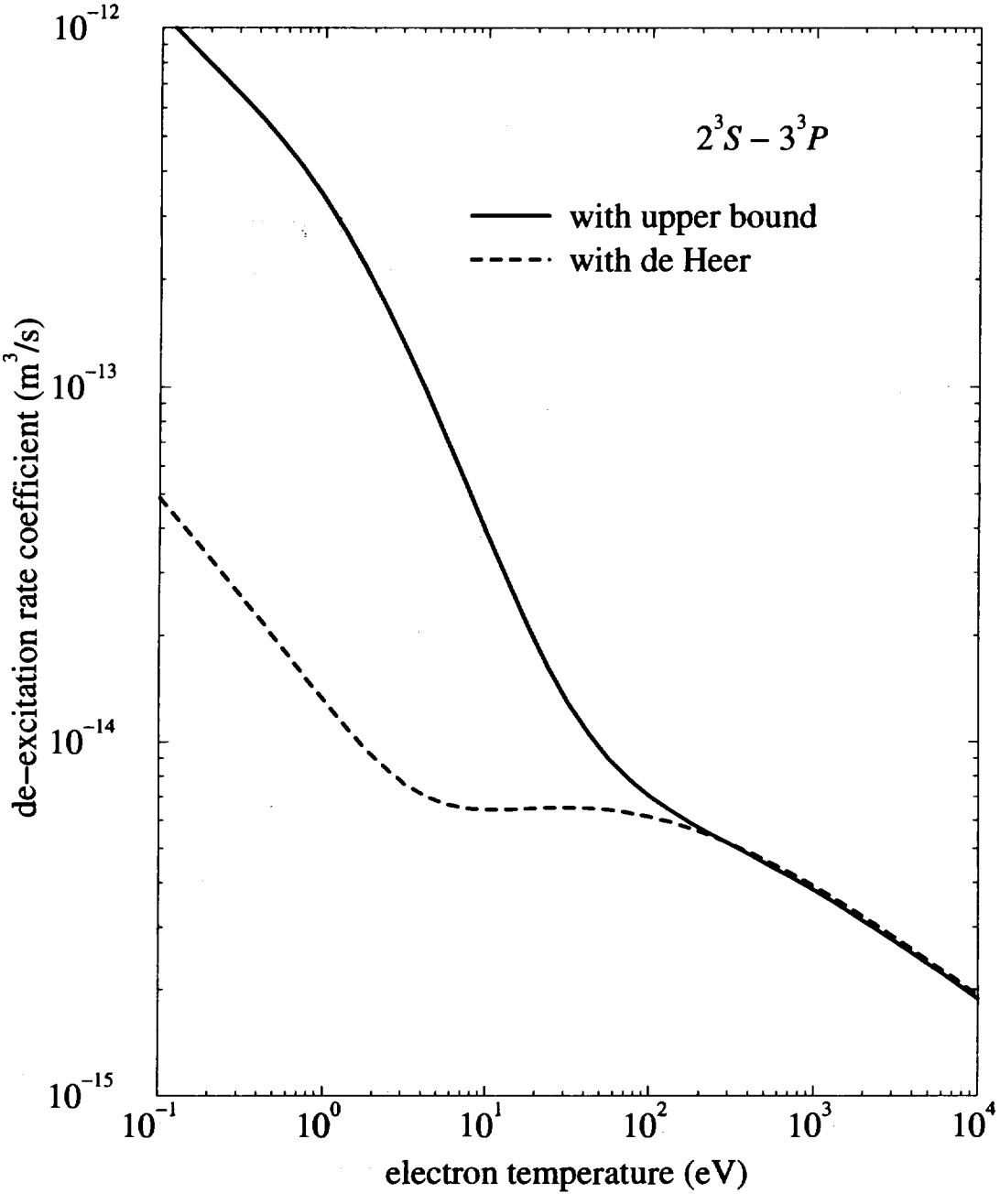

FIG. 45. De-excitation rate coefficient for $2^3S \rightarrow 3^3P$.

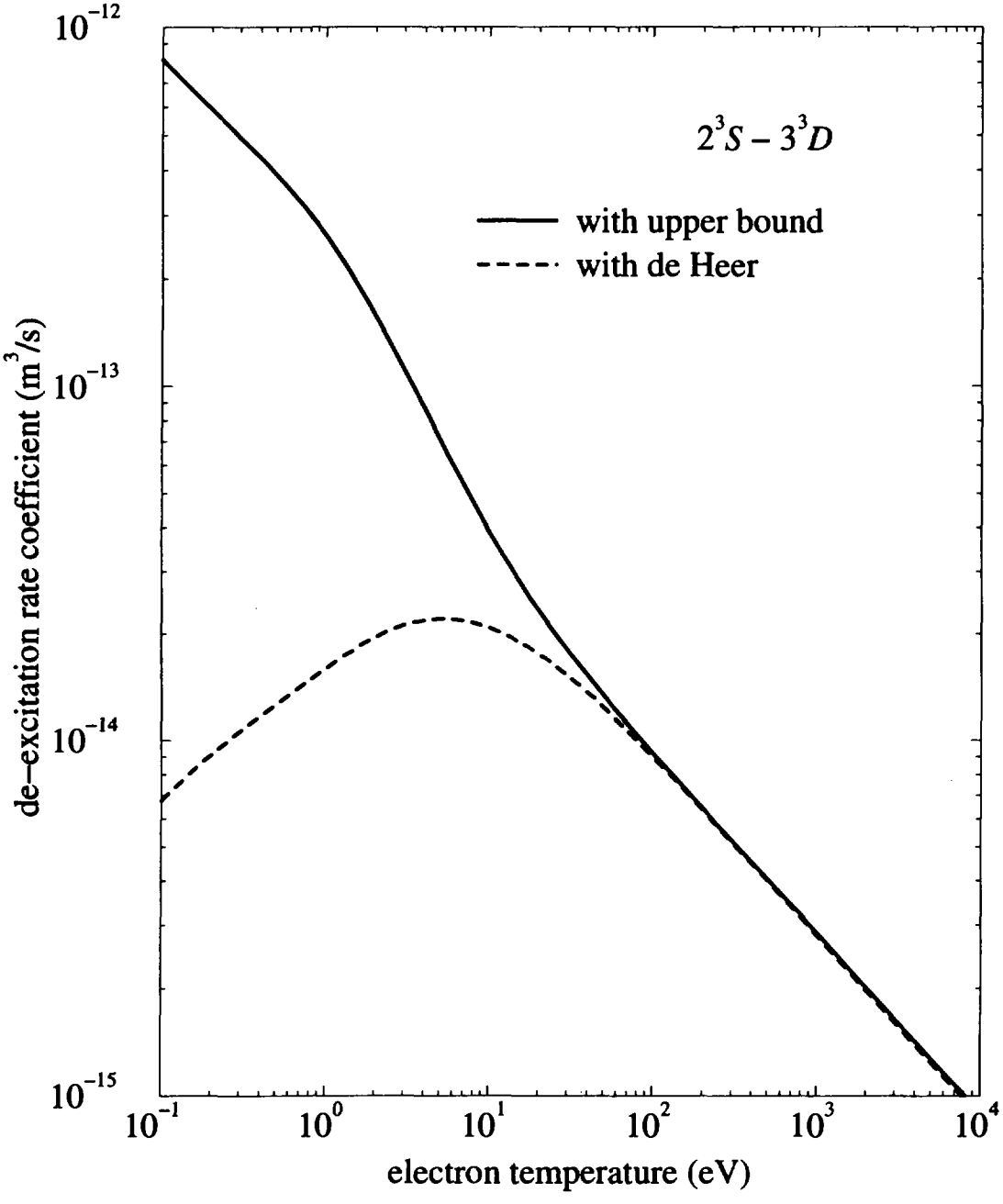

FIG. 46. De-excitation rate coefficient for $2^3S \rightarrow 3^3D$.

Publication List of NIFS-DATA Series

NIFS-DATA-1 Y. Yamamura, T. Takiguchi and H. Tawara,
Data Compilation of Angular Distributions of Sputtered Atoms;
Jan. 1990

NIFS-DATA-2 T. Kato, J. Lang and K. E. Berrington,
Intensity Ratios of Emission Lines from OV Ions for Temperature and Density Diagnostics ; Mar. 1990 [At Data and Nucl Data Tables 44(1990)133]

NIFS-DATA-3 T. Kaneko,
Partial Electronic Straggling Cross Sections of Atoms for Protons;
Mar. 1990

NIFS-DATA-4 T. Fujimoto, K. Sawada and K. Takahata,
Cross Section for Production of Excited Hydrogen Atoms Following Dissociative Excitation of Molecular Hydrogen by Electron Impact ; Mar. 1990

NIFS-DATA-5 H. Tawara,
Some Electron Detachment Data for H^- Ions in Collisions with Electrons, Ions, Atoms and Molecules –an Alternative Approach to High Energy Neutral Beam Production for Plasma Heating– ;
Apr. 1990

NIFS-DATA-6 H. Tawara, Y. Itikawa, H. Nishimura, H. Tanaka and Y. Nakamura,
Collision Data Involving Hydro-Carbon Molecules; July 1990
[Supplement to Nucl. Fusion 2(1992)25]

NIFS-DATA-7 H.Tawara,
Bibliography on Electron Transfer Processes in Ion-Ion/Atom/Molecule Collisions –Updated 1990–; Aug. 1990

NIFS-DATA-8 U.I.Safronova, T.Kato, K.Masai, L.A.Vainshtein and A.S.Shlyapzeva,
Excitation Collision Strengths, Cross Sections and Rate Coefficients for OV, SiXI, FeXXIII, MoXXXIX by Electron Impact ($1s^22s^2$-$1s^22s2p$-$1s^22p^2$ Transitions) Dec.1990

NIFS-DATA-9 T.Kaneko,
Partial and Total Electronic Stopping Cross Sections of Atoms and Solids for Protons; Dec. 1990

NIFS-DATA-10 K.Shima, N.Kuno, M.Yamanouchi and H.Tawara,
Equilibrium Charge Fraction of Ions of Z=4-92 (0.02-6 MeV/u) and Z=4-20 (Up to 40 MeV/u) Emerging from a Carbon Foil; Jan.1991
[AT.Data and Nucl. Data Tables 51(1992)173]

NIFS-DATA-11 T. Kaneko, T. Nishihara, T. Taguchi, K. Nakagawa, M. Murakami,

M. Hosono, S. Matsushita, K. Hayase, M.Moriya, Y.Matsukuma, K.Miura and Hiro Tawara,
Partial and Total Electronic StoppingCross Sections of Atoms for a Singly Charged Helium Ion: Part 1;Mar. 1991

NIFS-DATA-12 Hiro Tawara,
Total and Partial Cross Sections of Electron Transfer Processes for Be^{q+} *and* B^{q+} *Ions in Collisions with H,* H_2 *and He Gas Targets - Status in 1991-*; June 1991

NIFS-DATA-13 T. Kaneko, M. Nishikori, N. Yamato, T. Fukushima, T. Fujikawa, S. Fujita, K. Miki, Y. Mitsunobu, K. Yasuhara, H. Yoshida and Hiro Tawara,
Partial and Total Electronic Stopping Cross Sections of Atoms for a Singly Charged Helium Ion : Part II; Aug. 1991

NIFS-DATA-14 T. Kato, K. Masai and M. Arnaud,
Comparison of Ionization Rate Coefficients of Ions from Hydrogen through Nickel ; Sep. 1991

NIFS-DATA-15 T. Kato, Y. Itikawa and K. Sakimoto,
Compilation of Excitation Cross Sections for He Atoms by Electron Impact; Mar. 1992

NIFS-DATA-16 T. Fujimoto, F. Koike, K. Sakimoto, R. Okasaka, K. Kawasaki, K. Takiyama, T. Oda and T. Kato,
Atomic Processes Relevant to Polarization Plasma Spectroscopy ; Apr. 1992

NIFS-DATA-17 H. Tawara,
Electron Stripping Cross Sections for Light Impurity Ions in Colliding with Atomic Hydrogens Relevant to Fusion Research; Apr. 1992

NIFS-DATA-18 T. Kato,
Electron Impact Excitation Cross Sections and Effective Collision Strengths of N Atom and N-Like Ions -A Review of Available Data and Recommendations- ; Sep. 1992

NIFS-DATA-19 Hiro Tawara,
Atomic and Molecular Data for H_2O, CO & CO_2 *Relevant to Edge Plasma Impurities*, Oct. 1992

NIFS-DATA-20 Hiro. Tawara,
Bibliography on Electron Transfer Processes in Ion-Ion/Atom/Molecule Collisions -Updated 1993-; Apr. 1993

NIFS-DATA-21 J. Dubau and T. Kato,
Dielectronic Recombination Rate Coefficients to the Excited

States of C I from C II; Aug. 1994

NIFS-DATA-22 T. Kawamura, T. Ono, Y. Yamamura,
Simulation Calculations of Physical Sputtering and Reflection Coefficient of Plasma-Irradiated Carbon Surface; Aug. 1994

NIFS-DATA-23 Y. Yamamura and H. Tawara,
Energy Dependence of Ion-Induced Sputtering Yields from Monoatomic Solids at Normal Incidence; Mar. 1995

NIFS-DATA-24 T. Kato, U. Safronova, A. Shlyaptseva, M. Cornille, J. Dubau,
Comparison of the Satellite Lines of H-like and He-like Spectra; Apr. 1995

NIFS-DATA-25 H. Tawara,
Roles of Atomic and Molecular Processes in Fusion Plasma Researches - from the cradle (plasma production) to the grave (after-burning) -; May 1995

NIFS-DATA-26 N. Toshima and H. Tawara
Excitation, Ionization, and Electron Capture Cross Sections of Atomic Hydrogen in Collisions with Multiply Charged Ions; July 1995

NIFS-DATA-27 V.P. Shevelko, H. Tawara and E.Salzborn,
Multiple-Ionization Cross Sections of Atoms and Positive Ions by Electron Impact; July 1995

NIFS-DATA-28 V.P. Shevelko and H. Tawara,
Cross Sections for Electron-Impact Induced Transitions Between Excited States in He: n, n'=2,3 and 4; Aug. 1995

NIFS-DATA-29 U.I. Safronova, M.S. Safronova and T. Kato,
Cross Sections and Rate Coefficients for Excitation of $\Delta n = 1$ Transitions in Li-like Ions with $6<Z<42$; Sep. 1995

NIFS-DATA-30 T. Nishikawa, T. Kawachi, K. Nishihara and T. Fujimoto,
Recommended Atomic Data for Collisional-Radiative Model of Li-like Ions and Gain Calculation for Li-like Al Ions in the Recombining Plasma; Sep. 1995

NIFS-DATA-31 Y. Yamamura, K. Sakaoka and H. Tawara,
Computer Simulation and Data Compilation of Sputtering Yield by Hydrogen Isotopes ($^1H^+$, $^2D^+$, $^3T^+$) and Helium ($^4He^+$) Ion Impact from Monatomic Solids at Normal Incidence; Oct. 1995

NIFS-DATA-32 T. Kato, U. Safronova and M. Ohira,
Dielectronic Recombination Rate Coefficients to the Excited States of CII from CIII; Feb. 1996

NIFS-DATA-33 K.J. Snowdon and H. Tawara,
Low Energy Molecule-Surface Interaction Processes of Relevance to Next-Generation Fusion Devices; Mar. 1996

NIFS-DATA-34 T. Ono, T. Kawamura, K. Ishii and Y. Yamamura,
Sputtering Yield Formula for B_4C Irradiated with Monoenergetic Ions at Normal Incidence; Apr. 1996

NIFS-DATA-35 I. Murakami, T. Kato and J. Dubau,
UV and X-Ray Spectral Lines of Be-Like Fe Ion for Plasma Diagnostics; Apr. 1996

NIFS-DATA-36 K. Moribayashi and T. Kato,
Dielectronic Recombination of Be-like Fe Ion; Apr. 1996

NIFS-DATA-37 U. Safronova, T. Kato and M. Ohira,
Dielectronic Recombination Rate Coefficients to the Excited States of CIII from CIV; July 1996

NIFS-DATA-38 T. Fujimoto, H. Sahara, G. Csanak and S. Grabbe,
Atomic States and Collisional Relaxation in Plasma Polarization Spectroscopy: Axially Symmetric Case; Oct. 1996

NIFS-DATA-39 H. Tawara (Ed.)
Present Status on Atomic and Molecular Data Relevant to Fusion Plasma Diagnostics and Modeling; Jan. 1997

NIFS-DATA-40 Inga Yu. Tolstikhina,
LS-Averaged 1/Z Method as a Tool of Studying the Interactions of Highly Charged Ions with a Metal Surface; Jan. 1997

NIFS-DATA-41 K. Moribayashi and T. Kato,
Atomic Nuclear Charge Scaling for Dielectronic Recombination to Be-like Ions; Apr. 1997

NIFS-DATA-42 H. Tawara,
Bibliography on Electron Transfer Processes in Ion-ion / Atom / Molecule Collisions -Updated 1997 -; May 1997

NIFS-DATA-43 M. Goto and T. Fujimoto,
Collisional-radiative Model for Neutral Helium in Plasma: Excitation Cross Section and Singlet-triplet Wavefunction Mixing; Oct. 1997